PREDICTIVE MUSCULOSKELETAL SIMULATION FOR FUNCTIONAL ELECTRICAL STIMULATION CYCLING: FROM OPTIMIZATION TO EXPERIMENTAL VALIDATION IN SPINAL CORD INJURY

ALEXANDRE BERNARDI PERES

DISSERTAÇÃO DE MESTRADO
EM ENGENHARIA ELÉTRICA

DEPARTAMENTO DE ENGENHARIA ELÉTRICA

FACULDADE DE TECNOLOGIA

UNIVERSIDADE DE BRASÍLIA

Universidade de Brasília
Faculdade de Tecnologia
Departamento de Engenharia Elétrica

Predictive musculoskeletal simulation for functional electrical stimulation cycling: from optimization to experimental validation in spinal cord injury

Alexandre Bernardi Peres

DISSERTAÇÃO DE MESTRADO SUBMETIDA AO PROGRAMA DE PÓS-GRADUAÇÃO EM ENGENHARIA ELÉTRICA DA UNIVERSIDADE DE BRASÍLIA COMO PARTE DOS REQUISITOS NECESSÁRIOS PARA A OBTENÇÃO DO GRAU DE MESTRE.

APROVADA POR:

Roberto de Souza Baptista, Dr. (Universidade de Brasília - UnB)
(Orientador)

Ana Carolina Cardoso de Sousa, Dra. (Institut Químic de Sarrià - IQS)
(Coorientadora)

Antônio Padilha Lanari Bó, Dr. (Oslo Metropolitan University - OsloMet)
(Examinador Externo)

Geovany Araújo Borges, Dr. (Universidade de Brasília - UnB)
(Examinador Interno)

Brasília/DF, Fevereiro de 2026.

FICHA CATALOGRÁFICA

PERES, ALEXANDRE B.

Predictive musculoskeletal simulation for functional electrical stimulation cycling: from optimization to experimental validation in spinal cord injury. [Brasília/DF] 2026.

11, 107p., 210 x 297 mm (ENE/FT/UnB, Mestre, Dissertação de Mestrado, 2026).

Universidade de Brasília, Faculdade de Tecnologia, Departamento de Engenharia Elétrica.

Departamento de Engenharia Elétrica

1. Functional electrical stimulation cycling
2. Spinal cord injury
3. Musculoskeletal modeling
4. Predictive simulation
5. Cycling rehabilitation
6. Muscle dynamics
7. Optimization
8. OpenSim

I. ENE/FT/UnB

II. Título (série)

REFERÊNCIA BIBLIOGRÁFICA

PERES, ALEXANDRE B. (2026). Predictive musculoskeletal simulation for functional electrical stimulation cycling: from optimization to experimental validation in spinal cord injury. Dissertação de Mestrado, Publicação PPGEE 838/25, Departamento de Engenharia Elétrica, Universidade de Brasília, Brasília, DF, 107p.

CESSÃO DE DIREITOS

AUTOR: Alexandre Bernardi Peres

TÍTULO: Predictive musculoskeletal simulation for functional electrical stimulation cycling: from optimization to experimental validation in spinal cord injury.

GRAU: Mestre ANO: 2026

Alexandre Bernardi Peres

Universidade de Brasília (UnB)

Campus Darcy Ribeiro

Faculdade de Tecnologia - FT

Departamento de Engenharia Elétrica(ENE)

Brasília - DF CEP 70919-970

"It is important to draw wisdom from many different places. If you take it from only one place, it becomes rigid and stale. Understanding others, the other elements and the other nations will help you become whole."
- Uncle Iroh, Avatar: The Last Airbender

ACKNOWLEDGEMENTS

I would like to express my deepest gratitude to my family, whose motivation, care, and understanding provided essential support during the most demanding phases of this work. I am especially grateful to my parents, Adriano Peres and Patrícia Peres, whose constant encouragement and presence accompanied me throughout this entire journey. I also thank my brother Victor Peres, my sister Bruna Viana, Paulo Viana and his family, as well as my girlfriend Nicole Guerreiro and her family. Their belief in my work and unwavering patience were fundamental to the completion of this thesis.

I would like to thank my advisors, Dr. Roberto Baptista and Dra. Ana de Sousa, for their guidance, trust, and continuous support throughout my research and academic projects. Their expertise and feedback were essential to the development of this work. I am especially thankful to Dr. Carlos Gonçalves, who taught me the foundations upon which my research was built. I also thank Dr. Amilton Vieira and Dr. Lucas Ugliara for the valuable interdisciplinary perspectives that enriched both my academic formation and this research. My sincere appreciation also goes to Dr. Josep Font-Llagunes, Dra. Rosa Pàmies-Vilà, and Dr. Massimo Cenciarini, who followed my research activities in Barcelona and contributed significantly to my academic growth. Special thanks to Estevão Lopes, one of the coordinators of Project EMA, who was not only a constant source of friendship and support, but also generously volunteered for data collection.

I am grateful to the staff of the Electrical Engineering Department, particularly Valter de Oliveira, Vera Simões, and Leonardo Botelho, whose availability and efficiency made many practical and administrative aspects of this journey much smoother.

Finally, I would like to thank my friends — Fábio Santos, Gabriel Pacheco, Guilherme Camargo, Lucas Ferreira, Luís Sanchez, Luiza Tedesque, Marina Garcia, Matheus Barbosa (in memoriam), Pedro Ferreira, Rafael Barbosa, Rafael Mascarenhas, Rodrigo Zamagno, Víctor Pacheco, and Vinícius Gomes — who were always patient and supportive, willing to listen, help, and encourage me throughout this process.

ABSTRACT

Functional electrical stimulation (FES) cycling is a promising rehabilitation and exercise modality for individuals with spinal cord injury, but its effectiveness depends critically on the design of stimulation patterns that coordinate muscle activation in a physiologically plausible and robust manner. Traditionally, these patterns are derived empirically through manual tuning, which limits reproducibility and systematic exploration of design choices. This thesis investigates the use of predictive musculoskeletal simulations to derive stimulation strategies for FES cycling and to translate them into experimentally viable control signals.

The work is organized around two sequential experimental studies addressing the same research questions from complementary perspectives. The first study presents a proof-of-concept framework in which fully predictive optimal control simulations are used to generate stimulation profiles for cycling, which are then implemented experimentally in an individual with complete spinal cord injury. This study establishes the feasibility of deriving stimulation timing directly from simulation without relying on pre-recorded electromyography or heuristic phase definitions. The second study extends this framework by incorporating additional physiological refinements, including antagonist muscle groups and synergy-based coordination constraints, and by performing a more comprehensive experimental validation. Together, the studies evaluate the robustness, physiological plausibility, and experimental viability of simulation-derived stimulation relative to a bang-bang control strategy.

Across both investigations, predictive simulations produced stimulation patterns that could be safely implemented and sustained experimentally, yielding stable cycling behavior and performance metrics comparable to empirically tuned stimulation. For the first study, measured power, cycling cadence and left-right leg balance was improved when compared to a simple bang-bang protocol. For the second study, alongside the improvements to the presented method, a more elaborate and refined bang-bang protocol was used as a reference. Although the performance metrics for power and cadence exceeded those of the established protocol, the left-right balance remained superior to the reference bang-bang approach. While the proposed appro-

ach does not aim to outperform established controllers, it demonstrates that physiologically structured, fully synthetic stimulation signals can be generated systematically and translated to real-world FES cycling.

By explicitly integrating methodological decision-making into the modeling and experimental pipeline, this thesis contributes a reproducible simulation-to-stimulation workflow and clarifies the trade-offs associated with predictive control, model abstraction, and experimental implementation. The results provide a foundation for future work on personalized modeling, adaptive and closed-loop control, and the broader application of predictive simulations in neurorehabilitation.

Keywords: Functional electrical stimulation cycling, Spinal cord injury, Musculoskeletal modeling, Predictive simulation, Cycling rehabilitation, Muscle dynamics, Optimization, OpenSim.

RESUMO

Título em português: Simulação musculoesquelética preditiva para ciclismo por eletroestimulação funcional: da otimização à validação experimental em lesão medular.

A estimulação elétrica funcional (FES) aplicada ao ciclismo é uma estratégia promissora de exercício e reabilitação para indivíduos com lesão medular, porém sua eficácia depende criticamente do projeto de padrões de estimulação capazes de coordenar a ativação muscular de forma fisiologicamente plausível e robusta. Tradicionalmente, esses padrões são definidos de maneira empírica, por meio de ajustes manuais, o que limita a reprodutibilidade e a exploração sistemática das decisões de projeto. Esta dissertação investiga o uso de simulações musculoesqueléticas preditivas para a derivação de estratégias de estimulação para o ciclismo com FES e sua tradução em sinais de controle experimentalmente viáveis.

O trabalho é organizado em torno de dois estudos sequenciais que abordam as mesmas questões de pesquisa a partir de perspectivas complementares. O primeiro estudo apresenta uma investigação de prova de conceito, na qual simulações de controle ótimo totalmente preditivas são utilizadas para gerar perfis de estimulação para o ciclismo, posteriormente implementados experimentalmente em um indivíduo com lesão medular completa. Esse estudo estabelece a viabilidade de derivar a temporização da estimulação diretamente a partir de simulações, sem recorrer a eletromiografia previamente coletada ou a definições heurísticas de fase. O segundo estudo estende esses princípios ao incorporar refinamentos fisiológicos adicionais, incluindo grupos musculares antagonistas e restrições de coordenação baseadas em sinergias, além de realizar uma validação experimental mais abrangente ao longo de múltiplos dias. Em conjunto, os estudos avaliam a robustez, a plausibilidade fisiológica e a viabilidade experimental de sinais de estimulação derivados de simulação em comparação com uma estratégia de controle do tipo bang-bang madura e empiricamente ajustada.

Ao longo de ambas as investigações, as simulações preditivas produziram padrões de estimulação que puderam ser implementados de forma segura e sustentada experimentalmente, resultando em comportamento cíclico estável e métricas de desempenho comparáveis às obtidas

com a estimulação empiricamente ajustada. No primeiro estudo, a potência medida, cadência de pedalada, e equilíbrio entre as pernas mostraram melhorias quando comparado com um protocolo simples liga-desliga. No segundo estudo, juntamente com as melhorias apresentadas no método, um protocolo liga-desliga mais maduro e elaborado foi utilizado como referência. Enquanto as métricas de performance de potência e cadência do sinal de referência foram superiores, o equilíbrio entre as pernas se manteve superior. Embora a abordagem proposta não tenha como objetivo superar controles estabelecidos, os resultados demonstram que sinais de estimulação totalmente sintéticos, estruturados fisiologicamente, podem ser gerados de forma sistemática e traduzidos para o ciclismo com FES no mundo real.

Ao integrar explicitamente as decisões metodológicas ao longo do processo de modelagem e experimentação, esta dissertação contribui com um fluxo de trabalho reprodutível de simulação para estimulação e esclarece as implicações das escolhas relacionadas ao controle preditivo, à abstração do modelo e à implementação experimental. Os resultados fornecem uma base para trabalhos futuros em modelagem personalizada, estratégias de controle adaptativas e em malha fechada, e para a aplicação mais ampla de simulações preditivas no contexto da neurorreabilitação.

Palavras-chave: Ciclismo com eletroestimulação funcional, Lesão medular, Modelagem musculoesquelética, Simulação preditiva, Reabilitação com ciclismo, Dinâmica muscular, Otimização, OpenSim.

TABLE OF CONTENTS

LIST OF FIGURES

LIST OF TABLES

LIST OF SYMBOLS

J_{actu}	Actuator effort cost
J_{total}	Weighted total cost function
J_{musc}	Muscle effort cost
t_0	Initial time of the simulation
t_f	Final time of the simulation
t_{sim}	Total simulation duration
$x_m(t)$	Excitation of muscle m
$x(t)$	System state (crank angular velocity)
$x_{\text{ref}}(t)$	Reference crank angular velocity
$x_i(t)$	Actuator input signal
w_{time}	Weight associated with time minimization
w_{actu}	Weight associated with actuator effort
w_m	Weight associated with muscle effort
w	Weight associated with speed tracking
θ	Crank angle
θ_{shift}	Crank angular shift
I	Current amplitude
I_{std}	Standardized current amplitude
$a(t)$	Muscle activation signal
$a_m(t)$	Activation of muscle m
a_{norm}	Normalized muscle activation m
W	Muscle synergy weight matrix
C	Muscle synergy activation matrix
P	Average power output (W)
V	Crank cadence / angular velocity (rpm)
B	Left-right balance metric (%)

GLOSSARY

FES	Functional electrical stimulation
SCI	Spinal cord injury
BB	Bang-bang control signal
uCS / CS	(Unnormalized) Simulation-derived control signal
sEMG / EMG	(Surface) Electromyography
MSK	Musculoskeletal
PW	Pulse-width
A	Ampere
Kg	Kilogram
s	Second
PI	Proportional-integral
FL	Fuzzy-logic
NMF	Non-negative matrix factorization
NLP	Nonlinear programming
RF	Rectus femoris
VI	Vasti
ICORR	International Consortium for Rehabilitation Robotics
JNER	Journal of NeuroEngineering and Rehabilitation
SEB	Simpósio de Engenharia Biomédica
CBEB	Congresso Brasileiro de Engenharia Biomédica
ICNR	International Conference on NeuroRehabilitation

CHAPTER 1

INTRODUCTION

1.1 ELECTRICAL STIMULATION AND FES

Electrical stimulation has long been employed as a means to activate neuromuscular structures when voluntary control is impaired. By delivering electrical pulses to peripheral nerves or muscles, it is possible to evoke contractions and generate functional movement even in the absence of descending neural input (ANDERSEN *et al.*, 2022). This principle underlies a broad family of neuroprosthetic interventions, in which externally applied electrical inputs are used to substitute, augment, or reorganize impaired neuromuscular control. It ranges from therapeutic applications (KIM *et al.*, 2023; KENNEDY *et al.*, 2025) to assistive technologies aimed at restoring lost motor functions (HAMID; HAYEK, 2008; MAFFIULETTI *et al.*, 2018).

Functional electrical stimulation (FES) represents a particular class of electrical stimulation in which patterned stimulation is used to produce purposeful, task-oriented movements (MARQUEZ-CHIN; POPOVIC, 2020). Over the past decades, FES has been applied as a form of active rehabilitation to a variety of motor tasks, including reaching and grasping (POPOVIC *et al.*, 2001; KAPADIA *et al.*, 2020; HöHLER *et al.*, 2025), standing (BRAZ *et al.*, 2009; ZOULIAS *et al.*, 2019; IBITOYE *et al.*, 2019), and walking (POPOVIC *et al.*, 2001; NIGHTINGALE *et al.*, 2007; THRASHER; POPOVIC, 2008; MOLL *et al.*, 2017), particularly in individuals after a stroke, children with cerebral palsy, and people with spinal cord injury (SCI).

Beyond functional assistance, FES has been shown to provide important physiological benefits, such as preservation of muscle mass (DELEY *et al.*, 2015), improvements in cardiovascular conditioning (DAVIS *et al.*, 2008), and mitigation of secondary complications associated with prolonged muscle inactivity (POPOVIC; SINKJÆR, 2000; HUNT *et al.*, 2012; SADOWSKY *et al.*, 2013; MARQUEZ-CHIN; POPOVIC, 2020; MATEO *et al.*, 2021).

1.2 FES-ASSISTED CYCLING

Among the applications, FES-assisted cycling has received sustained attention since its first proposal in the 1980s (GLASER, 1986). It was widely adopted due to its constrained kinematics, repetitive structure, favorable health outcomes (RABELO *et al.*, 2018; SCHEER *et al.*, 2021; FRAZãO *et al.*, 2024), compatibility with stationary training systems, and competitive settings such as the Cybathlon (RIENER, 2016; COSTE; WOLF, 2018; JAEGER *et al.*, 2023). Historically, research in FES cycling has progressed alongside advances in stimulation hardware, sensor integration, and mechanical design, culminating in rehabilitative platforms such as recumbent tricycles and stationary ergometers (HUNT *et al.*, 2012). Despite these advances, FES cycling remains characterized by low mechanical efficiency and limited power output when compared to able-bodied cycling, a limitation that has been consistently reported across clinical and experimental studies (HAKANSSON; HULL, 2009; ZHANG *et al.*, 2011; HUNT *et al.*, 2012; HAKANSSON; HULL, 2012).

The challenges associated with FES cycling are multifactorial. Electrically evoked contractions differ fundamentally from voluntary ones, both in terms of motor unit recruitment and fatigue behavior (POPOVIC; SINKJÆR, 2000; HUNT *et al.*, 2012). Surface stimulation imposes strict actuation constraints, including limited muscle selectivity (LAUBACHER *et al.*, 2016; BAPTISTA *et al.*, 2022) and synchronous activation of multiple muscles per channel (POPOVIC; SINKJÆR, 2000; HUNT *et al.*, 2012). Moreover, effective power generation during cycling depends critically on the timing and coordination of muscle activation relative to crank position, as well as on the management of delays inherent to the neuromuscular and mechanical system (PERKINS *et al.*, 2001; FONSECA *et al.*, 2017; de Sousa *et al.*, 2016).

Most successful FES cycling implementations have relied on empirically tuned stimulation strategies and what is commonly referred to as on-off or bang-bang control. These approaches involve fully activating or deactivating large muscle groups at advantageous intervals, often complemented by extensive manual adjustments and user-specific adaptations. Although such strategies have demonstrated robustness and practical effectiveness, including in competitive settings, their development is inherently heuristic, based on a simple biomechanical understanding of the cycling movement, presenting risks, requiring substantial experimental effort, and, when implementing in people with complete SCI, without sensory feedback from the user. As

a result, stimulation protocols are often highly user and system-specific, limiting their generalizability and reproducibility, motivating the need for systematic design frameworks that can account for neuromuscular dynamics and mechanical constraints in a principled manner.

1.3 MUSCULOSKELETAL SIMULATIONS

The use of musculoskeletal simulations offers a pathway to address these challenges (FREGLY, 2021; UHLRICH *et al.*, 2023; KAINZ *et al.*, 2024). By explicitly modeling the dynamics of the musculoskeletal system, simulations provide a framework in which muscle coordination, timing, and mechanical interactions can be explored systematically and safely. Fully predictive simulations eliminate the need for prior experimental data, generating physiologically plausible activation patterns based solely on the model's dynamics and cost function definitions (FEBRER-NAFRíA *et al.*, 2022). The use of "predictive"in this context therefore reflects the capability of the simulation to generate data without the need of previously obtained experimental data. Early work already recognized the potential of such tools to inform stimulation design, suggesting that stimulation patterns optimized in silico could serve as reference signals for real-world neuroprosthetic systems, provided that closed-loop control compensates for modeling errors and disturbances (POPOVIC; SINKJÆR, 2000). However, at the time, modeling and computational limitations restricted the practical realization of this vision.

Fully predictive simulations are particularly attractive for FES applications in people with SCI, as they allow stimulation design to be framed objectively as an optimal control problem subject to physiological, mechanical, and implementation constraints despite the absence of user feedback. In this context, stimulation signals are no longer tuned manually but are derived systematically from an explicit performance objective. Until recently, very few studies have demonstrated a full translation of predictive simulations into experimentally validated FES control signals (CO *et al.*, 2025). As far as it is known by the authors, Peres et al. 2025a was the first study to successfully implement the results of a fully predictive simulation pipeline in an individual with a complete SCI in a cycling setting.

The motivation for adopting predictive simulations in FES cycling is further reinforced by insights from the experimental literature. The most recent literature review on FES cycling

efficiency highlighted that its poor efficiency arises primarily from unfavourable biomechanics and non-physiological muscle recruitment, including crude activation of muscle groups, suboptimal timing, and the lack of synergistic and antagonistic joint control (HUNT *et al.*, 2012). Importantly, they hypothesised that improvements in stimulation timing, inclusion of additional muscle groups, and the use of constrained numerical optimization with dynamic models could substantially enhance performance.

1.4 PHYSIOLOGICAL COORDINATION AND MUSCLE SYNERGIES

A central concept in muscular control is that of muscle synergies. In physiological movement, muscles rarely act in isolation (BERNSTEIN, 1967). Instead, coordinated activation patterns allow the nervous system to reduce control dimensionality and individual muscle burden while maintaining functional flexibility (CHEUNG *et al.*, 2020). Although electrically induced contractions do not replicate natural recruitment mechanisms, imposing coordinated activation structures in FES control can better reflect the realities of surface stimulation, where multiple muscles are activated simultaneously. When this concept is applied to neuroprosthesis, especially in surface electrode FES where selectivity is limited, it provides a structured way to constrain control solutions to coordinated activation patterns that are experimentally feasible (HAYASHIBE; SHIMODA, 2014; LI *et al.*, 2015). In this context, muscle synergies are not interpreted as direct representations of neural control, but rather as a control abstraction that enforces coordinated activation consistent with surface FES constraints.

Incorporating muscle synergy principles into optimization-based FES control is still not fully explored, with only one application to walking (WARNER *et al.*, 2025), and one to exoskeleton-assisted walking (ALIBEJI *et al.*, 2018). Until Peres et al. 2025b, it had not been implemented in a FES cycling setting (CO *et al.*, 2025).

1.5 RESEARCH QUESTIONS

Within this framework, the present thesis investigates whether stimulation protocols derived entirely from predictive musculoskeletal simulations can be translated into a real FES cycling

system and validated experimentally. Rather than aiming to outperform well-established empirical protocols outright, the focus is on assessing whether a fully predictive, constraint-aware workflow can generate implementable stimulation strategies without manual tuning.

The objective of this thesis is to evaluate whether stimulation patterns generated through fully predictive musculoskeletal simulations are physiologically plausible and can be successfully implemented in a real FES cycling system and produce functional cycling performance comparable to an empirically tuned stimulation strategy.

Based on this objective, the following hypotheses are formulated:

H1: Predictive musculoskeletal simulations can generate stimulation signals that produce feasible FES cycling while maintaining physiologically coordinated muscle activation patterns.

H2: A stimulation signal derived entirely from simulation can achieve comparable cycling performance to a mature empirically tuned bang-bang protocol under matched experimental conditions.

To investigate these hypotheses, the following research questions are addressed:

1. Can stimulation protocols be systematically optimized to produce feasible FES cycling while preserving physiologically coordinated muscle activation patterns?

2. Under matched experimental conditions, how does a simulation-derived stimulation signal compare with a mature, empirically tuned bang-bang protocol in terms of power output, cadence regulation, and inter-limb balance?

1.6 RELEVANCE AND CONTRIBUTIONS OF THE THESIS

Addressing these questions is relevant not only for FES cycling, but more broadly for the design of neuroprosthetic controllers that balance performance, safety, and reproducibility. By demonstrating a systematic simulation-to-stimulation pipeline and validating it experimentally in an individual with complete SCI, this thesis aims to contribute a methodological foundation upon which more adaptive, personalized, and scalable FES control strategies can be developed.

1.7 STRUCTURE OF THE THESIS

This thesis is organized around two sequential experimental studies that address the same overarching research questions from complementary perspectives. The first study (presented in Chapters 4-6) corresponds to a proof-of-concept investigation, previously presented at the International Consortium for Rehabilitation Robotics (ICORR) (PERES *et al.*, 2025a). Its primary objective was to assess the feasibility of using fully predictive musculoskeletal simulations to derive stimulation profiles for FES cycling and to implement these profiles experimentally in an individual with complete spinal cord injury.

The second study (presented in Chapters 7-9), recently submitted to the Journal of NeuroEngineering and Rehabilitation (JNER) (PERES *et al.*, 2025b), is a case study that builds directly upon the outcomes and limitations identified in the proof-of-concept study. It extends the original framework by incorporating additional physiological refinements, including antagonist muscle groups and synergy-based coordination, and by performing a more comprehensive experimental validation under a structured multi-day protocol. While the first study establishes feasibility through a simplified implementation, the second study extends the framework to include an additional muscle group and address the synchronous muscle recruitment inherent of superficial FES. For clarity, the methods, results, and discussions of each study are presented separately. The discussion of the case study is intentionally broader, synthesizing insights that apply across both investigations.

The thesis adopts a deliberately pedagogical structure. In contrast to more conventional thesis organizations, the methods chapters include not only the formal description of models, experimental protocols, and optimization procedures, but also explicit explanations of the methodological decisions that guided their design. The corresponding discussion chapters then expand on the consequences, trade-offs, and implications of these decisions. This structure was chosen intentionally to make the reasoning process behind the proposed framework transparent, reproducible, and to facilitate knowledge transfer.

Chapter 2 presents the theoretical background, contextualizing the challenges of FES cycling and providing a state of the art of optimization-based control strategies. Chapter 3 is intended as a cross-study common material, with information relevant to both studies. Chapters 4-6

detail the proof-of-concept study, while Chapters 7-9 present the case study. Finally, Chapter 10 synthesizes the main findings of the thesis and outlines future research directions.

CHAPTER 2

THEORETICAL BACKGROUND - FES CYCLING

2.1 FES CYCLING REHABILITATION

Functional electrical stimulation (FES) cycling can be implemented as a stationary or mobile active rehabilitation modality, in which electrical stimulation is used to evoke cyclic contractions of lower-limb muscles in synchrony with crank rotation (BO *et al.*, 2017; SCHMOLL *et al.*, 2022; JAEGER *et al.*, 2023). Unlike locomotor tasks such as walking, cycling imposes constrained and repeatable kinematics, requires minimal balance control, and allows continuous mechanical support throughout the movement. These characteristics make cycling particularly suitable for individuals with severe motor impairments, including people with complete spinal cord injury (SCI), for whom voluntary motor control and postural stabilization are absent (BAPTISTA *et al.*, 2022), but also make cycling particularly amenable to systematic control design and modeling. The use of FES cycling in clinical rehabilitation programs has steadily increased over the years in research settings, specialized rehabilitation centers, and long-term training contexts, driven by its cardiovascular, musculoskeletal, and metabolic benefits (RABELO *et al.*, 2018; FRAZãO *et al.*, 2024).

Most contemporary FES cycling systems are implemented either as stationary ergometers or recumbent tricycles. The recumbent posture provides enhanced trunk stability, reduces fall risk, and minimizes the need for postural control (BAPTISTA *et al.*, 2022). From a mechanical perspective, the recumbent configuration also promotes a more consistent alignment between the hips, knees, and crank axis across sessions, reducing variability in joint kinematics and force transmission. For these reasons, recumbent platforms have become the prevalent configuration in experimental FES cycling studies and competitive settings for users with complete spinal cord injury.

To ensure safe and effective transmission of electrically evoked forces to the crank, orthope-

dic boots or rigid foot fixation systems are commonly employed. These devices secure the feet to the pedals, limit motion outside the desired plane, and prevent excessive ankle movement, compensating for the absence of voluntary control and reflex-mediated joint stabilization. Beyond preventing slippage, rigid fixation plays a critical role in maintaining joint alignment and protecting the lower-limb joints from uncontrolled abduction or rotation, which could otherwise lead to injury (BO *et al.*, 2017). Although studies have explored the stimulation of lower-leg muscles to improve power generation (HAKANSSON; HULL, 2010), such approaches raise significant safety concerns in individuals with complete SCI when rigid fixation is not used. In practice, stability and safety take precedence over increased power generation, making rigid lower-leg fixation a standard component in FES cycling systems.

At the stimulation level, FES cycling systems typically rely on bipolar, symmetric, charge-balanced electrical pulses, delivered at fixed stimulation frequencies and modulated through either current amplitude or pulse width. This configuration is widely adopted to ensure reliable muscle activation while minimizing skin irritation, discomfort, and tissue damage (POPOVIC; SINKJÆR, 2000). The choice between these modulation strategies depends on hardware capabilities, safety considerations, and the desired resolution of control, but both preserve the same fundamental temporal structure of muscle activation (POPOVIC; SINKJÆR, 2000).

The electrodes used in FES systems, including FES cycling, are most commonly self-adhesive surface electrodes with relatively large contact areas. Larger electrodes distribute current over a wider region, reducing current density at the skin-electrode interface and improving comfort during prolonged sessions. However, this comes at the expense of spatial selectivity, as smaller or deeper muscles cannot be selectively activated without first exciting more superficial structures (POPOVIC; SINKJÆR, 2000; BO *et al.*, 2017).

Electrode placement therefore remains a critical yet inherently imprecise process, often refined empirically to achieve consistent muscle activation across sessions. While alternative electrode technologies, such as percutaneous, implanted (MCDANIEL *et al.*, 2017), or spatially distributed superficial electrodes (BAPTISTA *et al.*, 2022) can offer improved selectivity and stimulation efficiency, they introduce additional drawbacks related to surgical risk, infection, long-term maintenance, and cost (POPOVIC; SINKJÆR, 2000). For these reasons, stimulation through a single pair of surface electrodes (single electrode stimulation) per muscle group

remains the most practical and widely used option in FES cycling research and applications, including the ones reported in this thesis.

In practical implementations, only a restricted set of muscle groups is typically stimulated. The quadriceps muscle group is almost universally targeted due to its mechanical effectiveness and consistent contribution to the knee extension phases of the cycle. In more elaborate setups, additional muscle groups such as the hamstrings or gluteal muscles may be included to assist with knee flexion or hip extension (BO *et al.*, 2017), but the number of independently controllable muscle groups remains small. This restriction arises from several practical constraints: namely the limited number of stimulation channels available in most commercial electrical stimulators and the difficulty of achieving selective activation (POPOVIC; SINKJÆR, 2000). As a result, FES cycling systems generally operate with a small number of stimulation channels, each corresponding to a predefined muscle group rather than individual muscles.

Despite these practical limitations, FES cycling has demonstrated substantial physiological and rehabilitative benefits, motivating continued research and technological development. At the same time, the very constraints that make surface-stimulated FES cycling feasible and safe, may also define the boundaries within which novel control and stimulation strategies can operate. Understanding this practical context is essential for framing the technical challenges of surface-stimulated FES cycling and for identifying which aspects of the system can realistically be addressed for improvement.

2.2 PHYSIOLOGICAL AND TECHNICAL ORIGINS OF THE CHALLENGES IN FES CYCLING

FES-assisted cycling is constrained by a set of physiological, technical, and control-related factors that fundamentally distinguish electrically evoked movement from voluntary cycling. While these limitations were introduced at a high level in Chapter 1, a more detailed examination is required to clarify their physiological origins and technical implications, particularly in the context of surface-stimulated systems used by people with spinal cord injury (SCI).

Building on experimental and theoretical insights from the literature, particularly those synthesized by Hunt et al. 2012 and Popović et al. 2000, the challenges of FES cycling can be

organized around three core factors.

The first core challenge concerns unfavourable biomechanics arising from crude muscle group actuation, suboptimal timing of activation, and limited capacity for synergistic and antagonistic joint coordination. These factors directly affect mechanical power transfer and efficiency, and constitute the primary targets for optimization strategies explored in this thesis.

The second core challenge relates to the non-physiological nature of electrically evoked muscle recruitment, including altered motor unit recruitment order, synchronous firing, and deterministic stimulation patterns. While these properties cannot be eliminated with surface stimulation, they must be explicitly acknowledged when designing and evaluating stimulation strategies.

The third core challenge arises from neuromuscular alterations following spinal cord injury, including structural, metabolic, and functional changes in muscle tissue, as well as the absence of voluntary control and sensory feedback. These factors define fundamental limits on adaptability and performance, but their consequences can benefit from FES cycling with improved coordination and timing.

The following sections examine each of these core challenges in detail, tracing their physiological and technical origins and clarifying their implications for control, modeling, and optimization in surface-stimulated FES cycling.

2.2.1 Core Challenge I: Unfavourable biomechanics in FES cycling

Unfavourable biomechanics in surface-stimulated FES cycling arises because the neuromuscular system is driven by the relatively small set of stimulation channels that evoke coarse muscle-group actions, rather than finely distributed joint-level coordination. As highlighted in the experimental literature, low efficiency in FES cycling is strongly linked to crude recruitment of muscle groups, non-optimal timing of activation, and limited capacity to reproduce the synergistic and antagonistic coordination patterns that support effective power transfer in able-bodied cycling (HUNT *et al.*, 2012). In practice, this biomechanical mismatch reduces the fraction of electrically evoked muscle force that contributes actively to crank rotation and increases the sensitivity of performance to timing and parameter tuning.

2.2.1.1 Crude muscle group actuation

Surface stimulation typically activates muscles in broad groupings determined by electrode placement and the limited number of channels available in commercial stimulators (HUNT *et al.*, 2012). As a result, stimulation inputs are mapped to composite mechanical actions rather than to selectively controlled muscle contributions. This coarse actuation limits the ability to shape the direction of pedal force throughout the crank cycle and restricts the capacity to redistribute effort across joints as conditions change (e.g., due to fatigue or cadence variations). From a biomechanical perspective, the consequence is that force is often produced with limited control over its tangential component, reducing effective power transfer to the crank.

2.2.1.2 Non-optimal timing of muscle activation

Because cycling is a phase-dependent task, the mechanical effectiveness of electrically evoked contractions depends critically on aligning stimulation onset and offset with crank position (SCHMOLL *et al.*, 2022). Even small timing errors can shift force production into mechanically disadvantageous regions of the cycle, decreasing net power output and, in extreme cases, generating braking torques that oppose rotation (HUNT *et al.*, 2012). This sensitivity is amplified in FES cycling by electromechanical delays and by the limited capacity to modulate force smoothly with surface stimulation. In most practical implementations, timing is therefore encoded as crank-angle windows, which are tuned empirically and may require adjustments as cadence and fatigue state change.

2.2.1.3 Limited synergistic and antagonistic joint coordination

In volitional cycling, effective power transfer is supported by coordinated multi-joint muscle function, including task-dependent redistribution of effort between hip and knee moments and controlled transitions between propulsive phases (SO *et al.*, 2005). In addition, the nervous system uses anticipatory coordination and stabilizing strategies to maintain smooth crank dynamics across phase transitions (WAKELING; HORN, 2009; HUG *et al.*, 2011; KONG *et al.*, 2024). In surface-stimulated FES cycling, such coordination is difficult to reproduce because stimulation channels do not provide independent access to individual muscles (BO *et al.*, 2017).

Instead, each channel produces a coupled mechanical effect that cannot be decomposed easily into joint-specific control objectives.

2.2.1.4 Biomechanical implications

Taken together, crude muscle-group actuation, strong timing sensitivity, and limited coordination flexibility define the principal biomechanical constraints of surface-stimulated FES cycling. These constraints are consistently associated with low mechanical efficiency and reduced power output relative to able-bodied cycling (HUNT *et al.*, 2012). Importantly, this core challenge is not merely a matter of insufficient tuning effort. It reflects the restricted actuation structure imposed by surface stimulation and the need to generate propulsion using a small number of coupled control inputs. For this reason, most of FES cycling research focuses on improving stimulation timing and parameters to control or increase specific metrics of performance as seen in Section 2.3.

2.2.2 Core Challenge II: Non-physiological muscle recruitment and fatigue

A second fundamental limitation of surface-stimulated FES cycling arises from the non-physiological manner in which muscle fibers are recruited and activated under electrical stimulation. Unlike voluntary movement, where force production is governed by orderly motor unit recruitment and adaptive firing behavior, electrically evoked contractions impose artificial activation patterns that directly affect endurance, efficiency, and sustainable power output (POPOVIC; SINKJÆR, 2000; HUNT *et al.*, 2012).

2.2.2.1 Altered motor unit recruitment order

In physiological muscle activation, force generation follows the size principle: smaller, fatigue-resistant motor units are recruited first, with progressively larger and more fatigable units activated as force demand increases (HENNEMAN *et al.*, 1965). This recruitment hierarchy allows force to be modulated efficiently while delaying fatigue. Under surface electrical stimulation, however, motor unit recruitment depends primarily on electrode position,

user-specific muscle properties, and local stimulation intensity rather than on neural drive.

As a consequence, recruitment order is non-physiological, and may be mixed and often inverted, with fast, fatigable motor units activated at relatively low stimulation intensities (POPOVIC; SINKJÆR, 2000). This disruption of physiological recruitment fundamentally alters the relationship between stimulation input and force output, reducing endurance and contributing to the rapid decline in performance commonly observed during FES cycling sessions.

2.2.2.2 Synchronous activation and deterministic firing behavior

In addition to altered recruitment order, electrically evoked contractions differ markedly from voluntary contractions in their firing characteristics. Surface FES typically activates motor units synchronously and at fixed and high stimulation frequencies, whereas physiological force production relies on asynchronous motor unit firing and rate modulation (HUNT *et al.*, 2012). This synchronous, deterministic activation concentrates mechanical and metabolic load across fibers, accelerating fatigue and reducing the efficiency of force production (ZHANG *et al.*, 2011).

2.2.2.3 Implications for endurance and performance assessment

The combined effects of non-physiological recruitment order and synchronous firing behavior impose a constraint on sustainable performance in surface-stimulated FES cycling. While short-term power output may be increased through more intense stimulation, endurance and session-to-session repeatability remain limited. Importantly, these fatigue mechanisms are intrinsic to surface stimulation and cannot be eliminated through control design alone. Instead, their impact may only be taken into consideration when improving coordination, timing, and distribution of activation across muscle groups.

2.2.3 Core Challenge III: Neuromuscular alterations following spinal cord injury

Beyond the intrinsic limitations of surface electrical stimulation, FES cycling in people with SCI is further constrained by long-term neuromuscular changes that occur below the level of in-

jury. These alterations modify muscle structure, metabolism, and mechanical behavior, fundamentally changing how electrically evoked muscle activation translates into movement (HUNT *et al.*, 2012).

2.2.3.1 Structural and metabolic changes in paralyzed muscle

Shortly after a spinal cord injury, significant changes in muscle morphology and composition can be noted. These include muscle atrophy, reductions in fiber cross-sectional area, and shifts in fiber-type distribution, typically characterized by a decrease in fatigue-resistant fibers and an increased proportion of fast-fatigable fibers. Muscle tissue may also exhibit increased intramuscular fat content and altered connective tissue composition (HUNT *et al.*, 2012).

Such changes affect both active and passive muscle properties. Force-length and force-velocity relationships are modified, maximal force-generating capacity is reduced, and susceptibility to fatigue is increased. Passive stiffness and viscoelastic behavior may also change, influencing joint mechanics and altering the interaction between stimulated and non-stimulated muscles during cycling (POPOVIC; SINKJÆR, 2000). Consequently, identical stimulation inputs can produce substantially different mechanical outputs depending on the training history and muscle condition.

2.2.3.2 Absence of voluntary control and sensory feedback

A defining characteristic of FES cycling in individuals with complete SCI is the absence of voluntary motor control and sensory feedback from the stimulated musculature. Users cannot directly perceive muscle effort, joint loading, discomfort, or early signs of fatigue below the level of injury. In contrast to voluntary movement, where sensory feedback plays a critical role in refining coordination and preventing injury, electrically evoked movement must rely entirely on predefined stimulation strategies (POPOVIC; SINKJÆR, 2000).

From a control perspective, this absence of feedback places strict demands on the robustness and safety of stimulation design. Errors in timing, excessive stimulation intensity, or prolonged activation cannot be corrected reflexively or consciously by the user, increasing the risk of inefficient force production or musculoskeletal strain. This limitation further motivates

conservative and interpretable stimulation strategies, particularly in experimental and clinical contexts (FRAZãO *et al.*, 2024).

2.2.3.3 Limited capacity for physiological adaptation

Although repeated FES training can induce partial improvements in muscle condition, these adaptations occur gradually and do not restore physiological recruitment mechanisms. Neuroplastic changes and peripheral adaptations may improve certain functional and metabolic conditions (SANDRINI *et al.*, 2018), but fundamental aspects of electrically evoked muscle activation, including recruitment order and synchronous firing, remain unchanged.

As a result, many neuromuscular alterations following SCI represent long-term constraints rather than transient limitations. Stimulation strategies must therefore be designed to operate effectively within an altered and only partially adaptable neuromuscular system, rather than assuming convergence toward able-bodied muscle behavior.

2.2.3.4 Implications for optimization and control

The neuromuscular consequences of spinal cord injury define a boundary on what can realistically be achieved through stimulation optimization. While aspects such as timing, coordination, and force alignment may be improved through informed control strategies, fundamental properties such as recruitment order, reflex modulation, and sensory-guided adaptation remain inaccessible. Recognizing these constraints is essential for framing realistic optimization objectives and for interpreting experimental outcomes in FES cycling research.

Table 2.1 summarizes these three core challenges and clarifies which aspects can be optimized and which must be treated as intrinsic constraints when designing stimulation strategies.

2.3 STATE OF THE ART OF FES CYCLING PARAMETER OPTIMIZATION

Over the past three decades, a wide range of strategies have been proposed to improve the performance of surface-stimulated FES cycling, addressing one or more of its challenges (Section 2.2). These approaches vary substantially in their underlying assumptions, required

Table 2.1. Summary of the three core challenges in surface-stimulated FES cycling highlighting which aspects can be optimized and which can be considered when developing stimulation protocols using single electrode stimulation.

Category	Core Challenge I	Core Challenge II	Core Challenge III
Can be optimized?	**Yes.** Primary target for optimization	**No.** Intrinsic to surface stimulation	**No.** Intrinsic to SCI physiology
Can be considered?	**Yes.**	**Yes.**	**Partially.** Via subject-specific constraints

sensing modalities, and levels of physiological realism.

Across the literature, the majority of FES cycling strategies remain constrained by the same fundamental actuation structure: stimulation is applied to a limited number of muscle groups using surface electrodes, in a bang-bang (BB) fashion, with performance improvements sought through better timing, parameter tuning, or feedback regulation. As a result, prior work reflects different ways of selecting when and how strongly to stimulate muscles, rather than fundamentally altering the recruitment mechanisms imposed by surface stimulation.

This section reviews the state of the art in FES cycling parameter optimization, organizing prior work into four broad categories: (1) heuristic and empirically tuned strategies (Section 2.3.1), (2) kinematics and superficial electromyography (sEMG)-informed approaches (Section 2.3.2), (3) classical feedback control methods (Section 2.3.3), and (4) simulation-based optimization studies (Section 2.3.4).

Rather than providing a complete historical account, the review references studies and emphasizes how each class of methods addresses, or fails to address, the core challenges identified earlier, thereby motivating the framework choices adopted in this thesis.

2.3.1 Heuristic and empirically tuned stimulation strategies

The most widely adopted FES cycling strategies rely on empirically defined stimulation patterns, implemented as a bang-bang control. In these approaches, large muscle groups are activated at predefined crank-angle intervals with fixed stimulation intensity. Activation windows are selected to coincide with mechanically advantageous regions of the crank cycle and

are refined through repeated experimental testing.

Comprehensive descriptions of these strategies can be found in early surveys and experimental studies, particularly those summarized by Popović et al. 2000, who formalized phase-based stimulation paradigms and highlighted their practical advantages in clinical and experimental settings. The appeal of heuristic approaches lies in their simplicity, robustness, and minimal requirements, producing cycling motion without complex feedback or modeling (HUNT *et al.*, 2004; MCDANIEL *et al.*, 2017; TONG *et al.*, 2017; BAPTISTA *et al.*, 2022).

However, empirical tuning is inherently time-consuming and user-specific. Achieving acceptable performance often requires extensive trial-and-error procedures conducted over weeks or months of training, with periodic tuning due to subject changes. Moreover, because these strategies rely on abrupt, binary activation of muscle groups, they exacerbate non-physiological recruitment and accelerate fatigue. As noted by Hunt et al., even highly refined bang-bang protocols exhibit low mechanical efficiency, with a significant fraction of electrically evoked muscle force failing to contribute constructively to crank propulsion (HUNT *et al.*, 2012).

From the perspective of the core challenges identified earlier (Section 2.2), heuristic strategies partially address unfavourable biomechanics by roughly aligning stimulation with crank phase. However, they do not resolve crude muscle-group actuation, limited joint-level coordination, or non-physiological recruitment patterns. Consequently, while empirically tuned bang-bang stimulation remains the practical standard in competitive and many experimental settings (LAUBACHER *et al.*, 2017; BO *et al.*, 2017; BAPTISTA *et al.*, 2022), it provides limited insight into how stimulation parameters can be systematically optimized or generalized across users and conditions (AMBROSINI *et al.*, 2014).

2.3.2 sEMG and kinematics-informed stimulation strategies

A second class of approaches sought to improve stimulation timing by leveraging biomechanical measurements or muscle activation patterns observed during able-bodied cycling. These strategies are motivated by an important practical limitation in complete SCI: physiological signals that normally guide coordination, such as voluntary muscle coordination, are absent, and stable cycling kinematics cannot be assumed a priori without an initial trial-and-error

process. As a result, several studies used able-bodied kinematics, and/or sEMG recordings as reference patterns to inform stimulation design.

A few works in this category relied primarily on kinematic and kinetic measurements. Joint angles, crank position, pedal forces, or crank dynamics were used to define stimulation onset and offset through fixed mappings or adaptive phase-detection rules (AMBROSINI *et al.*, 2014; SCHMOLL *et al.*, 2022). Compared with purely manual heuristics, these approaches improved temporal consistency and reduced gross timing errors, partially addressing the strong timing sensitivity inherent to FES cycling (Section 2.2.1). The resulting stimulation patterns demonstrated improvements arising from the better stimulation phase selection.

Other studies incorporated sEMG recordings obtained from able-bodied cycling to guide stimulation timing. In these approaches, electromyographic (EMG) envelopes are processed to identify phases of high activation for target muscle groups, and these phases are translated into stimulation windows (PETROFSKY, 2003; METANI *et al.*, 2017; KAJGANIC *et al.*, 2023). Conceptually, these methods acknowledge that effective cycling depends on coordinated activation across muscles and joints, with improvements reflecting a more physiological muscle recruitment pattern.

Despite this conceptual advance, several limitations restrict the applicability of kinematics and sEMG-informed strategies in surface-stimulated FES cycling for complete SCI. Reference patterns derived from able-bodied individuals reflect neural control, reflex modulation, and muscle properties that do not translate to the muscles of people with SCI. Electrical stimulation preserves altered recruitment order, synchronous firing, and different fatigue dynamics (Section 2.2.2). Moreover, in people with complete SCI, the use of EMG reading is not recommended due to the lack of voluntary muscle contraction (Section 2.2.3), with FES-induced muscle activations being a reflection of the stimulation signal itself. Consequently, these strategies replicate observed activation timings without explicitly accounting for muscle dynamics or coupled muscle-group actuation.

In summary, kinematics and sEMG-informed approaches highlight the importance of coordination and timing in FES cycling and improve upon purely heuristic designs. However, it mostly relies on able-bodied reference data and has limited capacity to address intrinsic stimulation constraints.

2.3.3 Classical control strategies in FES cycling

A substantial body of work has explored the application of classical control theory to FES-assisted cycling, with the primary objective of regulating cadence, improving robustness to disturbances, or stabilizing cycling dynamics. In these studies, controlled variables commonly include crank cadence, crank torque, or pedal-related measures, while control inputs are limited to stimulation timing, pulse width, or current amplitude applied to predefined muscle groups.

In Fonseca et al. 2017, a proportional-integral (PI) controller was used to determine the ideal pulse width (PW) for regulating cycling cadence, and Ahmad et al. 2023 had a similar proposal using a fuzzy logic (FL) controller. Conversely, Farhoud et al. 2014 employed an FL controller to manage pulse amplitude while a higher-order sliding mode controller adjusted the PW, enhancing cadence control in a motorized system. In the context of PW-modulated and motor-assisted systems, Casas et al. 2024 utilized an adaptive approach to control cadence and reduce muscle fatigue. Another approach involved robust switched control, implemented by Bellman et al. 2016 to determine the stimulation timing for each muscle group while tracking a reference cadence through PW modulation.

These methods can compensate for non-linearities and uncertainties in the neuromusculoskeletal system. Nevertheless, classical control strategies face inherent limitations in surface-stimulated FES cycling. Feedback signals such as cadence or crank torque provide only indirect information about muscle state and force-generating capacity. Controllers may therefore compensate for declining performance by increasing stimulation intensity, inadvertently accelerating fatigue rather than resolving underlying biomechanical mismatch (Section 2.2.2). Moreover, because stimulation channels activate muscle groups rather than individual muscles, classical controllers cannot independently regulate synergistic and antagonistic actions, limiting their ability to shape joint-level coordination (Section 2.2.1).

In populations with complete SCI, the absence of voluntary control and sensory feedback further constrains classical control designs (Section 2.2.3). Users cannot provide corrective actions or perceptual feedback that might guide adaptation, requiring conservative safety margins that limit achievable performance gains. As a result, while classical control strategies demonstrate the value of closed-loop regulation and hybrid architectures, they remain fundamentally

limited by coarse actuation, non-physiological recruitment, and simplified system representations.

2.3.4 Simulation-based approaches to FES cycling optimization

Musculoskeletal (MSK) modeling and simulation have emerged as powerful tools. Unlike purely experimental or controller-centric approaches, simulation-based methods allow explicit representation of musculoskeletal geometry, muscle dynamics, joint mechanics, and task constraints. This enables systematic exploration of coordination strategies that would be difficult, risky, or impractical to test experimentally (FREGLY, 2021; UHLRICH *et al.*, 2023; KAINZ *et al.*, 2024). By combining optimal control theory with direct collocation methods, these simulations can estimate muscle forces and activations responsible for complex movements (KELLY, 2017; PARK *et al.*, 2022), and have been successfully implemented in applications such as walking (WARNER *et al.*, 2025).

In addition, controllers such as the aforementioned FL and PI controllers can still be implemented in a simulation environment, as in Sousa et al. 2016, in which the cadence was controlled to follow a target reference. However, most existing cycling studies have relied on experimental kinematic datasets (PARK *et al.*, 2022; CLANCY *et al.*, 2023), and EMG data from able-bodied subjects to inform their models (PARK *et al.*, 2012; WORSEY *et al.*, 2025; CROSSLEY *et al.*, 2025), limiting their application to populations with SCI.

In contrast, fewer studies employed fully predictive simulations, which eliminates the need for prior experimental data, generating physiologically plausible activation patterns based solely on the model's dynamics and cost function definitions (FEBRER-NAFRíA *et al.*, 2022). In Hakansson et al. 2009, predictive simulations optimized the bang-bang stimulation timings for muscle activation and deactivation. This simulation study was then validated in Hakansson et al. 2012 with 11 people with complete SCI, achieving comparable results to established and commercially-implemented bang-bang signals. A different simulation study by Kim et al. 2008, despite not having experimental validation, was the first study to deviate from the BB stimulation, proposing a stimulation pattern with four different muscle activation intensities throughout the cycle, approximating it to a physiological activation curve.

Despite these advances, most simulation-based FES cycling studies stop short of directly translating optimized solutions into experimentally validated stimulation protocols for individuals with complete SCI. Consequently, a gap remains between predictive simulation and real-world FES cycling implementation.

2.3.5 Synthesis and positioning of the present work

Taken together, the literature on FES cycling parameter optimization reveals a coherent methodological landscape. Heuristic and empirically tuned strategies established feasibility and robustness but relied heavily on manual calibration. Kinematics and sEMG-informed approaches improved temporal alignment with physiological inspiration, yet remained dependent on able-bodied reference data. Classical control strategies demonstrated the value of feedback regulation, but were constrained by coarse actuation and indirect performance measures. Simulation-based methods expanded the design space, enabling systematic exploration of timing, coordination, and control strategies, often integrating elements from different paradigms.

However, across these approaches, stimulation remains predominantly bang-bang in structure, and few studies explicitly address non-physiological recruitment and coordination constraints in a principled optimization framework. In particular, the use of fully predictive, muscle-driven simulations that generate physiologically plausible stimulation strategies without reliance on experimental reference data, and their direct experimental validation in individuals with complete SCI, remains unexplored (CO *et al.*, 2025) outside of Peres et al. 2025a and Peres et al. 2025b.

The present thesis addressed this gap by proposing and validating a simulation-to-stimulation workflow in which stimulation strategies are derived from predictive musculoskeletal simulations that explicitly account for surface stimulation constraints and altered neuromuscular physiology. By directly implementing and experimentally evaluating these strategies, this work builds upon and unifies prior heuristic, control-based, and simulation-driven approaches, advancing the state of the art toward a more systematic, transparent, and reproducible framework for FES cycling control.

CHAPTER 3

THEORETICAL BACKGROUND - METHODS

3.1 MUSCULOSKELETAL MODELING FRAMEWORK

Musculoskeletal (MSK) modeling provides a computational framework for representing the human body as a biomechanical system composed of interconnected rigid bodies actuated by muscles and external forces. By combining multibody dynamics with models of muscle-tendon units and neural excitation, MSK models enable the estimation of internal variables, such as muscle forces, joint moments, and joint contact loads, that are difficult or impossible to measure directly in vivo (DELP *et al.*, 2007).

Early MSK models were largely planar and task-specific, focusing on simplified representations of human movement. Over time, advances in computational power, anatomical data, and numerical methods enabled the development of three-dimensional, muscle-driven models capable of simulating whole-body movements with increasing physiological fidelity (FREGLY, 2021).

Within this framework, the human body is typically modeled as a system of rigid segments connected by joints, subject to kinematic constraints and governed by the equations of motion derived from Newton-Euler or Lagrangian mechanics. Muscles are represented as force-generating actuators spanning one or more joints, introducing redundancy, where multiple muscle activation patterns can produce the same net joint motion or force (GROOTE *et al.*, 2016). This redundancy necessitates the use of optimization or control-based approaches to resolve muscle coordination strategies.

A control-oriented perspective on musculoskeletal modeling is articulated in Popović et al. 2000, which frames human movement as the result of hierarchical control processes acting on a nonlinear, redundant biomechanical system. In this view, the musculoskeletal system is described as a controlled multibody plant, where neural commands (excitations) are transfor-

med into muscle activations and forces through activation and contraction dynamics, ultimately producing joint torques and movement.

Despite their growing sophistication, translating MSK modeling into clinical decision-making requires careful consideration of model validity, personalization, uncertainty, and interpretability (FREGLY, 2021). A conceptual blueprint for achieving clinical impact emphasizes the need for transparent modeling assumptions, robust validation against experimental data, and workflows that align with clinical constraints such as time, data availability, and interpretability of results. Rather than aiming for maximal model complexity, clinically useful MSK models must strike a balance between physiological detail and practical applicability, focusing on actionable insights rather than exhaustive descriptions of the system (FREGLY, 2021).

Recent perspectives highlight that clinical usefulness emerges when MSK models are embedded within well-defined workflows that address specific clinical questions, such as predicting treatment outcomes, identifying primary contributors to pathological movement, or evaluating assistive and rehabilitative interventions. Achieving this goal requires interdisciplinary collaboration and a clear separation between model predictions, uncertainty, and clinical interpretation, ensuring that simulation results support clinical reasoning (UHLRICH *et al.*, 2023).

3.1.1 OpenSim

OpenSim is an open-source software platform for modeling, simulating, and analyzing the neuromusculoskeletal system (DELP *et al.*, 2007). It provides a computational framework that allows researchers to construct subject-specific musculoskeletal models and to perform forward and inverse dynamic simulations of human and animal movement. OpenSim integrates rigid-body dynamics, muscle-tendon actuators, and control inputs to estimate internal biomechanical variables such as muscle forces, joint moments, and metabolic cost that cannot be directly measured experimentally.

The platform is widely used in biomechanics, rehabilitation engineering, and motor control research due to its modular architecture, transparency of physical assumptions, and support for reproducible simulation-based studies.

OpenSim supports multiple types of biomechanical analyses, including inverse kinematics,

inverse dynamics, static optimization, computed muscle control, and forward dynamic simulations (DELP *et al.*, 2007). These tools enable the study of movement coordination, muscle redundancy, pathological gait, assistive devices, and neuromuscular interventions such as functional electrical stimulation (FES). Additionally, OpenSim allows the incorporation of external devices (e.g., orthoses, prostheses, exoskeletons) and custom controllers, making it suitable for predictive simulations and control-oriented investigations.

3.1.1.1 Bodies

Bodies in OpenSim represent rigid segments of the musculoskeletal system, such as bones or external mechanical components. Each body is characterized by inertial properties, including mass, center of mass location, and inertia tensor. Bodies serve as the fundamental elements upon which forces and moments act, and their motion is governed by Newton-Euler equations of rigid-body dynamics.

3.1.1.2 Frames

Frames define coordinate systems attached to bodies or existing independently in space. They are used to specify the location and orientation of joints, muscles, markers, and external forces. By explicitly defining frames, OpenSim ensures consistent transformations between local and global reference systems, which is essential for accurate kinematic and dynamic computations.

3.1.1.3 Joints

Joints describe the kinematic relationships between bodies by constraining their relative motion. In OpenSim, joints are modeled as idealized mechanical connections with predefined degrees of freedom, such as revolute, prismatic, or custom joints. Joint definitions determine how generalized coordinates describe system motion and play a critical role in defining the model's kinematic structure.

3.1.1.4 Constraints

Constraints impose additional restrictions on system motion beyond those defined by joints. They are commonly used to enforce kinematic relationships such as closed-loop mechanisms, symmetry conditions, or prescribed motion patterns. Constraints reduce the effective degrees of freedom of the system and are handled internally by OpenSim's constraint stabilization and solver algorithms.

3.1.1.5 Ideal actuators

Ideal actuators represent abstract force or torque generators that apply generalized forces directly to coordinates or bodies. Unlike muscles, ideal actuators do not model physiological properties and can generate forces instantaneously and without fatigue. They are frequently used to represent motors, assistive devices, or simplified control inputs in simulation studies.

3.1.1.6 Muscles

Muscles in OpenSim are modeled as force-generating actuators that convert neural excitation into mechanical force through a muscle-tendon unit. Most OpenSim muscle models are based on Hill-type formulations, which represent the interaction between contractile elements, elastic tendon components, and force-length-velocity relationships (HILL, 1938). Muscle force production depends on muscle activation, fiber length, contraction velocity, and tendon compliance, allowing physiologically meaningful simulations of movement and load sharing among muscles.

Muscle excitation represents the neural control signal applied to a muscle, typically normalized between zero and one. Activation is the muscle's internal state that determines its force-generating capacity. Due to electrochemical and mechanical processes within muscle tissue, activation does not follow excitation instantaneously. Instead, the relationship between excitation and activation is governed by activation dynamics.

This dynamic behavior introduces a physiologically realistic delay and smoothing effect between control inputs and force generation, which is especially relevant in simulations involving

rapid changes in stimulation or neural drive, such as in FES.

3.1.1.7 Reserve actuators

Reserve actuators are auxiliary ideal actuators automatically added to joints to assist the simulation at specific instants where muscles alone are insufficient to reproduce the desired motion. They provide small corrective torques that help maintain numerical stability and ensure convergence of optimization-based simulations. While reserve actuators are useful for identifying model deficiencies or inconsistencies, their magnitudes are typically monitored and minimized to preserve the physiological validity of the simulation results.

3.2 OPTIMAL CONTROL PROBLEM

An optimal control problem consists of finding control inputs and corresponding system trajectories that minimize, or maximize, a predefined objective function while satisfying the system dynamics and a set of constraints. In biomechanical applications, the system dynamics are typically governed by multibody equations of motion coupled with muscle activation and contraction dynamics, while controls represent neural excitations or external actuation signals.

Formally, it seeks optimal time histories of states and controls over a finite time horizon such that the governing differential equations, path constraints, and boundary conditions are satisfied.

Cost function defines the performance criterion of the optimization problem and encodes the assumed objectives of the motor task or control strategy. In musculoskeletal simulations, cost functions commonly include terms related to effort minimization, tracking of kinematic or kinetic reference trajectories, smoothness of control signals, or metabolic energy expenditure.

Cost functions may be composed of multiple weighted terms, allowing the simultaneous consideration of competing objectives, such as accurately tracking an experimentally measured motion while minimizing muscle activations or actuator effort.

In this study, optimal control formulations are used as a computational tool to obtain dynamically consistent muscle excitation patterns that reproduce biomechanical behavior under

specific modeling assumptions. The optimization framework enables the estimation of muscle-level quantities that are not directly measurable, while enforcing physiological and mechanical constraints.

Importantly, the objective function used in this work balances trajectory tracking with effort-related penalties, ensuring that the resulting solutions are both mechanically accurate and physiologically plausible.

It is important to distinguish between solving an optimal control problem offline and implementing optimal control as a real-time control strategy. In this work, the musculoskeletal system is not optimally controlled in real time. Instead, an optimized solution is computed offline by solving a finite-horizon optimal control problem.

The resulting muscle excitation and state trajectories represent one optimal solution under the chosen model structure, constraints, and cost functions. These trajectories are then analyzed as outcomes of the optimization process, rather than being used to control the system during simulation execution. This distinction ensures that the methodology is interpreted as trajectory optimization rather than closed-loop optimal control. In this context, the optimization approach adopted in this study produces open-loop control trajectories. Although the optimized excitations are computed using full knowledge of the system dynamics, they are applied without feedback.

3.2.1 OpenSim Moco

OpenSim Moco (DEMBIA *et al.*, 2020) is an optimal control toolkit integrated into the OpenSim platform that enables the formulation and solution of musculoskeletal optimal control problems. Moco provides a high-level interface for defining states, controls, dynamics, constraints, and cost functions, while internally translating these components into a nonlinear programming problem.

Moco is designed to support both tracking-based and predictive simulations, allowing researchers to compute dynamically consistent solutions that satisfy musculoskeletal dynamics and physiological constraints. In Moco, the continuous-time optimal control problem is transcribed into a finite-dimensional nonlinear optimization problem. System states and controls are dis-

cretized over a predefined time grid, and the governing differential equations are enforced as algebraic constraints at the discretization points. The resulting problem is then solved using numerical optimization techniques.

3.2.1.1 How OpenSim Moco solves a problem

Moco provides an interface between the OpenSim musculoskeletal models and the CasADi (ANDERSSON *et al.*, 2018) framework for symbolic representation and automatic differentiation of the system equations, enabling efficient and accurate computation of gradients required by the optimizer. CasADi converts the optimal control formulation into a nonlinear programming problem (NLP).

The resulting NLP is solved using IPOPT (WäCHTER; BIEGLER, 2005), a large-scale interior-point optimization solver well suited for constrained nonlinear problems. IPOPT is responsible for iteratively finding the optimal solution that minimizes a specified cost function. Moco employs the direct collocation method (PARK *et al.*, 2022) to transcribe the continuous-time optimal control problem into a finite-dimensional NLP. In this approach, the time domain is discretized into a mesh of collocation points, where both the states, e.g., joints positions and speeds, and control variables, e.g., muscles activations, are defined.

The system dynamics are enforced through algebraic constraints that ensure consistency between consecutive nodes, allowing the optimizer to simultaneously determine the trajectory and the control signals that best satisfy the problem's objectives and constraints. This transcription greatly improves numerical stability and enables efficient convergence when solving complex musculoskeletal simulations. Upon convergence of the iterative process, IPOPT returns the optimized states and controls to Moco, which reconstructs the complete simulated motion and exports the results for post-processing in Python and OpenSim.

3.2.1.2 Meshes and tolerances

The temporal discretization of the optimal control problem is defined by a mesh, which specifies the number and distribution of collocation points over the simulation time interval. Mesh density directly affects solution accuracy and computational cost, with finer meshes pro-

viding more accurate approximations of the continuous dynamics at the expense of increased computation time.

Solver tolerances determine the acceptable levels of constraint violation and optimality error in the numerical solution. Appropriate selection of mesh resolution and solver tolerances is essential to ensure convergence to physically meaningful solutions while maintaining computational efficiency.

3.2.2 EMA setup

The cycling system employed in this work is based on customized and commercial electronic equipment and a tricycle in a tadpole configuration (HP3 Trikes, Brazil). It has the same architecture used since our team´s first Cybathlon participation in 2016 with mechanical upgrades (BO *et al.*, 2017; BAPTISTA *et al.*, 2022).

The experimental setup consisted of the trike adjusted for stationary cycling with a smart trainer (Wahoo Kickr V6), and dual-sided instrumented pedals (Wahoo Powrlink Zero), as the standard setup for the Cybathlon 2024 FES Bike Race. A 360-degree optical encoder (E38S6G5-600B-G24N, SHARVi Electronics) tracked crank angle variations at a sample rate of 100 Hz. In the Cybathlon 2024 event a custom game software integrated with *IndieVelo* was used. The same software was used during data collection in the proof-of-concept study of this thesis (PERES *et al.*, 2025a) (Chapter 4), but was discontinued afterwards. For the case study (PERES *et al.*, 2025b), we replaced it with the open-source software *GoldenCheetah* to connect the smart trainer and the instrumented pedals to measure cadence, power, and left-right balance during cycling (Chapter 7). A human-machine interface (with two push-buttons and a 16x2-character LCD screen display) and batteries complete the system.

3.2.3 Mapping simulated muscle activation to electrical stimulation

In both studies, muscle activation trajectories obtained from optimal control simulations were used to define the temporal structure of the electrical stimulation applied during cycling. After post-processing and normalization, the muscle activation signal was treated as a dimensi-

onless control profile, representing the relative activation demand as a function of crank angle, independent of absolute stimulation intensity. These profiles were then discretized and ordered into a look-up table as functions of crank angle using 360 points per cycle, matching the angular resolution of the crank encoder used in the experimental setup. A higher resolution would only increase computational load and processing latency without providing additional control fidelity.

The normalized activation profile was mapped linearly to a stimulation parameter according to

$$I(\theta) = a_{norm}(\theta)\, I_{std} \tag{3.1}$$

where $a_{norm}(\theta) \in [0,1]$ is the normalized muscle activation and I_{std} is the standardized current amplitude (in mA) set by the experimental protocol. The mapping preserved the temporal structure of the simulation-derived activation profile while allowing the overall stimulation intensity to be controlled in a standardized manner during data collection.

Two modulation strategies were employed across the studies, both at stimulation frequency of 50 Hz. In current amplitude modulation, the stimulation pulse width was held constant at 450 μs, while the value of I_{std} was varied according to the data collection protocol, effectively scaling the overall amplitude of the stimulation-current profile. In pulse-width modulation, I_{std} was held constant at 100 mA, such that $I(\theta) = a_{norm}(\theta) \cdot 100\ mA$, while the effective stimulation intensity was regulated by varying the stimulation pulse width according to the data collection protocol. Although both approaches preserve the same activation-derived temporal profile, pulse-width modulation provides finer control resolution due to the wider available parameter range.

The activation-to-stimulation mapping was implemented using the Robot Operating System 2 (ROS 2) (MACENSKI *et al.*, 2022) as a modular framework running in a Raspberry Pi 4 with Ubuntu 22.04. In this setup, the crank-angle encoder continuously provided joint angle measurements to a control node that queried a predefined angle-stimulation lookup table. When the measured angle did not correspond to an explicit entry in the table, linear interpolation was used to compute the appropriate stimulation value, which was then sent to the stimulation device (Hasomed RehaStim 4) (Figure 4.1 d)).

In all cases, stimulation parameters were constrained by software-imposed limits to ensure

safe operation. The pilot interface displayed real-time stimulation metrics, and attempts to exceed the predefined maximum current or pulse width resulted in saturation at the corresponding limit, without further changes to the stimulation output. This design ensured that the activation-derived stimulation signal remained within safe and reproducible bounds during experimental trials.

CHAPTER 4

METHODS - PROOF OF CONCEPT STUDY

This study followed a multi-step methodology to develop, implement, and validate predictive simulation-derived stimulation profiles for functional electrical stimulation (FES) cycling in a participant with complete spinal cord injury (SCI). The process involved (1) creating cycling models in an musculoskeletal (MSK) simulation environment, (2) solving an optimal control problem to derive stimulation profiles, (3) extracting and processing the stimulation profile, and (4) implementing and testing these signals in an experimental setup (Figure 4.1).

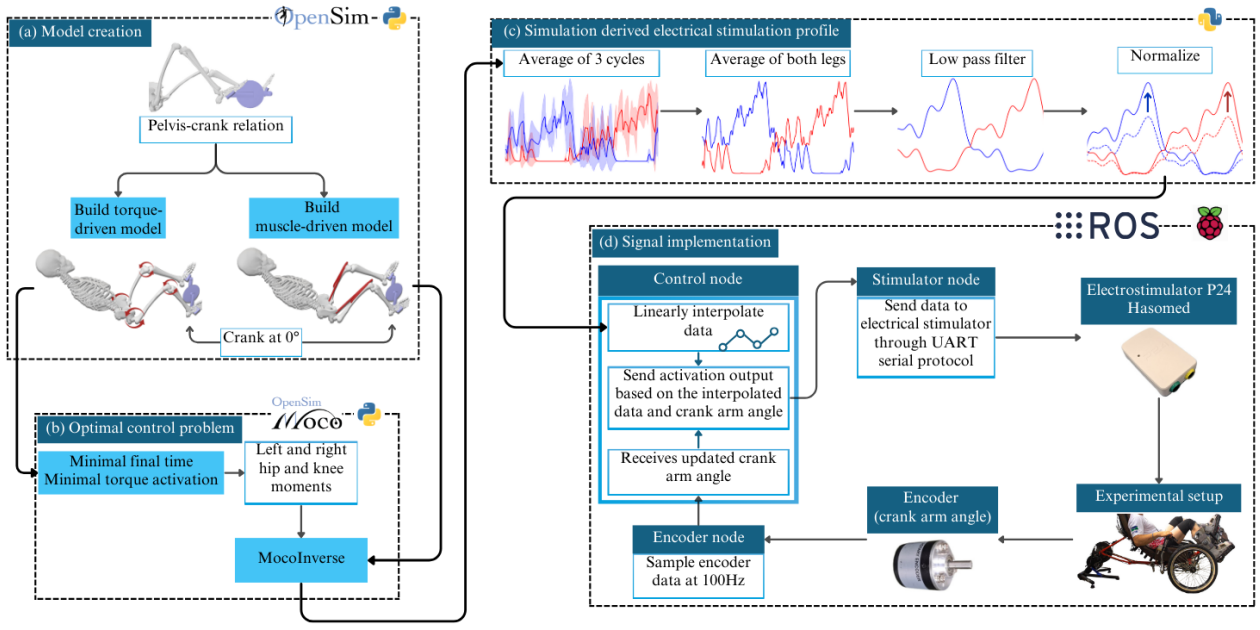

Figure 4.1. Framework for generating muscle activation from predictive simulations. (a) Model creation: torque-driven and muscle-driven models were developed using the geometry and pelvis-crank relationship from the physical setup. (b) Optimal control problem: simulations that minimize movement time and joint and muscle excitation effort using predictive algorithms. (c) Simulation-derived electrical stimulation profile: the necessary steps to obtain the stimulation profile from the simulated data. (d) Signal implementation: the control node receives the stimulation profile and data from the encoder, where angle values are processed and interpolated to generate the stimulation signal, which is then sent to the stimulation topic for delivery via the electrical stimulator.

4.1 MUSCULOSKELETAL CYCLING MODEL

The musculoskeletal model used in this study was based on the Gait10dof18musc (DELP *et al.*, 1990) model available in OpenSim (Section 3.1), which has been widely used for gait and lower-limb simulations. The original model comprises 10 degrees of freedom and 18 muscle-tendon units acting on the lower extremities. Although originally developed for walking, this model provides a suitable starting point for cycling applications (YAMAGUCHI; ZAJAC, 1989; ANDERSON; PANDY, 1999; ANDERSON; PANDY, 2001).

The cycling model's design was based on previous studies (SOUSA *et al.*, 2021; SOUSA; FONT-LLAGUNES, 2024). First, the model was constrained to a sagittal-plane motion, restricting the degrees of freedom. This not only reduces the model computational complexity, but also reflects the experimental configuration, in which the participant uses rigid orthopedic boots that limits out-of-plane motion for stability and safety.

The model was positioned in a cycling posture according to the geometry of the Project EMA FES trike, including the pelvis-crank relationship and crank axis location (Figure 4.1 a)). The upper-body, ankle and feet joints were replaced by weld joints, to further reduce computational cost by eliminating unnecessary degrees of freedom. A resistive crank and pedal mechanism was added to the model, applying a constant 8 Nm torque opposing crank rotation, in order to approximate the mechanical resistance imposed by the cycling system during the experiments. The feet were connected to the pedals through a kinematic constraint that limited the maximum distance between the calcaneus and the pedals to 1.2 cm. This formulation avoided the creation of a closed kinematic chain, which is not supported by OpenSim, while still allowing minimal relative motion between the foot and pedal. The small permitted movement is consistent with the experimental setup, where a slight relative motion is observed due to compliance in the orthopedic boots.

Two distinct versions of the model were created for this study: (1) a torque-driven model and (2) a muscle-driven model. In the torque-driven model, all muscle actuators from the original OpenSim model were removed. Instead, ideal torque actuators (Section 3.1.1) were inserted at the hip and knee joints (Figure 4.1 a)). These actuators were capable of generating joint torques up to $40Nm$, consistent with experimental values reported in the literature for

cycling applications (CLANCY *et al.*, 2023).

In the muscle-driven model, the joint torques were generated by muscles (Section 3.1.1) rather than ideal actuators. The muscle representation was updated from the Millard implementation (MILLARD *et al.*, 2013) of the Hill-type model (HILL, 1938), to the De Groote-Fregly muscle model (GROOTE *et al.*, 2016), which provides improved numerical stability and smoother activation-contraction dynamics compared to traditional Hill-type formulations. Despite the model having 18 lower-limb muscles, to replicate a quadriceps-only FES cycling configuration, all muscles except the quadriceps group, represented by the rectus femoris and a simplification of the three vastus named vasti, were effectively deactivated. This was achieved by limiting the maximum isometric force of the non-quadriceps muscles to $0.5N$, restricting active contribution to the motion.

Similar to (CLANCY *et al.*, 2023), the muscle-driven model had its maximum isometric force doubled and reserve actuators were added at the hip and knee joints of the muscle-driven model to improve numerical convergence (Section 3.1.1). Their activation occurred primarily in the so-called dead zones of the crank cycle, such as the horizontal crank positions, where the configuration limits effective power generation. This approach ensured convergence of the optimal control problem without artificially dominating the muscle-generated motion.

4.2 CYCLING OPTIMAL CONTROL PROBLEM

The problem structure was based on a previous study (SOUSA; FONT-LLAGUNES, 2024), which explored two optimal control formulations using a torque-driven model: (1) minimization of effort and motion duration, adopted in (PERES *et al.*, 2025a), and (2) minimization of trajectory error relative to a constant target speed, adopted in (PERES *et al.*, 2025b) and detailed in Chapter 7. The current cycling problem was based on the first approach.

The strategy focused on optimizing the kinematics of four consecutive cycles performed by the torque-driven model. The model was required to complete the motion within 7 seconds while minimizing the motion's time and effort needed by the ideal actuators. The initial position of the model is defined as 0°, with the left crank at the top dead center (Figure 4.1 a)). Additionally, the model is allowed to assume initial speeds for the crank, hips, and knee joints, provided

these speeds remain within the crank speed set range of 0 to 40rpm. This boundary ensured a moderate and safe FES cycling speed while preventing backwards cycling.

For the torque-driven simulation the first goal was to minimize the time to complete the prescribed motion (t_{sim}), bringing and stabilizing the crank speed closer to the maximum value of 40 rpm. Additionally, the time minimization ensured a reasonable and predictable time for the motion, which directly impacts the computational time to complete the simulation (Figure 4.1 b)).

The second goal of the torque-driven simulation was to minimize the motion's effort (J_{actu}) (Figure 4.1 b)). Minimizing the effort is an important element in a rehabilitation context, since among all the possible muscle activations that can satisfy the motion's requirements, we wanted a safe and less demanding solution. The effort minimizing cost function is expressed by

$$J_{actu} = \int_0^{t_{sim}} \sum_{i \in actu} |x_i(t)|^2 \, dt, \tag{4.1}$$

where the total effort is the sum of the squared effort ($x_i(t)$) made by each of the ideal actuators (i) throughout the prescribed motion. Combining the cost functions for minimizing time and effort, the final element to be minimized (J_{total}) is indicated by

$$J_{total} = w_{time}\, t_{sim} + w_{actu}\, J_{actu}, \tag{4.2}$$

in which the weights w_{time} and w_{actu} had to be balanced due to the conflicting nature of the two cost functions. The only way to reduce the motion's execution time is by cycling faster, requiring more intense muscle activation and subsequently increasing the effort. The same logic can be applied to minimizing the effort, it results in a longer time to complete the motion. Through iterative tuning, the final values for the weights w_{time} and w_{actu} were 6 and 2, respectively, achieving a good balance of execution time and effort needed.

Due to boundary effects associated with the finite-horizon formulation of the torque-driven predictive optimal control problem, the first crank revolution did not exhibit steady cyclic behavior. This initial cycle reflects the transition to a stable cadence and was therefore excluded from subsequent analysis. The remaining three revolutions, which showed consistent kinematic and dynamic patterns, were selected as representative of steady-state motion.

After the torque-driven predictive simulation, the resulting steady-state kinematics were used as input to a muscle-driven inverse optimal control problem to address the muscle re-

dundancy problem. This problem arises from the multiple possible muscle excitation patterns capable of producing the same joint kinematics, given that the musculoskeletal system contains more actuators (muscles) than mechanical degrees of freedom (POPOVIC; SINKJÆR, 2000; GROOTE *et al.*, 2016). This step was implemented using the *MocoInverse* function in OpenSim, which prescribes the reference joint kinematics as constraints and computes muscle excitations that satisfy the system dynamics (DEMBIA *et al.*, 2020).

In this formulation, the kinematic states are enforced exactly and are not influenced by an optimization objective. The inverse problem therefore focuses solely on determining a feasible combination of muscle excitations capable of reproducing the prescribed motion using the available actuators. Similar to Eq. 4.1, muscle redundancy is resolved through quadratic regularization of the muscle excitation signals over a specified interval of the prescribed motion:

$$J_{musc} = \int_{t_i}^{t_{sim}} \sum_{m \in musc} w_m \, x_m(t)^2 dt, \tag{4.3}$$

where $x_m(t)$ represents the excitation of actuator m, and $musc$ denotes the total number of muscle actuators in the model, and all actuator weights (w_m) were set to 1. The *MocoInverse* function was beneficial not only for identifying the desired sequence of muscle excitation signals but also for its ease of implementation and computational efficiency, allowing for quick verification of results throughout the development process. The optimal control problem solving process is described in the theoretical background (Section 3.2).

4.3 DERIVING THE OPTIMAL CONTROL SIGNAL

Following the solution of the muscle-driven inverse optimal control problem, only the three steady-state crank revolutions selected from the predictive and inverse analyses were considered in this step. These revolutions exhibited consistent cyclic behavior and served as the basis for extracting representative muscle activation profiles.

Although the inverse solution included activation trajectories for both the rectus femoris (RF) and vasti (VI) muscles, only the RF activation was retained for subsequent signal processing. The VI activations were consistently of lower magnitude and temporally overlapped with RF activation. In the context of surface FES, stimulation applied over the RF is expected to concurrently recruit the VI muscles due to current spread within the quadriceps muscle group.

Therefore, the RF activation was used as a representative quadriceps control signal. The resulting RF muscle activation trajectories were then processed to generate stimulation signals suitable for experimental implementation (Figure 4.1 c)).

To reduce inter-cycle variability and emphasize steady-state characteristics, the muscle activation signals corresponding to the three revolutions were first time-normalized to the crank cycle and averaged separately for each leg (Figure 4.1 c)). This procedure resulted in one representative activation profile for the RF muscle for the left leg and one for the right leg, each characterizing steady cycling at the target cadence.

Cycling is a fundamentally bilaterally symmetric task, and promoting symmetric muscle recruitment is an important aspect of balanced and effective rehabilitation. Motivated by this principle, the leg-specific activation profiles were subsequently averaged across the left and right limbs, yielding a single symmetric activation pattern for the RF muscle (Figure 4.1 c)). This step enforced inter-limb symmetry at the signal level and provided a consistent basis for the experimental FES cycling protocol.

The resulting muscle activation signals were then low-pass filtered with a 5^{th} order Butterworth filter to remove high-frequency numerical artifacts arising from the optimal control solution and signal interpolation (Figure 4.1 c)). Although the activation dynamics included in the musculoskeletal model impose temporal smoothing, simulation-derived activations can still exhibit rapid transitions that are not representative of physiological muscle recruitment, particularly when compared to muscles activated through surface functional electrical stimulation.

In FES-driven contractions, muscle activation dynamics are influenced by factors such as motor unit recruitment order, stimulation pulse properties, and muscle-electrode coupling, which collectively result in slower and smoother activation profiles than those typically observed in simulation-based activations. Filtering therefore served to produce activation patterns that were more compatible with physiological behavior and safer for experimental implementation, while preserving the essential temporal structure of the cycling task.

Finally, the processed muscle activation signals were normalized to the range [0,1] (Figure 4.1 c)). In the inverse optimal control solution, the raw activation amplitudes typically ranged between 0 and approximately 0.6, indicating that relatively low RF activation levels were sufficient to reproduce the prescribed joint kinematics. This behavior was influenced by

the presence of reserve actuators and by modifications to the muscle model parameters, including increased maximum isometric force, which reduced the activation demand required to generate joint moments.

Moreover, the musculoskeletal model assumes physiological excitation–activation coupling, whereas the experimental setup relied on surface functional electrical stimulation, which is inherently less efficient in eliciting muscle activation due to factors such as current dispersion, electrode placement, and selective motor unit recruitment. Normalization therefore served to decouple the temporal structure of the activation patterns from their absolute magnitude, enabling consistent mapping to the stimulation amplitude while compensating for differences between simulated muscle activation and experimentally achievable FES-induced activation.

The resulting normalized RF activation profiles were implemented experimentally using a current-modulated functional electrical stimulation strategy, as described in Section 3.2.3.

4.3.1 Computational details

All simulations and post-processing steps were performed on a computer equipped with a Ryzen 9 5950X CPU, with 64 GB of RAM, and Windows 11 operating system. For both the torque-driven predictive simulation and the muscle-driven inverse problem, the number of meshes were configured to 600, and convergence and constraint tolerances were set to 10^{-2} and 10^{-4}, respectively (Section 3.2). On the specified hardware, the average convergence time was approximately 6 minutes for both the torque-driven and the muscle-driven inverse simulations. The models, codes and data are publicly available [1].

4.4 PARTICIPANT CHARACTERISTICS

The volunteer of this study was a 46-year-old male, 170 cm tall and weighing 78 kg, with a complete spinal cord injury (SCI) classified as T9 AIS A, indicating no voluntary motor function below the level of injury, agreed to participate in the study via written consent. The experiments were performed under the ethics committee from the University of Brasília code

[1] Currently being developed and maintained at: FES cycling project.

CAAE: 75441323.4.0000.8093.

4.5 DATA COLLECTION PROTOCOL

Data were collected over three non-consecutive days, allowing adequate recovery between sessions and minimizing the effects of interday muscle fatigue. Each data collection session followed the same preparation and warm-up procedure to ensure consistent experimental conditions.

Each session began with 20 minutes of supervised stretching, followed by 20 minutes of electrical stimulation warm-up, during which low-intensity stimulation was applied to prepare the muscles for cycling. Stimulation electrodes (8 cm × 13 cm) were positioned bilaterally over the quadriceps muscle group under the supervision of a licensed physiotherapist, following established guidelines for surface electrode placement (SCOTT *et al.*, 2019).

On the first day of data collection, an initial proof-of-concept protocol was conducted using the unnormalized simulation-derived activation profile. This preliminary session was intended solely to verify the feasibility of directly applying the simulation output and was not included in the comparative analysis presented in this study.

On the second and third data collection days, experimental data were collected using two stimulation strategies: the simulation-derived control signal (CS) and a bang-bang (BB) baseline control signal. For each day, four data collection sets were performed, alternating between CS and BB to reduce ordering effects, as indicated in table 4.1. A rest period of 5 minutes was provided between sets to mitigate muscle fatigue.

For both CS and BB conditions, stimulation was delivered using current amplitude modulation, with the pulse width fixed at 450 μs. Stimulation current was initialized at 30 mA and increased in increments of 2 mA every 10 seconds, following a cautious and progressive protocol. Once the current reached 100 mA, corresponding to the maximum stimulation level defined by the study protocol, stimulation intensity was held constant and one minute of cycling data was recorded without external assistance.

During data collection, the cycling environment was simulated using IndieVelo, a virtual cycling platform configured to reflect the participant's body mass and a flat terrain profile

(Section 3.2.2). This setup provided a consistent and controlled cycling environment and facilitated standardized data collection across sessions.

Table 4.1. Summary of data collection protocol, including the type of control signal applied on each day and the sequence of trials conducted over three non-consecutive days

day 1	1 set of data	uCS
day 2	4 sets of data	CS_1, BB_1, CS_2, BB_2
day 3	4 sets of data	BB_3, CS_3, BB_4, CS_4

4.5.1 Simulation-derived control signal

The simulation-derived control signal (CS) refers to the optimal stimulation profile obtained from the post-processed muscle activation trajectories derived from the optimal control simulations described in this chapter. This signal defines a continuous, crank-angle-dependent stimulation pattern designed to reproduce near-physiological muscle activation timing throughout the cycling cycle.

4.5.2 Bang-bang control signal

The bang-bang control signal (BB) was used as a baseline stimulation strategy for comparison with the proposed simulation-derived control signal (CS). In this study, BB consisted of a discrete on-off stimulation pattern applied bilaterally to the quadriceps muscle group over predefined crank-angle intervals corresponding to the power-producing phase of cycling.

Crank angles were defined assuming the left crank at top dead center as the absolute 0° reference, with angles increasing in the direction of forward pedaling. Using this convention, stimulation windows were defined separately for each leg to account for the 180° phase shift between left and right cranks. Stimulation was activated for the left leg when the crank angle entered the interval from 300° to 55°, and for the right leg when the crank angle entered the interval from 120° to 235° (Figure 5.1). Outside these intervals, stimulation was inactive.

During the active phase, stimulation was delivered at a constant current amplitude corresponding to the stimulation level defined by the data collection protocol, while no stimulation was applied during the remainder of the cycle. This bang-bang strategy represents a conventio-

nal FES cycling approach based on fixed angular stimulation windows and serves as a reference for evaluating the benefits of the continuous, simulation-derived control signal proposed in this study.

4.5.3 Cycling metrics collected

For subsequent data analysis, the following cycling metrics were collected: mechanical power output (P), crank angular velocity (V), and interlimb balance (B), defined as the symmetry percentage between left and right leg contributions during cycling.

In a rehabilitation context, mechanical power output is directly related to the user's strength and mass-related force generation capacity, making it one of the most commonly used metrics for evaluating cycling performance and motor recovery when applicable (FRAZãO *et al.*, 2024). Crank angular velocity reflects the intensity of cardiovascular exercise and provides insight into overall work efficiency during cycling (HUNT *et al.*, 2012). Finally, interlimb balance is an important indicator of lower-limb symmetry and coordinated muscle recruitment, which are key goals in rehabilitation following neurological injury (AMBROSINI *et al.*, 2012).

These variables were recorded using instrumented cycling components described in the theoretical background chapter (Section 3.2.2).

CHAPTER 5

RESULTS - PROOF OF CONCEPT STUDY

5.1 SIMULATION-DERIVED CONTROL SIGNAL

Figure 5.1 presents the simulation-derived rectus femoris (RF) activation profile obtained from the muscle-driven inverse optimal control problem, alongside the bang-bang (BB) stimulation pattern used for comparison. Activation profiles are shown over the crank cycle using a polar representation, with crank angle defined such that 0° corresponds to the left crank at top dead center and angles increase in the direction of forward pedaling.

The simulation-derived control signal (CS) exhibits a continuous activation profile distributed over a broad angular range, with smooth onset and offset transitions across the crank cycle. In contrast, the BB strategy applies stimulation within fixed angular windows, resulting in abrupt activation transitions and extended periods of zero activation outside the predefined stimulation intervals.

Left and right RF activation profiles follow complementary angular patterns, reflecting the alternating contribution of each limb during the cycling motion. Because bilateral symmetry was enforced during post-processing, the resulting CS provides a consistent and repeatable temporal structure for stimulation across crank revolutions.

5.2 CYCLING PERFORMANCE METRICS

Figure 5.2 presents the time evolution of cycling performance metrics during one minute of steady-state cycling, comparing the simulation-derived control signal (CS) and the bang-bang control strategy (BB). Metrics shown include power output, crank angular velocity, and left-right balance, reported as mean trajectories with corresponding standard deviation envelopes across trials.

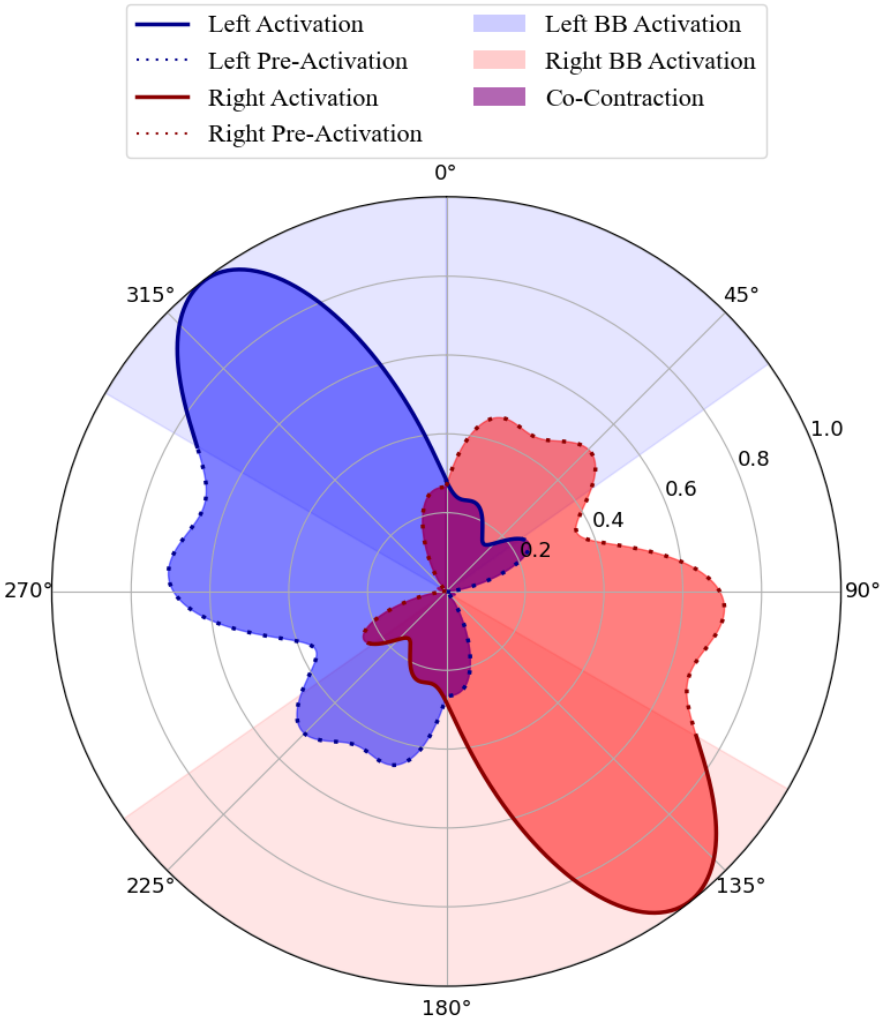

Figure 5.1. Simulation-derived rectus femoris (RF) activation profiles over the crank cycle for the left and right legs. Activations are shown using a polar representation, where the angular coordinate corresponds to crank position and 0° denotes the left crank at top dead center, with angles increasing in the direction of forward pedaling. The solid colored profiles represent the normalized RF activation obtained from the simulation-derived control signal (CS), while the shaded regions indicate the bang-bang (BB) stimulation pattern used for comparison. The radial coordinate represents normalized activation magnitude.

Across all metrics, CS consistently resulted in higher average performance compared to BB. As summarized in Table 5.1, CS trials exhibited greater mean power output (14.9 ± 1.7 W) than BB trials (12.8 ± 0.9 W), alongside higher average cadence (44.4 ± 4.4 rpm for CS versus 40.8 ± 2.1 rpm for BB). These differences were observed consistently across individual trials on both days of data collection.

Temporal trends in Figure 5.2 further indicate that cadence variability increased toward the end of the data collection period in CS trials, as reflected by the widening standard deviation envelope in the cadence subplot. This effect was less pronounced for BB, which showed comparatively lower variability in cadence over time. Despite this increased variability, CS maintained

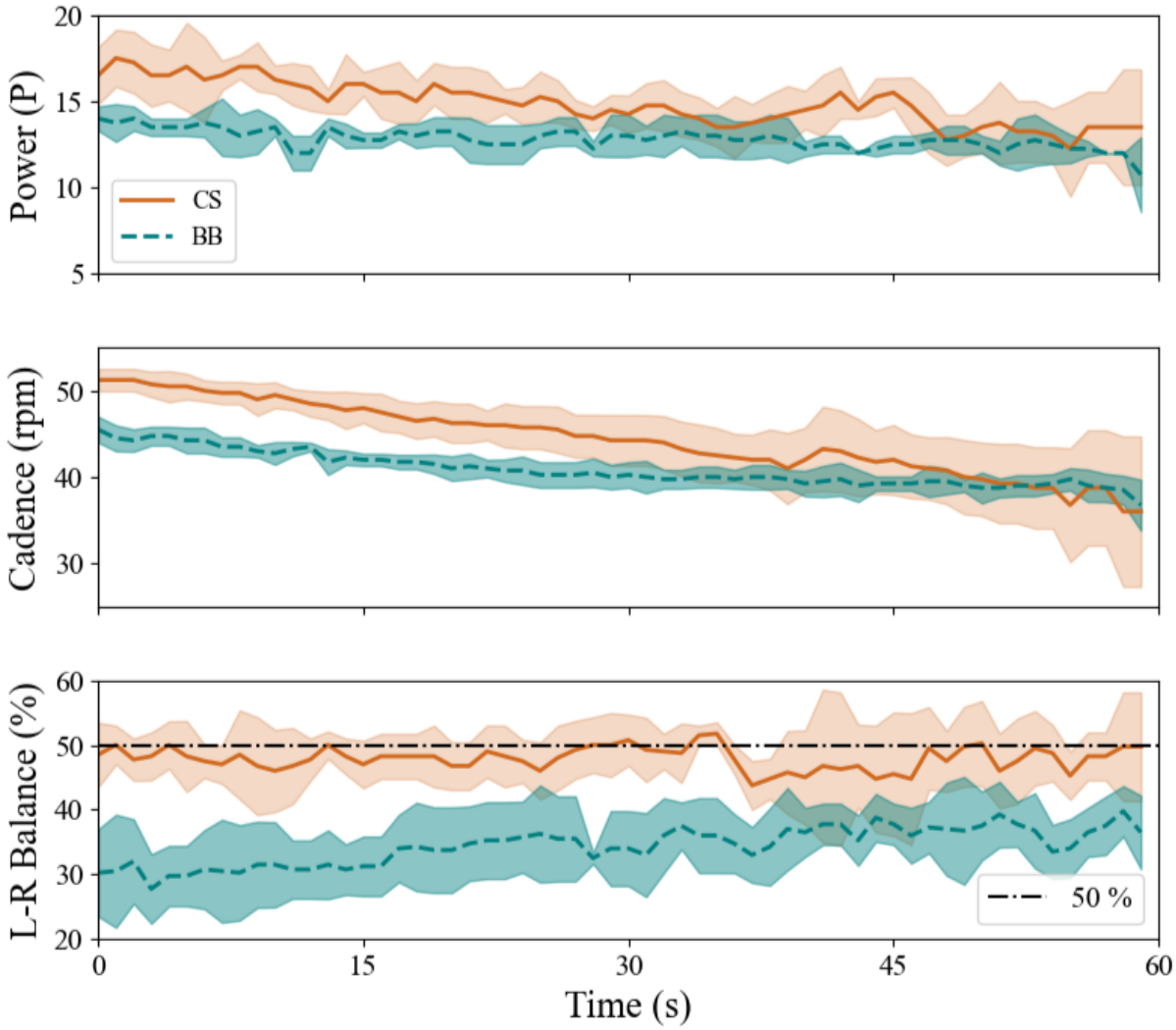

Figure 5.2. Comparison of cycling performance during one minute of unassisted cycling using the simulation-derived control signal (CS, solid lines) and the bang-bang control strategy (BB, dashed lines). Shown variables include power output (top), crank angular velocity (middle), and left-right balance (bottom). Curves represent mean trajectories across all trials, with shaded regions indicating one standard deviation. Quantitative results are summarized in Table 5.1.

higher average cadence values throughout the collection window.

The most pronounced difference between control strategies was observed in the left-right balance metric. CS trials consistently produced balance values closer to the ideal symmetric condition of 50%, with a pooled average of 47.9 $\pm$ 3.7%, whereas BB trials resulted in lower balance values of 34.4 $\pm$ 4.1%. This separation is evident both in the time-series representation and in the aggregated statistics, indicating a substantial improvement in inter-limb symmetry when using the simulation-derived control signal.

Overall, the experimental results demonstrate that CS yields higher power output, higher cadence, and markedly improved left-right balance compared to BB, with balance showing the

Table 5.1. Summary of cycling performance metrics collected during experimental trials. Reported variables include average power output (W), crank angular velocity (rpm), and left-right balance (%), expressed as: mean ± standard deviation of each trial. Results are organized by trial and day of data collection for the simulation-derived control signal (CS) and the bang-bang control strategy (BB). The total data summary reports: pooled mean ± standard deviation across all CS and BB trials, respectively.

	$\overline{Power}$	$\overline{Velocity}$	$\overline{Balance}$
Day 1 of data collection			
uCS	—	—	—
Day 2 of data collection			
$\mathbf{CS}_1$	13.7 ± 1.7	44.1 ± 3.9	44.1 ± 5.0
$\mathbf{BB}_1$	12.7 ± 0.6	42.3 ± 1.8	34.6 ± 4.4
$\mathbf{CS}_2$	15.2 ± 1.2	49.0 ± 2.4	44.0 ± 3.4
$\mathbf{BB}_2$	11.9 ± 0.8	41.3 ± 2.2	27.1 ± 4.2
Day 3 of data collection			
$\mathbf{BB}_3$	13.2 ± 1.0	39.4 ± 2.8	35.6 ± 4.2
$\mathbf{CS}_3$	14.2 ± 2.5	40.9 ± 7.0	54.7 ± 3.2
$\mathbf{BB}_4$	13.4 ± 1.2	40.5 ± 1.6	40.1 ± 3.4
$\mathbf{CS}_4$	16.3 ± 1.4	43.7 ± 4.2	48.8 ± 3.2
Total data summary			
CS	14.9 ± 1.7	44.4 ± 4.4	47.9 ± 3.7
BB	12.8 ± 0.9	40.8 ± 2.1	34.4 ± 4.1

largest relative improvement among the evaluated metrics.

CHAPTER 6

DISCUSSION - PROOF OF CONCEPT STUDY

6.1 MAIN CONTRIBUTIONS AND OUTCOMES

This study demonstrated the successful development, implementation, and experimental validation of a fully predictive simulation framework for functional electrical stimulation (FES) cycling as illustrated by the simulation-to-experiment pipeline(Figure 4.1). By integrating musculoskeletal modeling, optimal control theory, and direct collocation methods, it was possible to predict muscle activation patterns required to generate a stable cycling motion and to translate these patterns into stimulation signals suitable for experimental application.

A key outcome of this work is the successful implementation of simulation-derived stimulation patterns in an individual with complete spinal cord injury, bridging the gap between predictive simulation and real-world FES cycling. The proposed framework not only produced feasible stimulation profiles but also enabled their direct deployment in an experimental setting, where they were shown to consistently outperform a simple form of bang-bang control strategy in terms of power output, cadence, and inter-limb balance.

These results highlight the potential of predictive simulations as a powerful tool for the design and evaluation of FES cycling strategies. By demonstrating that simulation-derived control signals can be effectively implemented and can lead to improved cycling performance compared to conventional stimulation approaches, this study establishes a solid foundation for further developments aimed at enhancing the physiological relevance, efficiency, and clinical applicability of FES-based rehabilitation interventions.

To the best of our knowledge, this is the first study to validate the use of a fully predictive musculoskeletal simulation pipeline to derive and implement electrical stimulation patterns for FES cycling in a human participant. Unlike inverse approaches that rely on experimentally measured kinematics or predefined stimulation timing, the proposed framework predicts both

the motion and the underlying muscle activation patterns, providing a principled and model-based basis for stimulation design.

6.2 INTERPRETATION OF SIMULATION-DERIVED STIMULATION PATTERNS

The simulation-derived control signal exhibited smooth activation transitions, overlapping muscle activation across crank phases, and activation occurring outside the mechanically optimal power-producing regions typically associated with bang-bang stimulation. These characteristics contrast with the discrete, phase-limited activation pattern of the bang-bang strategy and reflect fundamental differences in how the two approaches define stimulation timing (Figure 5.1).

It is important to note that neither pre-activation nor co-contraction was explicitly encouraged or penalized by the cost functions used in this study. In the torque-driven predictive simulation, the optimization balanced execution time and mechanical effort to determine cycling kinematics (Equations 4.1 and 4.2). Whereas in the muscle-driven inverse simulation, muscle redundancy was resolved by minimizing muscle excitation for a prescribed, already optimized motion (Equation 3.3). As a result, the emergence of overlapping activation patterns cannot be attributed to a direct optimization objective targeting stability or coordination.

Instead, these activation features are understood as emergent properties arising from the interaction between imposed task constraints and the musculoskeletal structure of the model. In particular, the rectus femoris is a bi-articulated muscle, contributing simultaneously to knee extension and hip flexion, which enables it to influence crank motion across a broad range of joint configurations (RYAN; GREGOR, 1992). This dual mechanical role provides a plausible explanation for activation extending beyond a narrow power-producing phase and for partial overlap between left and right limb activations across the crank cycle.

Pre-activation, although it may initially appear counterproductive in cyclic propulsion tasks, is well documented in high-performance cycling and has been associated with reduced force loss during mechanically less efficient phases of the crank cycle (HERING *et al.*, 2023). By reducing effective muscle reaction time, pre-activation may contribute to smoother force transitions and improved inter-limb coordination (KIMURA *et al.*, 2002), which is consistent with the incre-

ased balance observed during experimental trials using the simulation-derived control signal (Figure 5.2).

Similarly, co-contraction is a recognized mechanism for movement stabilization and joint protection under dynamic conditions (SO *et al.*, 2005; BAUTMANS *et al.*, 2011; HUG *et al.*, 2011; TURPIN; WATIER, 2020). While in a simulation environment, co-contraction can be a result of excessive passive forces from the hip and knee extensors (LAI *et al.*, 2017). Within the present framework, overlapping activation may also reflect the combined effects of quadriceps-only stimulation and the imposed maximum crank speed constraint. In the absence of antagonist muscle stimulation, activation outside mechanically advantageous regions may serve to regulate crank velocity and prevent excessive acceleration, rather than exclusively generate forward propulsion.

Alternative framework choices, such as the inclusion of antagonist muscle groups in the model or relaxation of hard kinematic constraints in the problem formulation, may lead to different activation distributions.

6.3 EXPERIMENTAL PERFORMANCE COMPARISON BETWEEN CONTROL STRATEGIES

The experimental results demonstrated consistent performance improvements when using the simulation-derived control signal (CS) compared to the bang-bang (BB) stimulation strategy across all evaluated metrics. As summarized in Table 5.1 and illustrated in Figure 5.2, CS trials generally resulted in higher average power output, higher crank cadence, and improved left-right balance.

Power output was consistently higher during CS trials, both on individual days and in the aggregated results. This suggests that the smoother and more continuous stimulation timing derived from the predictive simulations enabled more effective force transmission to the crank. Importantly, this improvement was achieved without increasing stimulation amplitude beyond the study limits, indicating that the observed gains were primarily attributable to stimulation timing rather than intensity.

Cadence values followed a similar trend, with CS trials generally achieving higher average

crank angular velocity, but with its performance declining faster than BB, indicating a faster fatigue effect. Additionally, greater variability in cadence was observed during some CS trials, particularly toward the end of the one-minute collection periods. This variability may reflect the increased responsiveness of the simulation-derived stimulation pattern to transient changes in crank dynamics, as well as fatigue-related effects during sustained unassisted cycling. While BB stimulation produced more uniform cadence profiles, this stability was accompanied by lower overall cadence values, suggesting a trade-off between responsiveness and uniformity.

The observed improvements in left-right balance during CS trials should not be interpreted as evidence of increased strength in one limb relative to the other. Instead, the results suggest differences in activation timing and responsiveness between the two control strategies. Although stimulation amplitude and protocol were symmetric across limbs, the simulation-derived control signal incorporated pre-activation phases that reduced the effective delay between electrical excitation and force production. This reduced activation latency likely enabled a more timely contribution of each leg during its respective power phase, resulting in a more synchronized bilateral cycling motion. In contrast, the phase-limited nature of bang-bang stimulation may delay force generation relative to crank position, leading to greater apparent asymmetry despite symmetric stimulation parameters.

6.4 IMPLICATIONS FOR FES CYCLING REHABILITATION

The results of this study demonstrate that predictive musculoskeletal simulations can generate stimulation timing strategies that outperform traditional phase-based control approaches when implemented experimentally. At the same time, the structure of the simulation framework necessarily imposed several simplifying assumptions that influence the resulting activation patterns.

In particular, the present formulation relied on a quadriceps-only muscle set and enforced symmetry at the signal-processing level to enable controlled experimental validation. While this approach proved effective for demonstrating feasibility and performance improvements, it also limited the range of coordination strategies that could emerge from the simulations. The absence of antagonist muscle groups and the reliance on a single representative muscle for

stimulation timing constrain the physiological richness of the derived control signal.

These observations motivate the exploration of alternative modeling strategies that explicitly account for coordinated muscle group activation and interaction under functional electrical stimulation. Extending the predictive framework to incorporate muscle synergies and more realistic representations of electrically induced muscle recruitment offers a natural pathway to further refine stimulation timing and distribution. Such extensions form the basis for the subsequent study, which builds directly upon the simulation and experimental insights established here.

6.5 STUDY LIMITATIONS AND SCOPE

While the results of this study are encouraging, its limitations should be acknowledged. First, the musculoskeletal cycling model was not scaled to the participant's anthropomorphic dimensions, and the experimental validation was conducted with a single participant, which limits the generalizability of the findings. Individual-specific factors such as muscle condition and prior experience with functional electrical stimulation (FES) cycling may influence responsiveness to different stimulation strategies. Future studies involving individualized models and more participants will be necessary to assess inter-subject variability and robustness.

Beyond participant-related constraints, a methodological limitation arises from the use of a torque-driven formulation to optimize cycling kinematics. While torque-driven models are computationally efficient and well suited for feasibility analyses, they do not explicitly represent muscle activation dynamics or the physiological constraints governing force production. As a result, the optimized kinematic solutions may include motion patterns that are mechanically valid at the joint level but not fully reproducible through muscle-driven actuation.

Related to this modeling abstraction, an additional limitation of this proof-of-concept study concerns the use of static stimulation profiles that were independent of cycling cadence and activation delays. Stimulation timing was defined solely as a function of crank angle and applied uniformly across conditions, without accounting for the electromechanical delay between stimulation onset and force generation. In the context of FES cycling, such delays arise not only from muscle activation dynamics but also from sensing, signal processing, and stimulation

delivery. As cycling speed varies, fixed phase-based stimulation profiles may therefore become misaligned with the mechanical response of the system, reducing their effectiveness and limiting robustness across operating conditions.

From a neuromuscular perspective, the stimulation strategy was further constrained by the use of a quadriceps-only musculoskeletal model and experimental configuration. While this simplification facilitated both modeling and experimental control, it necessarily restricted the range of achievable muscle coordination patterns. The absence of antagonist muscle stimulation, combined with the imposition of a hard maximum crank speed, may have influenced the emergence of activation outside mechanically optimal phases, as discussed previously.

More fundamentally, a central limitation of the present study—and a primary motivation for subsequent work—lies in how muscle activation under functional electrical stimulation is represented within the simulation framework. The musculoskeletal model assumes physiological excitation-activation coupling, whereas electrically induced contractions are characterized by non-physiological motor unit recruitment order, reduced selectivity, and spatially diffuse activation. Surface FES typically stimulates a broad region of the quadriceps muscle group simultaneously, rather than selectively activating individual muscles or motor units.

As a consequence, deriving stimulation timing solely from rectus femoris activation may represent an oversimplification of the true neuromuscular response during FES cycling. It is plausible that inclusion of the vasti muscles, together with explicit modeling of coordinated muscle group behavior, would alter the resulting activation profiles and their interaction with crank dynamics. Addressing this limitation requires moving beyond single-muscle representations toward group-based or synergy-based control formulations, which directly informed the design and objectives of the subsequent study.

Despite these limitations, the study establishes a clear proof of concept for using predictive musculoskeletal simulations to derive and experimentally validate stimulation strategies for FES cycling. By demonstrating both feasibility and performance benefits, this work provides a solid foundation for subsequent investigations aimed at refining model fidelity, expanding muscle group involvement, and exploring more adaptive and physiologically grounded control paradigms.

CHAPTER 7

METHODS - CASE STUDY

This chapter presents the methodology adopted in the case study, which builds directly upon the findings and limitations identified in the previous investigation (Chapter 6). While the first study demonstrated the feasibility of deriving functional electrical stimulation (FES) cycling control signals from fully predictive simulations and validating them experimentally, methodological and physiological simplifications remained. These included the use of a simplified musculoskeletal model, with a limited muscle set focused on the quadriceps, and an optimal control problem with kinematic boundaries and the absence of explicit coordination structures capable of representing how muscle groups are activated under FES.

The present study was designed to address these limitations by extending the simulation framework toward greater physiological realism and control structure abstraction. In particular, this study introduces muscle synergies as a control strategy, incorporates additional muscle groups, consider participant-specific muscle activation limitation, and reformulates the optimal control problem to explicitly track a target cycling speed while resolving muscle redundancy through synergy-based excitation patterns. By doing so, this work moves beyond a proof-of-concept implementation and advances toward stimulation strategies that better reflect the constraints and characteristics of FES-driven muscle activation.

Similarly to the previous study, the methods are organized into a simulation phase, data processing, and implementation steps for experimental validation (Figure 7.1). While the outcomes of the two studies are not intended to be directly compared due to differences in participant condition and data acquisition protocol, maintaining a consistent methodological structure allows the studies to be presented as complementary and conceptually aligned investigations. This parallel organization highlights the evolution of the proposed framework while preserving

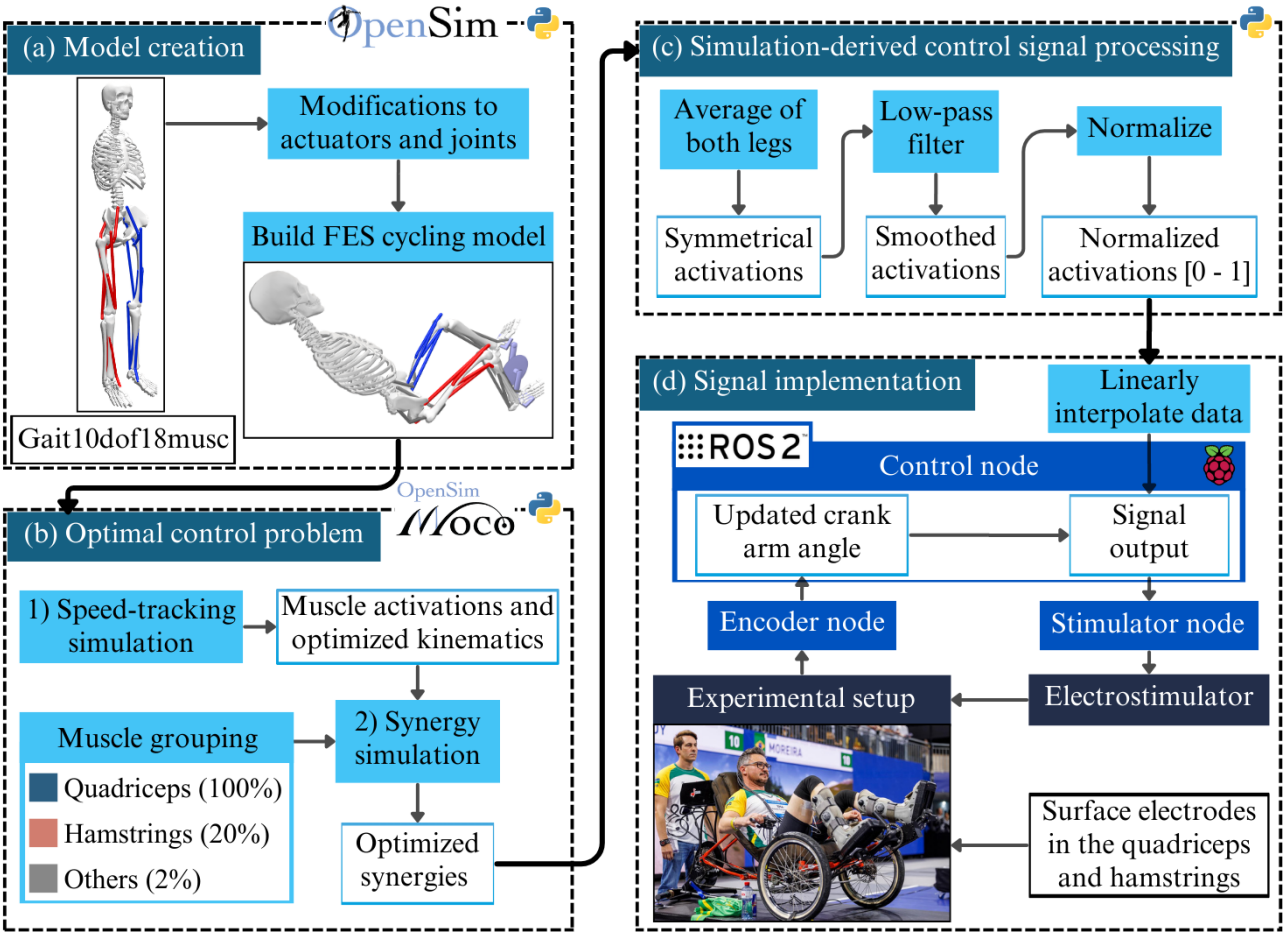

Figure 7.1. Overview of the simulation-to-stimulation framework used to generate and experimentally implement a synergy-based FES cycling control signal. (a) Model creation, including modification of muscle actuators, subject-specific activation constraints, and construction of the FES cycling model in OpenSim. (b) Optimal control formulation in OpenSim Moco, consisting of a speed-tracking simulation followed by a synergy-based optimization using non-negative matrix factorization to obtain coordinated muscle excitations. (c) Post-processing of simulation-derived activations, including bilateral averaging, low-pass filtering, and normalization to obtain smooth, bounded stimulation profiles. (d) Real-time signal implementation using ROS2, where crank angle measurements are used to index the stimulation lookup table and drive the electrical stimulator during experimental cycling. Pilot and investigator image rights: (ETH Zurich / CYBATHLON / Alessandro Della Bella).

continuity across the thesis.

7.1 MUSCULOSKELETAL CYCLING MODEL

The musculoskeletal model used in this study builds upon the muscle-driven cycling model described in the first investigation (Section 4.1), which was based on the Gait10dof18musc model implemented in OpenSim. The same fundamental modeling assumptions were retained, including sagittal-plane motion, locked feet and ankle joints to replicate the use of orthopedic cycling boots, and the inclusion of a resistive crank-pedal mechanism matching the experimental cycling setup. These design choices ensure methodological continuity while allowing the present

study to focus on extending the model toward greater physiological relevance under functional electrical stimulation (FES).

To better represent a clinically and competitively relevant FES cycling configuration, the set of actively contributing muscles was expanded relative to the proof-of-concept study. In addition to the quadriceps group (rectus femoris and vasti), the hamstrings muscle group (hamstrings and biceps femoris short head) was included as an active contributor to the cycling motion (Figure 7.1). This muscle configuration reflects a traditional FES cycling strategy and corresponds to the stimulation setup employed by Project EMA during the most recent Cybathlon 2024 edition. Incorporating both knee extensors and knee flexors allows the simulations to capture a more realistic distribution of muscular contributions throughout the crank cycle.

All remaining muscles in the model were restricted to a maximum activation of 2%, while preserving their passive force-length and force-velocity properties. Maintaining this small activation kept the muscles' contribution negligible and was essential for ensuring numerical convergence of the optimal control problem. This approach differs from the strategy adopted in the first study, where muscles were effectively deactivated by modifying their force-generating capacity. Limiting activation instead of force output ensures that non-stimulated muscles provide negligible active contribution while maintaining their passive mechanical effects, which play an important role in joint stability and overall system dynamics (Section 2.2.3).

In addition to defining the active muscle set, subject-specific activation constraints were incorporated to reflect the participant's physiological response to FES. In particular, the maximum activation of the hamstring muscles was limited to 20%. This constraint was motivated by experimental observations in the participant indicating that stimulation intensities above this level consistently induced involuntary spasms and unpredictable muscle behavior. This constraint effectively embeds experimentally observed neuromuscular limitations into the optimization problem.

Overall, these modeling choices extend the framework introduced in the proof-of-concept study by enabling a more realistic representation of FES-driven muscle coordination while preserving numerical robustness. Importantly, they also demonstrate the flexibility of computational approaches to incorporate participant-specific constraints, an essential requirement for translating simulation-derived stimulation strategies into practical and safe experimental

implementations. The key modeling differences can be seen in Table 7.1.

7.2 CYCLING OPTIMAL CONTROL PROBLEM

The formulation of the optimal control problem in this study follows the theoretical framework proposed by (SOUSA; FONT-LLAGUNES, 2024), which describes two complementary approaches for deriving stimulation strategies for functional electrical stimulation (FES) cycling using torque-driven musculoskeletal simulations. The proof-of-concept study expanded on the first of these approaches by employing a fully predictive formulation to generate cycling kinematics optimized with respect to time and effort (Section 4.2). The present work expands on the second approach.

The optimal control problem was structured as a two-stage optimization process. In the first stage, a speed tracking problem was formulated in which the cycling model completed one full crank revolution, starting with the left crank at top dead center, with no predefined joint initial speed, tracking a constant target cadence of 40 rpm against a constant resistive torque of 8 Nm. This simulation optimized the joint kinematics and corresponding muscle activations required to achieve the desired cycling behavior (Figure 8.1). The implementation used the *MocoStateTrackingGoal* function, with a cost term weight ω set to 1, to minimize the error between the instantaneous crank angular velocity $x(t)$ and the reference velocity $x_{ref}(t)$ throughout the duration of the motion (t_f), according to

$$J = \int_{t_0}^{t_f} \sum w(x(t) - x_{ref}(t))^2 dt. \tag{7.1}$$

In the second stage, the resulting muscle activation trajectories and kinematics obtained from the speed tracking simulation were used as reference inputs to a subsequent optimization. This second problem focused on resolving muscle coordination by grouping individual muscle activations into a reduced set of predefined muscle synergies while minimizing overall muscle excitation effort.

The number of groups and the assignment of muscles to each group were determined based on the anatomical layout of the model and the set of muscles that can be synchronously activated using single electrode stimulation (Fig. 7.2). Within each group, all muscles were constrained

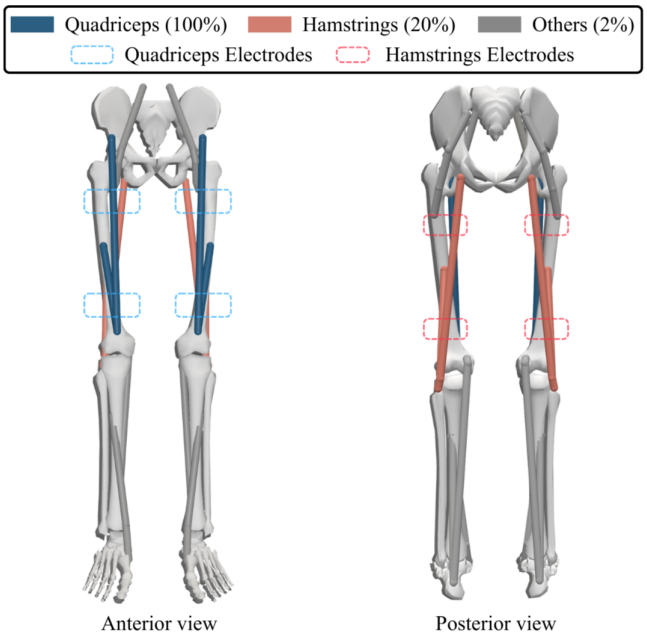

Figure 7.2. Muscle grouping and electrode placement used for synergy-based FES cycling control. Muscles in the cycling model are grouped according to anatomical function and surface stimulation feasibility, forming six muscle groups per leg: iliopsoas, quadriceps, tibialis anterior, gluteus maximus, hamstrings, and triceps surae. Anterior and posterior views illustrate the muscles included in each group and the corresponding surface electrode placements for the quadriceps and hamstrings, which were the only groups actively stimulated in this study. Dashed outlines indicate electrode locations, highlighting the correspondence between simulated muscle groups and experimentally available stimulation channels.

to share identical synergy weights, reflecting the inability to independently modulate individual muscles under surface stimulation. Importantly, only the quadriceps and hamstrings muscle groups actively contributed to the motion, with the other muscle groups' contributions being considered negligible.

To better represent the constraints imposed by surface functional electrical stimulation (FES), a synergy-based OC formulation was implemented. Under surface stimulation, multiple muscles are activated simultaneously and cannot be controlled independently. Consequently, muscles were not treated as independent actuators, but instead followed coordinated activation patterns defined by muscle synergies.

Although only two muscle groups were stimulated experimentally, the optimal control problem initially included additional muscles to allow physiologically consistent force redistribution during the simulation. The synergy decomposition was therefore used to extract two experimentally implementable control signals from the higher-dimensional excitation space produced by the optimal control solution.

The primary motivation for using muscle synergies was to ensure that the optimized control

signals were both physiologically plausible and experimentally implementable. By prescribing synergies aligned with the stimulation capabilities of surface electrodes, the optimization problem inherently accounted for the synchronous activation of multiple muscles during FES cycling.

Reference excitation trajectories obtained from the speed-tracking simulation were used to parameterize the synergy-based controller. For each leg, the simulated excitations were first aggregated according to the predefined muscle groups (Fig. 7.2), resulting in N_s group-level excitation signals. These trajectories were arranged into a data matrix $A \in \mathbb{R}^{T \times N_s}$, where T denotes the number of time samples and each column corresponds to one muscle group.

Non-negative matrix factorization (NMF) was then applied to decompose A into the product $A \approx WH$, where $W \in \mathbb{R}^{T \times N_s}$ contains time-varying excitation signals and $H \in \mathbb{R}^{N_s \times N_s}$ is a fixed weighting matrix. The factorization was obtained by minimizing a divergence between the original matrix A and its reconstruction WH, subject to non-negativity constraints on all matrices (LEE; SEUNG, 2000; FéVOTTE; IDIER, 2011).

In the synergy-based formulation, the time-varying excitation signals ($c_s(t)$) contained in W were treated as the control variables optimized by Moco. The excitation applied to each muscle group was obtained as a linear combination of these signals according to Eq. 7.2:

$$u_m(t) = \sum_{s=1}^{N_s} w_{ms}\, c_s(t), \tag{7.2}$$

where $c_s(t)$ denotes the excitation of the s-th synergy, corresponding to the s-th column of W, w_{ms} are fixed weighting coefficients from H, and $u_m(t)$ represents the resulting optimized excitation applied to muscle group m.

Although NMF is most commonly applied to electromyographic data, it is employed here as a mathematically convenient and physiologically consistent factorization to parameterize grouped excitation patterns derived from fully simulated muscle excitations. Ensuring experimental implementability under surface functional electrical stimulation, the optimized excitations $u_m(t)$ were applied uniformly to all muscles belonging to the corresponding muscle group.

Importantly, despite six muscle groups being included in the musculoskeletal model (iliopsoas, quadriceps, tibialis anterior, gluteus maximus, hamstrings, and triceps surae), only the quadriceps and hamstrings groups were stimulated in the experimental setup. Consequently,

the synergy decomposition effectively reduced the stimulation space to experimentally implementable activation profiles. In practice, this resulted in one synergy corresponding to the quadriceps muscles (rectus femoris and vasti) and another corresponding to the posterior thigh muscles (hamstrings and short head of the biceps femoris), consistent with the two available stimulation channels per leg.

In addition, the synergy-based formulation included a control effort term that penalized the magnitude of the synergy excitation signals. This effort term was defined in Eq. 7.3:

$$J_{syn} = \int_{t_0}^{t_f} \sum_{s=1}^{N_s} |c_s(t)|^2 \, dt, \tag{7.3}$$

encouraging low-amplitude synergy excitation profiles. Unlike the speed-tracking simulation, in which the objective function penalized only kinematic tracking error and did not include an explicit effort term on the controls, the effort term in the synergy simulation acted on the reduced set of synergy excitation controls c_s.

Minimizing the synergy control effort is particularly relevant in a rehabilitation context, as multiple synergy excitation profiles may satisfy the kinematic tracking requirements. Among these feasible solutions, the proposed formulation favors excitation patterns that are less demanding and potentially safer for prolonged applications.

7.3 DERIVING THE OPTIMAL CONTROL SIGNAL

Following the solution of the synergy-based muscle-driven optimal control problem, the resulting muscle synergy activation signals were post-processed to generate stimulation profiles suitable for experimental implementation. The post-processing steps adopted in this study follow the same rationale described in the previous study (Section 4.3), with adaptations reflecting the structure of the present optimal control formulation.

Because the simulated cycling motion consisted of a single crank revolution, no inter-cycle averaging was required. To enforce bilateral symmetry of the cycling task, the synergy activation signals obtained for the left and right legs were averaged, yielding a single symmetric activation profile per synergy.

The resulting signals were then filtered using a fifth-order Butterworth low-pass filter with a

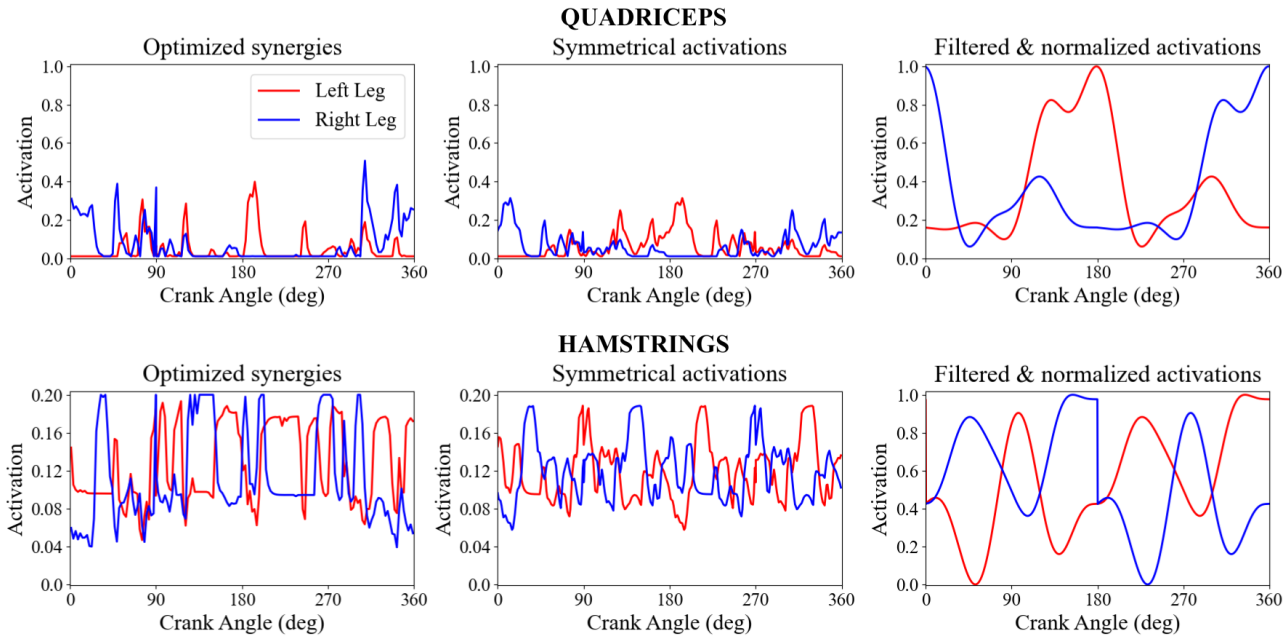

Figure 7.3. Post-processing of the synergy activation signals for the quadriceps and hamstrings muscle groups. Left-leg (blue) and right-leg (red) activations were first averaged to generate a symmetrical quadriceps pattern. The resulting signal was then filtered to attenuate abrupt activation transitions and normalized between 0 and 1 to compensate for doubled isometric force in the musculoskeletal model, the use of reserve actuators, and the reduced efficiency of surface electrical stimulation. The final filtered and normalized profile corresponds to the quadriceps stimulation command implemented in real time during the experimental trials.

normalized cutoff frequency of 0.6 Hz and a sampling rate of 100 Hz, ensuring smooth temporal transitions compatible with physiological muscle recruitment and functional electrical stimulation. Finally, the filtered signals were normalized to the range [0,1] to compensate for the modeling assumptions adopted in the simulations, including doubled maximum isometric muscle forces, the presence of reserve actuators, and the direct excitation of muscle fibers inherent to the computational model (Figure 7.3).

The resulting normalized synergy activation profiles were implemented experimentally using pulse width modulation FES strategy (Section 3.2.3). The key methodological differences between the proof-of concept study and the case study can be seen in Table 7.1.

7.3.1 Computational details

The speed tracking simulation had 380 meshes, and 10^{-4} for convergence and constraint tolerances, converging in just over eight hours. The muscle synergy simulation had 150 meshes, and 10^{-1} for convergence and constraint tolerances, being solved in 31 seconds. The simulations were executed on the same workstation described in the previous study (Section 4.3.1). The

Table 7.1. Summary of key methodological differences between the proof-of-concept study and the case study.

Aspect	Proof-of-concept study	Case study
Objective	Framework feasibility	Physiological refinement
Muscle set	Quadriceps only	Quadriceps and hamstrings
Muscle deactivation	Reduced isometric force	Limited muscle activation
Subject-specificity	Not explicitly modeled	Hamstrings activation limit
Kinematic constraints	Maximum speed limit	Constant speed tracking
Kinematics prediction	Torque-driven model	Muscle-driven model
Muscle control	Independent muscles	Synergy-based coordination

model, codes and data are publicly available [1].

7.4 PARTICIPANT CHARACTERISTICS

An experienced male participant with a complete spinal cord injury (T9 SCI, ASIA A) volunteered for this study. The same participant had taken part in the previous investigation (Section 4.4), allowing continuity across the two experimental protocols. At the time of this second study, the participant was 47 years old, weighed 65 kg, and measured 1.70 m in height.

Prior to participation, the volunteer provided written informed consent in accordance with the Declaration of Helsinki. The study protocol was approved by the Universidade de Brasília Institutional Research Ethics Committee (protocol number: 75441323.4.0000.8093).

7.5 DATA COLLECTION PROTOCOL

Data were collected over four non-consecutive days, following a standardized preparation and testing sequence designed to ensure participant safety and consistency across sessions. Each session began with a stretching routine conducted under the supervision of a physiotherapist while the participant lay on a stretcher. The routine targeted the quadriceps, hamstrings, gluteals, ankles, and lumbar regions to promote flexibility and reduce spasticity.

[1] Currently being developed and maintained at: FES cycling project.

After stretching, a 5-minute passive warm-up phase was performed. During this phase, the participant was positioned in a standardized manner on the recumbent trike, and an investigator manually assisted the pedaling motion. Surface electrodes were then placed bilaterally over the quadriceps and hamstring muscle groups. An active warm-up phase followed, during which assisted cycling continued while stimulation intensity was gradually increased by the participant until sustained unassisted pedaling was achieved. This active warm-up lasted 12 minutes, after which the participant rested for 5 minutes before the start of the experimental trials.

For each data collection day, the simulation-derived Control Signal (CS) and the bang-bang (BB) stimulation protocols were tested in alternating order to minimize systematic bias. The order of the protocols was counterbalanced across days such that each protocol was tested first and second an equal number of times: (day 1) BB followed by CS, (day 2) CS followed by BB, (day 3) BB followed by CS, and (day 4) CS followed by BB. During each session, two experimental trials were performed, one for each protocol (Table 8.1).

Each trial lasted 2 minutes. The first 30 seconds, consistent with the Cybathlon 2024 race start protocol, were assisted by an investigator and maintained between 55 and 60 rpm to facilitate the transition to unassisted cycling and to standardize initial conditions for subsequent data analysis. Stimulation parameters were standardized across trials, with pulse width starting at 225 μs and increasing by 25 μs every 10 seconds, while the current amplitude varied according to the active stimulation protocol. All trials were performed under constant mechanical resistance on the cycling system to match the simulated conditions. Power output, crank cadence, and inter-limb balance were recorded continuously for subsequent analysis (Section 3.2.2).

7.5.1 Simulation-derived control signal

For the simulation-derived Control Signal (CS), stimulation followed the normalized synergy activation profiles obtained from the optimal control simulations. The stimulation current varied smoothly as a function of crank angle, ranging from 0 to 100 mA for the quadriceps muscle group and from 0 to 20 mA for the hamstrings muscle group, corresponding to the minimum and maximum values of the activation profiles (Figure 8.3). Meanwhile, the pulse

width increased according to the data collection protocol. These limits were selected to respect participant-specific tolerance thresholds while preserving the relative temporal structure of the simulation-derived activation patterns.

7.5.2 Bang-bang control signal

In the bang-bang (BB) protocol, stimulation was applied within fixed crank-angle activation windows for the quadriceps and hamstrings, including linear ramp-up and ramp-down transitions at the onset and offset of each window. In addition, BB stimulation was intentionally asymmetric to compensate for previously observed left-right imbalance (Figure 5.2). The left leg received a 30% higher stimulation command than the right leg. This increase was implemented by scaling the commanded pulse width by a factor of 1.3, with an upper limit of 480 μs for both muscle groups. Thus, for quadriceps and hamstrings alike, the left leg pulse width stimulation followed the same phase-based BB windows but with a 30% higher command until reaching the 480 μs limit. When the right leg reaches the limit of 450 μs, the stimulation intensity difference becomes constant at 6.7% (Figure 8.3). This asymmetry was applied consistently throughout BB trials and should be considered when interpreting BB balance outcomes in this study.

Quadriceps stimulation was applied over a broad power-producing region of the crank cycle. For the left leg, stimulation onset occurred at 300°, preceding top dead center, and was maintained through the downstroke until 55°. Hamstring stimulation was applied over a shorter angular window associated with knee flexion, beginning 100° and ending at 160°. The corresponding stimulation windows for the right leg were defined symmetrically by a 180° phase shift relative to the left leg, ensuring bilateral temporal symmetry across the crank cycle.

To improve comfort and reduce abrupt changes in stimulation intensity, activation and deactivation were not applied instantaneously. Instead, linear ramps were incorporated at both the onset and offset of stimulation, spanning 20° of crank rotation. Within these ramp regions, stimulation current increased or decreased linearly between zero and the prescribed maximum value. Outside the defined activation windows, stimulation was set to zero. The resulting bang-bang stimulation pattern, including activation windows and ramp regions, is illustrated in the polar representation shown in Figure 8.3.

7.5.3 Crank-speed-dependent phase shifting

To account for variations in crank cadence during experimental cycling, both the simulation-derived Control Signal (CS) and the bang-bang (BB) stimulation profiles were subjected to a crank-speed-dependent phase adjustment. This phase-shifting strategy ensured that the timing of stimulation relative to crank position remained consistent despite variations of cycling speed.

Specifically, stimulation onset and offset angles were adjusted dynamically as a function of the instantaneous crank angular velocity, introducing a phase advance at higher cadences to compensate for neuromuscular activation delays. This adjustment was applied uniformly across both stimulation strategies to ensure a fair comparison between CS and BB. The phase-shifting relationship was implemented according to the equation described in (de Sousa *et al.*, 2016)

$$\theta_{shift} = \frac{K}{\omega_{max}}\,\omega, \tag{7.4}$$

where θ_{shift} represents the phase adjustment applied to the stimulation profile, K is an empirically defined correction factor equals to 30°, ω_{max} is a maximum speed of 300° per second (60 rpm), and ω denotes the instant crank angular velocity. The stimulation profiles depicted in Figure 8.3 correspond to the maximum stimulation at a 40 rpm crank angular velocity.

CHAPTER 8

RESULTS - CASE STUDY

The computational framework was composed of two consecutive optimal control problems: a speed-tracking simulation followed by a muscle synergy-based simulation. The objective of the speed-tracking problem was to minimize the error between the instantaneous crank cadence and a constant target cadence of 40 rpm. The optimized solution successfully tracked the reference cadence throughout the simulated cycle, resulting in stable and periodic kinematics.

8.1 SIMULATION RESULTS

Muscle activation patterns obtained from the speed-tracking simulation are shown in Figure 8.1. The rectus femoris and vasti muscles exhibited the expected oscillatory activation patterns associated with cyclic knee extension during pedaling. In contrast, the hamstrings and biceps femoris short head showed comparatively lower and nearly constant activation levels, reflecting the imposed activation constraints of the musculoskeletal model. These results confirm that the speed-tracking simulation produced physiologically plausible muscle dynamics while achieving the desired crank cadence.

The optimized kinematics and muscle dynamics from the speed-tracking problem were subsequently used as reference inputs for the muscle synergy-based optimal control problem. In this second simulation, muscle controllers were grouped into predefined synergies, resulting in one synergy for the quadriceps muscle group and one synergy for the hamstrings muscle group in each leg. Muscles not included in these synergies were allowed to remain independent, although their contribution to the solution was negligible due to minimal activation levels. The synergy-based simulation preserved the crank cadence trajectory obtained in the speed-tracking problem, indicating that the introduction of synergies did not compromise the optimized kinematics. At the same time, muscle activations were reorganized according to the imposed synergy structure, yielding a single activation pattern per muscle group and leg (Figure 8.2).

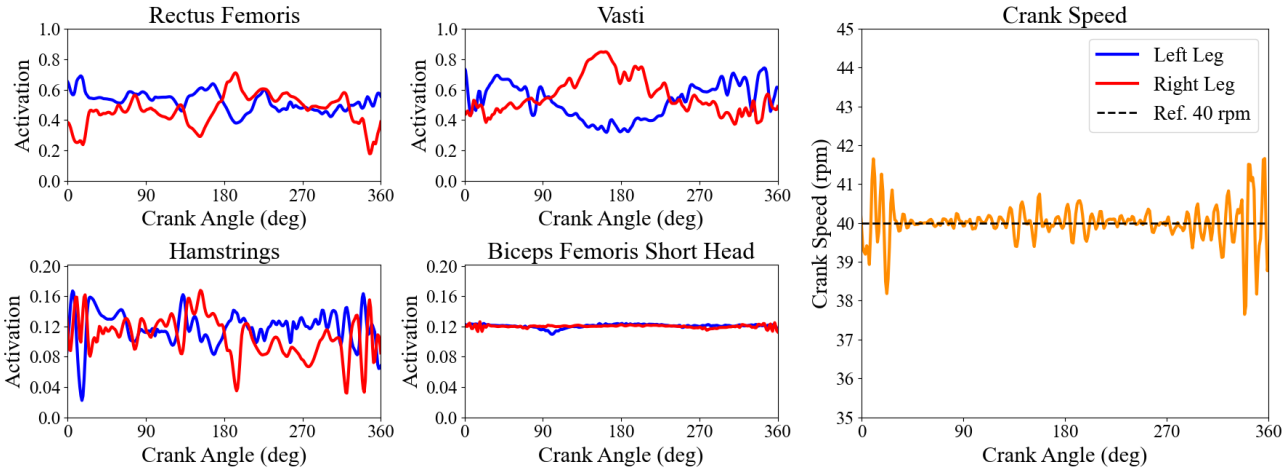

Figure 8.1. Muscle activations obtained from the speed-tracking simulation for rectus femoris, vasti, hamstrings, and biceps femoris short head over a full 360° crank cycle. Crank angle is defined starting at the left crank top dead center (0°). Blue lines represent the left leg and red lines the right leg. Quadriceps muscles (rectus femoris and vasti) exhibit the expected cyclic activation patterns associated with knee extension phases, whereas the hamstrings operate close to their imposed 20% activation limit throughout the cycle. The rightmost panel shows the instantaneous crank speed (solid yellow line), which closely tracks the constant reference cadence of 40 rpm (dashed line). Although the speed-tracking simulation was computed over 0-450°, only the steady-state interval from 90-450° is shown and re-indexed to 0-360° for clarity and consistency with subsequent figures and analyses. These muscle activation profiles and kinematics served as the input for the subsequent synergy-based optimal control problem.

Following the synergy-based simulation, the resulting activation signals were post-processed to derive stimulation profiles suitable for experimental implementation (Figure 7.3). The final simulation-derived control signal (CS), together with the empirically tuned bang-bang (BB) stimulation protocol used during the experiments, is presented in polar form in Figure 8.3. This representation facilitates direct comparison of the temporal structure, smoothness, and inter-limb symmetry of the two stimulation strategies across a full 360° crank cycle. Together, these simulation results establish the basis for the experimental comparison of CS and BB stimulation presented in the following section.

8.2 EXPERIMENTAL RESULTS (JNER)

The experimental phase compared the simulation-derived Control Signal (CS) with the empirically tuned bang-bang (BB) stimulation protocol previously used during the Cybathlon 2024 competition. Four experimental sessions were conducted on non-consecutive days, each consisting of two trials, one per stimulation protocol, with the order of protocol execution alternated across days. Cycling performance over the 120-s trials is shown in Figure 8.4, and quantitative summaries are reported in Table 8.1.

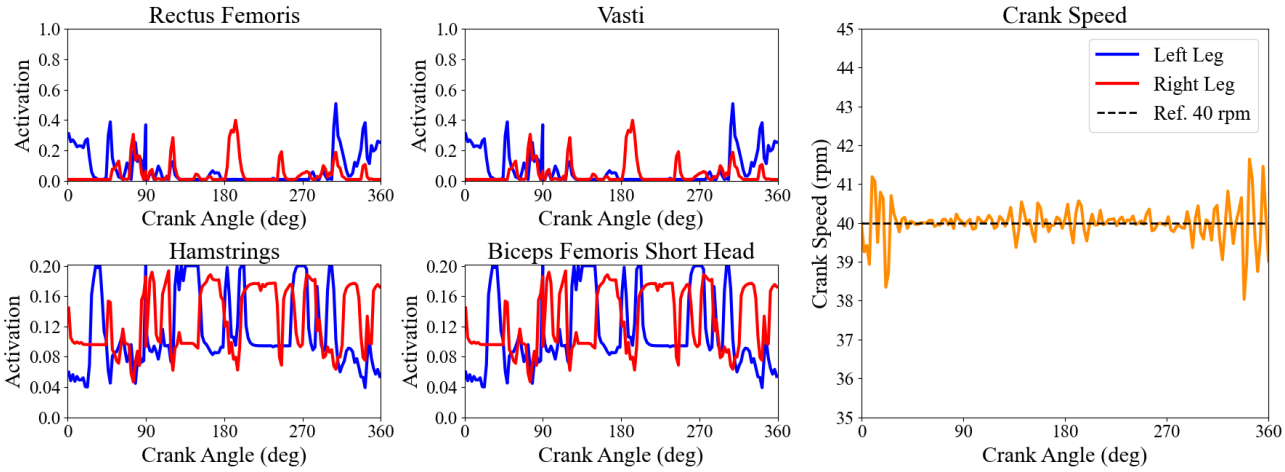

Figure 8.2. Muscle activations obtained after solving the synergy-based optimal control problem, following the reference kinematics from the speed-tracking simulation. Blue and red curves represent left and right leg activations, respectively. Six muscle synergies per leg were prescribed, but only two with active contribution: a quadriceps synergy grouping rectus femoris and vasti, and a hamstrings synergy grouping hamstrings and biceps femoris short head, with the last synergy being subject to a 20% activation limit as per modeling specification. As a result, rectus femoris and vasti exhibit identical activation profiles, as do the hamstrings and biceps femoris short head. Compared to the speed-tracking solution, activation patterns are substantially lower due to the additional objective of minimizing muscle excitation. The rightmost panel shows the crank cadence (solid yellow line), which closely matches the reference speed of 40 rpm (dashed line), indicating that the prescribed synergy structure preserved the optimized kinematics within solver tolerances.

Both control strategies enabled functional electrical stimulation (FES) cycling across all sessions, producing consistent power output and crank cadence profiles over multiple days. No systematic degradation in performance was observed across sessions, suggesting minimal inter-day fatigue and indicating reliable experimental conditions and data acquisition (Figure 8.4).

Distinct performance differences were observed between the two stimulation strategies during the unassisted cycling phase. The BB protocol maintained higher and more stable power output and cadence throughout the unassisted period. In contrast, the CS condition exhibited a noticeable reduction in both power and cadence immediately following the initial 30-s assisted phase, followed by a gradual recovery as pulse width increased during the trial. Despite these differences in performance magnitude, left-right balance remained close to 50% for both protocols, indicating relatively symmetrical contributions from both legs across conditions (Figure 8.4).

Across all sessions, the BB protocol resulted in higher mean power output and cadence with lower inter-session variability. Conversely, the CS condition demonstrated a consistently improved left-right balance, with the exception of the first day of data collection.

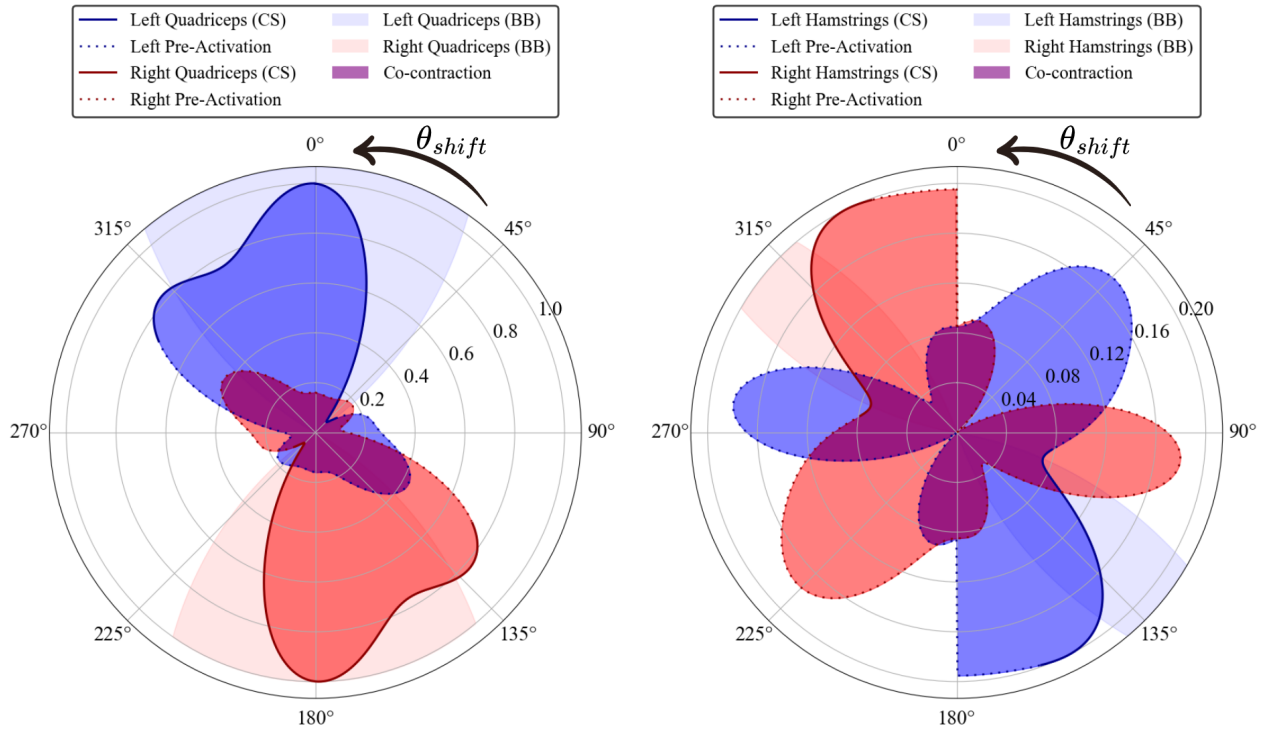

Figure 8.3. Polar representations of the two stimulation profiles used in the experimental protocol at maximum activation and 40 rpm. The simulation-derived control signal (CS) is shown as dark colored curves (blue for the left leg and red for the right leg), while the empirically tuned bang-bang (BB) protocol is shown as shaded regions. The plots span a full 360° crank cycle, with 0° corresponding to the left crank at top dead center. CS exhibits phases of pre-activation outside the mechanically advantageous regions (dotted segments) and intervals of simultaneous co-contraction between the muscle groups (purple shading). BB displays discrete activation windows, combined with linear 20° ramp-up and ramp-down transitions at the onset and offset of each window. The BB stimulation was intentionally asymmetric to compensate for unbalanced cycling, indicated by the larger radial extent of the shaded regions for the left leg. The left panel shows the quadriceps stimulation profiles, while the panel to the right shows the hamstrings profiles. Together, these plots highlight the fundamental differences in temporal structure, smoothness, and inter-limb symmetry between the CS and the empirically tuned BB profiles.

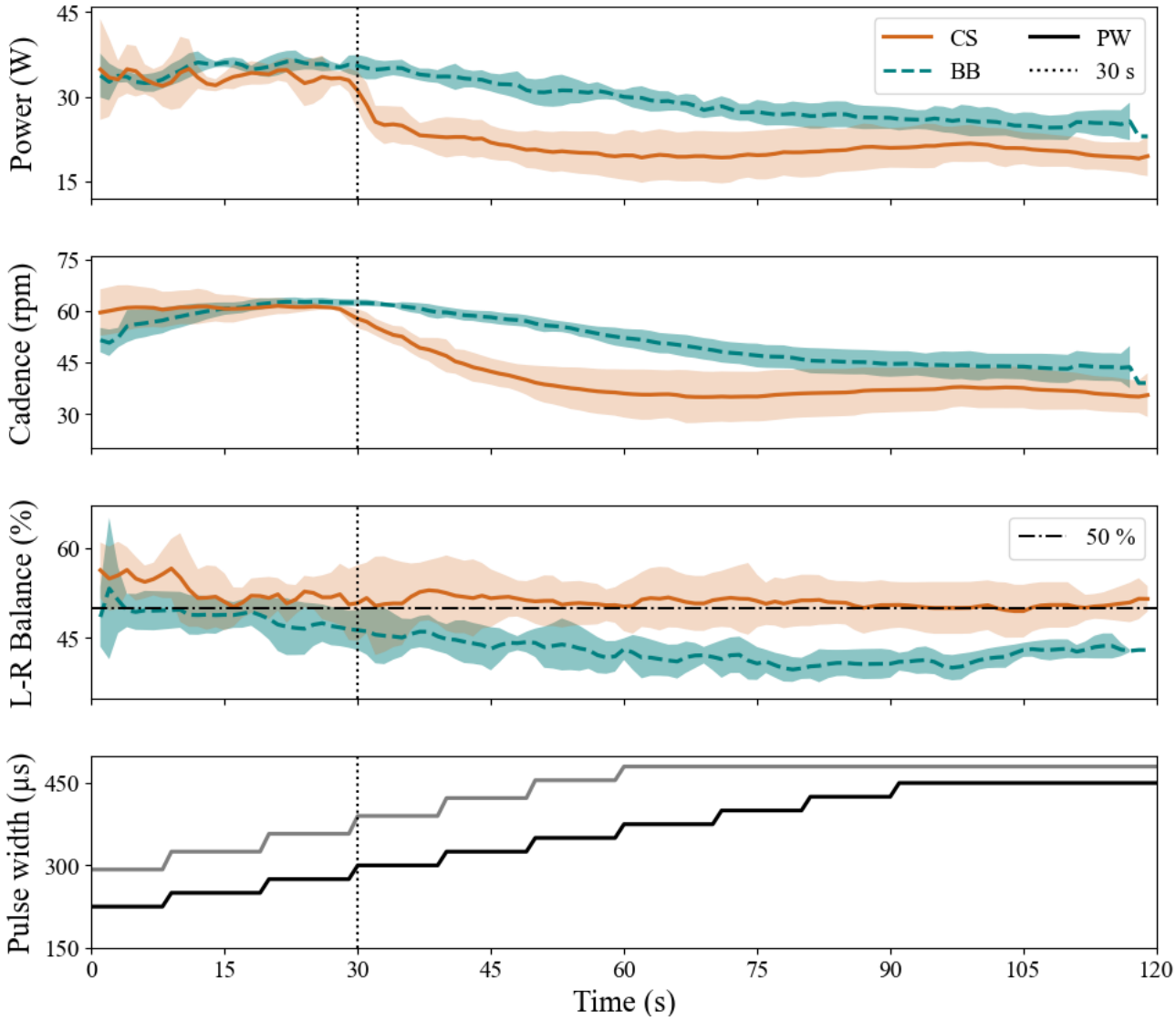

Figure 8.4. Experimental comparison of cycling performance using the simulation-derived control signal (CS, solid lines) and the empirically tuned bang-bang protocol (BB, dashed lines) averaged across four non-consecutive days of data collection sessions. From top to bottom, the panels show power output (W), crank cadence (rpm), left-right balance (%), and pulse width (μs) over 120-s trials. Shaded regions indicate one standard deviation across sessions. The vertical dotted line at 30 s marks the transition from assisted to unassisted FES cycling. Pulse width was increased automatically during each trial. The black line represents the pulse width used in CS and the right leg for BB, while the gray line indicates the left-leg pulse width used in the BB protocol. Quantitative data for the sessions and summaries for assisted and unassisted phases are reported in Table 8.1.

Table 8.1. Summary of cycling performance metrics collected during experimental trials across four non-consecutive days of data collection. Reported variables include average power output (W), crank cadence (rpm), and left-right balance (%), expressed as mean ± standard deviation for each trial. Results are organized by day and stimulation protocol, comparing the simulation-derived control signal (CS) and the bang-bang protocol (BB), with alternating protocol order across sessions. The data summary reports pooled mean ± standard deviation for assisted and unassisted cycling phases separately, for both CS and BB conditions.

	Power (W)	**Cadence** (rpm)	**Balance** (%)
Day 1 of data collection			
BB	29.58 ± 4.06	52.92 ± 7.30	47.96 ± 4.93
CS	22.55 ± 7.80	43.42 ± 14.15	57.02 ± 2.93
Day 2 of data collection			
CS	29.15 ± 6.77	53.08 ± 11.09	49.58 ± 4.66
BB	29.00 ± 4.34	51.49 ± 8.40	42.75 ± 2.24
Day 3 of data collection			
BB	30.94 ± 5.02	50.11 ± 7.74	42.27 ± 3.91
CS	22.93 ± 6.79	40.37 ± 11.33	50.78 ± 2.24
Day 4 of data collection			
CS	25.65 ± 4.47	48.55 ± 8.52	49.76 ± 3.39
BB	31.69 ± 2.76	55.58 ± 4.98	43.34 ± 3.18
Data summary			
CS assisted	33.41 ± 3.19	60.73 ± 3.80	52.90 ± 4.15
BB assisted	34.89 ± 1.52	59.52 ± 2.29	48.56 ± 3.65
CS unassisted	21.02 ± 3.55	38.96 ± 5.74	50.89 ± 4.35
BB unassisted	28.69 ± 1.96	50.03 ± 2.93	42.53 ± 2.45

CHAPTER 9

DISCUSSION - CASE STUDY

This study builds directly upon the predictive simulation framework introduced in the first investigation of this thesis (Chapter 4). While that initial proof-of-concept study demonstrated the feasibility of deriving functional electrical stimulation (FES) cycling control signals from simulations and validating them experimentally, several biomechanical and neuromuscular simplifications limited its physiological scope and translational robustness.

The present case study was therefore designed to systematically address these limitations by extending both the simulation framework and the experimental protocol toward greater realism and clinical relevance. Specifically, six interrelated limitations identified in the first study motivated the methodological advances presented here: (1) the use of a torque-driven formulation to optimize cycling kinematics, which may yield motion patterns not reproducible through muscle-driven actuation; (2) the use of static, cadence-independent stimulation profiles that do not account for activation delays or changes in cycling speed; (3) the exclusive use of the quadriceps muscle group in both simulations and experiments; (4) the absence of participant-specific neuromuscular constraints in the musculoskeletal model; (5) the simplified representation of non-physiological FES activation patterns; and (6) the lack of explicit modeling of coordinated muscle activation structures, such as synergies, that characterize FES-driven movement. Together, these limitations defined the scope and objectives of the present study.

9.1 EVOLUTION OF THE MODELING AND CONTROL FRAMEWORK

In the first study, cycling kinematics were optimized using a torque-driven formulation and subsequently prescribed to a muscle-driven model for activation optimization. While this approach was computationally efficient and sufficient for an initial feasibility analysis, it does not explicitly account for muscle activation dynamics or the physiological constraints governing force production. In the context of FES cycling, where excitation timing, muscle force-length-

velocity relationships, and stimulation-induced dynamics play a central role, this abstraction may lead to kinematic solutions that are not fully reproducible by electrically stimulated muscles. This limitation directly motivated the transition to a fully muscle-driven formulation in the present study, allowing kinematics, muscle activation dynamics, and subject-specific stimulation constraints to be optimized within a unified muscle-driven framework.

Beyond the formulation used to generate kinematics, the first study also simplified how stimulation timing was represented. Both the simulation-derived control signal and the bang-bang strategy employed static stimulation profiles that did not adapt to variations in cycling speed. The simulations assumed direct muscle excitation and physiological activation dynamics, whereas FES cycling introduces additional electromechanical delays associated with sensing crank position, signal processing, stimulation delivery, and surface-induced muscle activation. As a result, stimulation timing that is optimal at one cadence may become suboptimal as cycling speed changes. To address this limitation, the present study incorporated speed-dependent phase shifts that anticipate stimulation onset at higher cadences, compensating for these delays and improving temporal alignment between stimulation and mechanical output, following approaches previously explored in the literature (de Sousa *et al.*, 2016; FONSECA *et al.*, 2017).

For the first study, only the quadriceps muscle group was included in both the simulation framework and the experimental implementation, reflecting the most basic configuration of FES cycling. While this simplification facilitated modeling and experimental control, it no longer reflects current rehabilitation practices or competitive FES cycling configurations, such as those adopted in the Cybathlon (BO *et al.*, 2017; LAUBACHER *et al.*, 2017; METANI *et al.*, 2017). Contemporary approaches commonly incorporate both knee extensors and knee flexors, enabling more continuous power production, reduced periods of passive crank motion, and smoother cycling dynamics. From a rehabilitation perspective, activating additional muscle groups may also promote more balanced muscular engagement and reduce localized fatigue. In the present study, the inclusion of the hamstrings muscle group was therefore a deliberate extension of the framework, allowing the simulation and experimental protocols to more closely replicate realistic FES cycling configurations and enabling direct comparison with a bang-bang stimulation strategy using the same muscle set.

Expanding the stimulation framework beyond the quadriceps also exposed another impor-

tant limitation of the first study: the absence of participant-specific neuromuscular constraints within the musculoskeletal model. This was acceptable in the initial investigation, as stimulation of the quadriceps muscle group exhibited predictable and robust behavior under the activation limits used experimentally. However, with the inclusion of the hamstrings muscle group in the present study, this assumption no longer held. Experimentally, the participant exhibited a substantially lower tolerance to hamstring stimulation, with activation levels above 20% consistently inducing involuntary spasms and unpredictable behavior (BO *et al.*, 2017; METANI *et al.*, 2017). To ensure consistency between simulation outcomes and experimental implementation, this activation limitation was explicitly incorporated into the musculoskeletal model. Had this constraint been imposed only during experimental execution, the optimization process would likely have relied on hamstring activation strategies that could not be safely or reliably realized in practice. By embedding participant-specific activation limits directly into the simulation framework, the resulting control strategies remained physiologically feasible and directly translatable. This modification ensured that optimized activation strategies remained feasible under the participant's neuromuscular constraints.

Beyond muscle selection and activation limits, the first study also simplified how muscle activation under surface functional electrical stimulation was represented in the simulation framework. In that study, individual muscles within the quadriceps group were treated as independently actuated, even though experimental stimulation activates these muscles synchronously due to electrode size and placement (HUG *et al.*, 2011). This abstraction allowed the optimizer to selectively overload specific muscles, most notably the rectus femoris, while underutilizing others, as a means of minimizing effort. While mathematically valid, such solutions do not reflect the experimentally imposed synchronization of muscle activation in FES cycling. In practice, rectus femoris and vasti muscles are activated together and cannot be selectively recruited, meaning that force production is necessarily distributed across the muscle group. By not encoding this constraint, the first study's model could generate activation patterns that were optimal for the simulated system but suboptimal or unrealistic for translation to experimental stimulation, both in terms of timing and muscle loading. This limitation motivated the need for a control abstraction that explicitly reflects synchronized muscle activation under FES.

These actuation constraints directly motivated the introduction of an explicit control abstraction capable of representing coordinated muscle activation under surface FES. In such applications, control is fundamentally constrained by the stimulation hardware: each stimulation channel typically activates multiple muscles simultaneously, and selective recruitment of individual muscles is rarely feasible (KIM *et al.*, 2008; COUSIN *et al.*, 2021). To reflect this reality, the present study introduced muscle synergies as a control abstraction, not as emergent physiological entities, but as prescribed groupings that mirror the experimentally imposed actuation constraints. Muscle groupings were defined based on cycling literature (HUG *et al.*, 2011; CHEUNG *et al.*, 2020; WANG *et al.*, 2024) and practical considerations related to electrode size and placement, while the temporal behavior of each synergy was determined entirely by the optimizer. Six synergies per leg were prescribed to provide sufficient flexibility, although only the quadriceps and hamstrings synergies actively contributed to cycling. By enforcing synchronized activation within these muscle groups, the model was constrained to generate solutions that inherently account for shared activation and load distribution, preventing the optimizer from exploiting non-implementable muscle-specific strategies. This approach reduces control dimensionality, improves numerical robustness, and, most importantly, ensures that the resulting activation patterns are directly translatable to real-time FES implementation. Within this context, prescribing synergy structure represents a deliberate and necessary design choice aligned with the physical realities of surface stimulation.

9.2 SIMULATION RESULTS: INTERPRETATION & MECHANISMS

The simulation results of the present study are structured around a two-stage, fully muscle-driven optimal control framework designed to address the limitations identified in the first investigation. In the first stage, a speed-tracking optimal control problem was solved using a muscle-driven formulation, in which muscle activations and joint kinematics were optimized simultaneously to track a constant crank cadence of 40 rpm. This formulation ensured that the resulting kinematics were directly achievable through muscle actuation, in contrast to the torque-driven approach used previously. The optimized kinematics and muscle dynamics obtained from this simulation are illustrated in Figure 8.1.

In the second stage, these optimized kinematics were prescribed as reference inputs to a

synergy-based optimal control problem, in which muscles were grouped into predefined synergies and the temporal activation of each synergy was optimized to reproduce the movement while minimizing overall muscle effort. Despite this additional control abstraction, the synergy-based simulation preserved the crank cadence and kinematic trajectories obtained in the speed-tracking problem within the specified tolerances, as shown in Figure 8.2. Finally, the resulting simulation-derived control signal (CS) is presented in polar form in Figure 8.3, enabling a compact visualization of its temporal structure across the crank cycle.

9.2.1 Speed-Tracking Simulation

The speed-tracking simulation successfully achieved the target crank cadence of 40 rpm, as shown by the crank speed trajectory in Figure 8.1. While the average cadence closely follows the reference value, small oscillations are observed throughout the crank cycle. Notably, the largest deviations occur near 0°/360° and 180°, coinciding with crank positions where quadriceps activation reaches its peak. In contrast, cadence fluctuations are reduced near 90° and 270°, corresponding to mechanically disadvantageous crank positions, often referred to as dead zones, where muscle-generated forces contribute minimally to crank rotation. This behavior mirrors observations in able-bodied cycling (HUG *et al.*, 2011), where power production is concentrated during distinct pushing and pulling phases rather than being uniformly distributed across the cycle. The presence of cadence oscillations near peak force transmission suggests that the optimizer compensates for reduced mechanical effectiveness in the dead zones by increasing force production in the mechanically favorable regions. It can be hypothesized that greater engagement of knee flexor muscles could reduce this compensation, potentially smoothing crank speed by contributing torque during phases where quadriceps effectiveness is diminished.

The resulting muscle activation patterns from the speed-tracking simulation further support the physiological plausibility of the optimized solution. The rectus femoris and vasti muscles exhibit clear oscillatory activation profiles aligned with the cyclic demands of knee extension during pedaling. In contrast, activation of the hamstrings and biceps femoris short head remains comparatively low and exhibits limited modulation across the crank cycle. This behavior is primarily explained by the imposed activation constraints on these muscles, which restrict their maximum contribution and prevent the emergence of unconstrained physiological acti-

vation patterns. Under these limitations, the optimizer adopts a strategy in which hamstring muscles remain near their allowable activation ceiling, representing the most effective means of contributing torque within the imposed bounds. Despite these constraints, the resulting activation profiles remain feasible for experimental implementation and are consistent with those used in the first study. However, it is important to note that these activation patterns represent only one of many possible solutions capable of achieving the desired kinematics. Moreover, implementing these muscle-specific activations directly would neither minimize muscle effort nor reflect the synchronous activation imposed by surface FES, underscoring the need for subsequent signal processing and control abstraction

From a computational perspective, the speed-tracking simulation reflects a deliberate trade-off between physiological realism and numerical complexity. In the present study, the simulation was performed over 450° of crank rotation, with the first 90° discarded to ensure steady-state behavior for subsequent analyses. This simulation required approximately eight hours to converge. In contrast, the first study simulated four full crank cycles and discarded the initial cycle, achieving convergence within approximately 30 minutes. The increased computational cost in the present framework arises primarily from the transition to a fully muscle-driven formulation and the preservation of passive muscle properties. In the first study, non-stimulated muscles were effectively deactivated by reducing their maximum isometric force, which simultaneously limited both active and passive force contributions. In the present study, muscle deactivation was achieved by constraining activation levels to 2%, suppressing active force generation while fully preserving passive muscle dynamics. This choice more accurately reflects FES cycling in individuals with complete spinal cord injury, where non-stimulated muscles retain passive mechanical properties despite lacking voluntary activation. However, this imbalance between active and passive force contributions introduces additional numerical stiffness and significantly increases computational demands. Despite this cost, the approach was necessary to ensure that the simulated dynamics remained representative of the experimental conditions targeted in this study.

9.2.2 Synergy Simulation

The muscle synergy simulation was formulated by prescribing the kinematics obtained from the muscle-driven speed-tracking problem and optimizing muscle activation patterns to reproduce this motion under a reduced control dimensionality. Because the reference kinematics originated from a muscle-driven formulation, they inherently respected muscle activation dynamics and force-length-velocity constraints, ensuring physiological feasibility. As shown in Figure 8.2, the crank cadence closely followed the prescribed trajectory, with the characteristic oscillations around 40 rpm preserved across the cycle. Given the near-closed kinematic structure of the model, this implies that the remaining joint trajectories also followed the optimized motion. Minor deviations in crank speed reflect the higher numerical tolerances adopted in this second optimization stage, which were intentionally relaxed to improve computational tractability without altering the qualitative behavior of the solution.

The most substantial changes introduced by the synergy-based optimization are seen in the muscle activation patterns. Compared to the speed-tracking solution, activations no longer exhibited smooth oscillations around intermediate activation levels. Instead, both quadriceps and hamstrings activations converged toward sparse, low-amplitude profiles centered near zero, punctuated by brief activation bursts sufficient to satisfy the prescribed kinematics (Figure 8.2). This behavior is a direct consequence of the muscle effort minimization objective, which favors temporally compact activation strategies that reduce overall stimulation demand while preserving motion. Importantly, the imposed synergy structure enforced synchronized activation within muscle groups: rectus femoris and vasti followed an identical activation profile, as did the hamstrings and biceps femoris short head. This grouping prevented the optimizer from overloading a single muscle to minimize cost, promoting distributed force production consistent with experimentally realizable surface FES stimulation.

The imposed muscle groupings play a critical role in shaping these outcomes. In surface FES, selective recruitment of individual muscles is fundamentally limited by electrode size and placement, resulting in the simultaneous activation of multiple muscles per stimulation channel. Prescribing synergy structure therefore reflects the true actuation constraints of the system, rather than imposing an artificial coordination pattern. In this context, synergies are not intended to uncover underlying neural organization, but instead serve as a control abstraction

that reduces dimensionality while preserving functional flexibility. Non-negative matrix factorization (NMF) provides a convenient and principled mathematical framework for this purpose, enforcing non-negativity and coordinated activation while separating fixed muscle groupings from optimizable temporal coefficients. By constraining the optimizer to operate within experimentally meaningful groupings, this formulation restricts the solution space to activation strategies that are numerically robust, physiologically feasible, and directly translatable to real-time stimulation, while still allowing the emergence of timing features such as pre-activation and controlled co-contraction without manual tuning. Importantly, while the synergy structure was prescribed, the resulting activation patterns were not imposed but emerged from the interaction between musculoskeletal dynamics, task objectives, and stimulation constraints.

9.3 TRANSITION FROM SIMULATION TO STIMULATION

To enable experimental implementation, the synergy-derived activation signals were post-processed to obtain stimulation profiles suitable for real-time FES delivery, as illustrated in Figure 7.3. Owing to the cyclic nature of pedaling, these profiles can be naturally represented as functions of crank angle, facilitating interpretation in the polar domain (Figure 8.3). In this representation, the quadriceps control signal exhibits a smooth, graded activation largely confined to mechanically advantageous regions of the cycle. The pre-activation and co-contraction outside these regions is primarily attributable to the bi-articular function of the rectus femoris, whose contribution to hip flexion becomes necessary given the limited activation capacity of the hamstrings. In contrast, the hamstrings profile displays a more irregular structure, characterized by multiple activation peaks and reduced alignment with mechanically favorable crank angles. This behavior reflects both the imposed activation limit and the extraction of the control signal from a single steady-state cycle. A gradual FES conditioning towards greater hamstring activation capacity or averaging across multiple cycles would likely yield a more regular activation profile and alter the quadriceps-hamstrings interaction.

The polar representation further reveals important structural characteristics of the empirically tuned bang-bang (BB) stimulation protocol beyond its discrete timing. In contrast to the simulation-derived control signal (CS), BB relies on fixed crank-angle activation windows that were previously defined and applied uniformly across cycles. These windows are combined with

linear ramp-up and ramp-down transitions to reduce abrupt force transients, which appear as curved edges in the polar domain due to the angular parametrization. A key feature highlighted by this representation is the intentional asymmetry introduced in the BB protocol. The left leg received a systematically higher stimulation command, visible as a larger radial extent of the shaded activation regions. This asymmetry reflects a deliberate compensatory strategy adopted in response to the persistent left-right imbalance observed in the previous study (Figure 5.2), and was implemented as a 30% increase in commanded pulse width for the left leg, capped at 480 μs as a safety measure, where the stimulation difference drops to 6.7% (Figure 8.3).

An additional aspect of the transition from simulation to stimulation concerns the timing mismatch introduced by electromechanical and system-level delays inherent to surface FES. While the simulation framework assumes instantaneous muscle excitation and activation dynamics, experimental FES cycling involves delays associated with crank angle sensing, signal processing, stimulation delivery, and the muscle's excitation-activation coupling. To account for these effects, a speed-dependent phase shift was incorporated into both control strategies, anticipating stimulation onset proportionally to crank cadence. Although the proportionality constant governing this shift K was determined empirically, its behavior closely matches the measured delay of the participant, characterized in a simple experiment. Brief stimulation pulses applied to each leg produced measurable crank motion after delays of approximately 90 ms, closely aligned with the phase adjustment implemented in practice. For simplicity and to preserve direct comparability between stimulation protocols, the phase shift described by equation 7.4 was applied to BB and CS. While this empirical approach has proven robust over years of experimental refinement, it also highlights an element of the study framework that remains heuristic.

9.4 EXPERIMENTAL RESULTS: INTERPRETATION & COMPARISON

The experimental evaluation implemented the two stimulation strategies derived and discussed in the previous sections: the simulation-derived control signal (CS) and the empirically tuned bang-bang (BB) protocol depicted in the polar representation (Figure 8.3). Data were collected over four non-consecutive days to minimize interday fatigue effects, with two trials performed per session and the order of protocol execution alternated to reduce order-related

bias. Power output, crank cadence, and left-right balance were recorded continuously during each trial and subsequently analyzed. Trials means and variability metrics are summarized in Table 8.1, while the temporal evolution of these variables across the full 120-s trials is shown in Figure 8.4. Across sessions, the BB protocol consistently achieved higher average power output and cadence, whereas the CS generally exhibited improved left-right balance, indicating a more symmetrical contribution between limbs.

Examination of the trial-wise results in Table 8.1 reveals both consistent performance trends and notable session-dependent effects. An effect of protocol order was observed across days. On the first and third days, when the BB protocol was performed before CS, BB exhibited markedly higher power and cadence values than CS. Conversely, on the second and fourth days, when CS was tested first, its performance more closely matched that of BB within the same session. This pattern suggests a short-term carryover or priming effect, potentially related to muscle conditioning, neuromuscular readiness, or transient fatigue accumulation. Despite these order effects, the relative differences between protocols remained consistent, with BB favoring higher power output and cadence, and CS demonstrating improved balance.

The temporal evolution of power, cadence, and balance shown in Figure 8.4 provides additional insight beyond the trials averaged metrics. During the initial assisted phase, both stimulation strategies were assisted to achieve comparable power and cadence levels during that interval. Following the transition to unassisted cycling at 30 s, clear differences emerged. The BB protocol maintained relatively stable power output and cadence throughout the unassisted phase, whereas the CS exhibited an immediate drop in both variables, followed by a gradual recovery as pulse width increased automatically over time. This behavior highlights the greater robustness of BB to the removal of assistance and lower pulse width stimulation, while also illustrating the improvements of CS under progressive stimulation scaling. In contrast, left-right balance remained comparatively stable across time for both protocols, with CS consistently closer to 50%, suggesting that balance improvements were not strongly affected by the assisted-unassisted transition.

Although the empirically tuned bang-bang (BB) protocol outperformed the simulation-derived control signal (CS) in terms of power output and crank cadence, this result does not undermine the relevance or contribution of the proposed approach. The BB stimulation protocol

used in this study represents the outcome of more than a decade of empirical refinement (BO *et al.*, 2017), including iterative adjustments of stimulation timing, intensity, and asymmetry. In particular, the protocol incorporates an intentional 30% increase in stimulation applied to the left leg to compensate for persistent inter-limb imbalance, a feature that was previously shown to be effective and was successfully employed during the Cybathlon 2024 competition. Such BB protocols are the product of extensive experimentation, intuition, and participant-specific adaptations and conditioning (LAUBACHER *et al.*, 2017; METANI *et al.*, 2017).

In contrast, CS was generated from a fully predictive pipeline, starting from musculoskeletal optimal control and proceeding through a structured post-processing stage to obtain implementable stimulation profiles. Beyond the modeling and experimentally imposed activation constraints and a shared timing compensation strategy, CS did not rely on manual tuning of crank-angle windows, rider-specific asymmetry heuristics, or iterative shaping of stimulation behavior. In other words, the contribution of CS is not that it immediately replace an optimized BB pattern, but that it demonstrates a reproducible workflow capable of producing a functional stimulation strategy with minimal heuristic burden. This is particularly valuable for new FES cycling users, new research groups, or clinical contexts where extensive iterative tuning is not feasible, and where a safe, objective starting point can materially reduce setup time, uncertainty, and experimentation risk (FREGLY, 2021).

Two factors likely contributed to the higher power and cadence achieved by the BB protocol relative to the CS. First, the BB stimulation strategy maintains prolonged periods of near-maximal stimulation within the predefined crank-angle windows, which inherently favors greater torque production, particularly during lower effective pulse widths. In contrast, the CS exhibits a smoother, more graded activation profile that spends less time at active-contraction stimulation levels (Figure 8.3), thereby limiting instantaneous force output.

A second possible explanation for the observed performance differences is the participant's long-term training history with the BB stimulation. More than a decade of exposure to abrupt, high-intensity, BB recruitment patterns may have conditioned the neuromuscular system to respond more effectively to binary stimulation strategies than to smoothly varying activation profiles. Long-term FES training is known to induce task-specific adaptations, including changes in muscle contractile properties, reflex behavior, and central modulation of motor output (RUSH-

TON, 2002; HOOK; GRAU, 2007; ALASHRAM *et al.*, 2022). Under this interpretation, the CS protocol may require a dedicated adaptation period before its physiological advantages can translate into comparable mechanical performance, despite its closer resemblance to graded muscle activation.

The consistently improved left-right balance observed during CS trials should not be interpreted as a difference in limb strength or overall force-generating capacity, but rather as a consequence of differences in activation timing, coordination, and responsiveness between the two control strategies. Unlike the BB protocol, which relies on fixed activation windows and compensatory amplitude asymmetry, the CS incorporates pre-activation phases that initiate muscle excitation before the mechanically optimal crank regions. This anticipatory activation reduces the effective electromechanical delay between stimulation onset and force production, allowing each leg to contribute more synchronously during its respective power phase.

In addition, the CS promotes small, nearly continuous intervals of co-contraction between quadriceps and hamstrings, which may enhance crank control near phase transitions and reduce abrupt changes in angular acceleration. Together, pre-activation and controlled co-contraction likely improve temporal alignment between muscle force generation and crank mechanics, promoting smoother bilateral coordination. In contrast, the BB protocol compensates for delayed or a possible asymmetric force production, an issue also noted in prior FES cycling studies (COUSIN *et al.*, 2021; WANG *et al.*, 2024), primarily through increased stimulation amplitude applied to the left leg. While effective for sustaining power output and improving inter-limb balance, this strategy inherently relies on stimulation asymmetry, which may introduce practical concerns and potentially limit generalizability, particularly if substantial stimulation asymmetry is required to achieve acceptable balance.

These results suggest that balance improvements under CS originate from differences in when and how muscles are activated, rather than how much stimulation is delivered or reduced left leg strength. By promoting timing and coordination, the simulation-derived approach reduces reliance on amplitude-based compensation strategies and offers a pathway toward more symmetric FES cycling without requiring limb-specific tuning.

9.5 QUALITATIVE COMPARISONS ACROSS STUDIES

Although the two studies presented share the same overarching simulation-to-stimulation workflow and were conducted with the same participant at different time points, a direct quantitative comparison of outcomes across studies is not appropriate. The experimental conditions differ in several ways that impact the experimental results. First, the participant's physiological status changed over the intervening year (age, body mass, training status, and overall conditioning), which directly affects FES responsiveness and fatigue behavior. Second, the data acquisition environment differed, altering signal filtering, internal calibration, and metric computation. Third, the collection protocol was redesigned: trial duration increased, an explicit assisted phase was introduced, and stimulation intensity followed a structured pulse-width increase. Finally, the bang-bang stimulation used for comparison was not the same across studies, since the present study implemented an elaborate BB protocol including intentional inter-limb asymmetry, onset and offset activation ramps, and a speed-dependent phase shift. For these reasons, comparisons across studies in this thesis are treated as qualitative and mechanistic rather than statistical, focusing on whether specific control features persist under more realistic assumptions and protocols.

One qualitative comparison that remains meaningful across studies concerns the persistence of timing features in the simulation-derived control signal (CS) (Figures 5.1 and 8.3). In the first study, pre-activation and co-contraction were interpreted partly as emergent responses to modeling constraints, including quadriceps-only actuation and the imposed maximum crank speed. A reasonable hypothesis was that these features might be artifacts of the hard speed constraint, reflecting the need to regulate cadence by "braking" the crank through off-phase activation. In the second study, however, similar coordination features remained present despite substantial changes to the modeling and control formulation, including the removal of the hard crank-speed limitation and the addition of antagonist muscle groups. This persistence supports the interpretation that pre-activation and co-contraction are not merely constraint-driven artifacts, but can also arise from muscle properties and coordination demands (KIM *et al.*, 2008; HAKANSSON; HULL, 2009; HUG *et al.*, 2011).

The overall profile of the quadriceps in the CS was similar between studies (Figures 5.1 and 8.3), but not its positioning, and several factors could plausibly contribute to this shift. Preserving

passive muscle properties in the second study changes baseline joint torques and the effective mechanical demands on stimulated muscles across the cycle, which can shift optimal timing and amplitude. The inclusion of hamstrings adds an additional, although comparatively limited, torque source and an antagonist pathway, changing how the optimizer allocates work between muscle groups contributions, and potentially reducing the need for sustained quadriceps activation in certain regions. In addition, the second study extracted the control signal from a single steady-state cycle rather than averaging across multiple cycles, which can preserve sharper local features that might otherwise be smoothed out by cycle-to-cycle averaging. Together, these modeling and processing differences provide a coherent explanation for the changes observed in the CS across studies, even though key coordination features remained consistent.

9.6 LIMITATIONS

Despite the methodological advances introduced in this study, limitations should be acknowledged at both the modeling and experimental levels.

9.6.1 Model scaling

At the modeling level, the musculoskeletal representation was intentionally simplified. The model was not scaled to the participant's anthropometric dimensions and did not incorporate individualized muscle-tendon parameters, which influence activation dynamics, force-length-velocity relationships, and the timing of force transmission. While this level of abstraction was sufficient to generate experimentally viable stimulation profiles, further personalization would improve the physiological fidelity of the simulations (MACERATESI *et al.*, 2025).

9.6.2 Crank resistance

The resistive crank torque used in both simulation studies was fixed at 8 Nm. This value was not derived from a formal optimization or experimental setup characterization, but rather selected based on prior work by de Sousa et al. (SOUSA; FONT-LLAGUNES, 2024), where it demonstrated stable and physiologically reasonable cycling behavior. While this choice ena-

bled consistent comparison across studies and facilitated convergence of the optimal control problem, it remains a heuristic parameter. Different resistance levels would likely alter muscle coordination strategies and optimal stimulation timing.

9.6.3 Number of synergies

In addition, although six synergies per leg were prescribed to provide optimization flexibility, only two synergies per leg actively contributed to cycling, consistent with the literature (LI *et al.*, 2015; AMBROSINI *et al.*, 2016). When working with a simulation framework and FES cycling applications, more complex musculoskeletal representations, including additional muscles or three-dimensional joint dynamics, would not only likely require a richer synergy structure to adequately capture coordination demands and force redistribution (BRAMBILLA; SCANO, 2022), but also require substantially more computational power.

9.6.4 Fixed target cadence

The simulations were conducted around a fixed target cadence, which allowed for controlled optimization of activation timing and coordination. However, real-world FES cycling often involves cadence fluctuations due to fatigue, terrain, or voluntary upper-body input. Although speed-dependent phase shifting was applied experimentally, the simulation framework itself did not explicitly model cadence variability, which may limit the generality of the derived control signal under dynamically changing conditions.

9.6.5 Open-loop control

The proposed stimulation strategy operates in an open-loop configuration. Although the simulation-derived stimulation signal was designed to be robust and experimentally viable, it does not explicitly compensate for external disturbances, unmodeled dynamics, or time-varying physiological changes during cycling. As a result, perturbations such as abrupt fatigue onset, electrode displacement, or unexpected reflex activity may degrade performance or compromise stability. This limitation is inherent to open-loop FES systems and has long been recognized

in the literature, particularly in the presence of nonlinear neuromuscular dynamics and altered reflex pathways following spinal cord injury (POPOVIC; SINKJÆR, 2000).

9.6.6 Participants limitation

At the experimental level, variability in the participant's physiological state across non-consecutive testing days may have contributed to performance fluctuations. Moreover, the study was conducted with a single highly trained participant, which limits the generalizability of the quantitative findings.

It is also important to recognize that achieving and maintaining the level of fitness required for sustained FES cycling typically demands months or years of regular training, which inherently limits participant availability. While this constraint restricts larger scale experimental validation, lower-intensity FES protocols involving less trained participants may also benefit from the proposed simulation-derived stimulation approach.

9.6.6.1 Cautionary note

Prior to engaging in cyclic FES exercise, adequate muscle conditioning should be ensured, particularly in individuals with severe atrophy or long term muscle paralysis. Isometric training at lower stimulation intensities can serve as an effective preparatory phase, allowing gradual adaptation while providing valuable insight into patient-specific muscle properties.

As emphasized by Popović et al. (POPOVIC; SINKJÆR, 2000), neuroprosthetic systems may fail to produce adequate functional movement due to fatigue, reduced torque-generating capacity, altered reflexes, spasticity, joint contractures, osteoporosis, and increased fracture risk. Central nervous system injury also leads to reflex reorganization and spastic responses, which can result in inappropriate antagonist activation and unpredictable motor behavior. These factors underscore the importance of cautious progression, individualized assessment, and clinical supervision when translating simulation-derived stimulation strategies into practice.

CHAPTER 10

CONCLUSION

Functional electrical stimulation (FES) cycling remains a challenging control problem due to the intrinsic non-physiological nature of electrically evoked muscle activation, the presence of electromechanical delays, and the strong coupling between stimulation timing, muscle coordination, and mechanical power production. Despite decades of experimental refinement, most successful FES cycling strategies still rely on empirically tuned bang-bang stimulation protocols, whose effectiveness depends heavily on manual adjustments, long-term user adaptation, and trial-and-error calibration. This thesis set out to investigate whether predictive musculoskeletal simulations could be used not only as an analysis tool, but as a reliable source of stimulation commands that can be translated into a FES cycling setup and validated experimentally.

Within this context, the thesis addressed two central research questions. The first examined how stimulation signals can be optimized in a safe and effective manner while remaining closer to coordinated, physiologically inspired patterns of muscle activation. The second investigated how simulation-derived stimulation signals compare experimentally to a mature, empirically tuned bang-bang protocol when evaluated using power output, cadence, and inter-limb balance (Section 1.5).

This thesis demonstrates that stimulation signals can be optimized safely and effectively by embedding the optimization process within a predictive, muscle-driven simulation framework that explicitly accounts for the physiological and experimental constraints of surface FES. Rather than tuning stimulation heuristically at the hardware level, the proposed approach formulates stimulation design as an optimal control problem constrained by muscle activation dynamics, passive tissue properties, coordinated muscle group actuation, and participant-specific activation limits. By prescribing synergy structures that reflect the realities of surface stimulation and allowing the optimizer to determine their temporal behavior, the resulting control signals exhibit graded activation, anticipatory timing, and controlled co-contraction patterns

that are more consistent with known principles of neuromuscular coordination. Safety is ensured intrinsically, by constraining the solution space to activation patterns that are physiologically feasible and experimentally implementable. In this sense, optimization is achieved not by maximizing performance alone, but by balancing effectiveness, coordination, and translational validity within a unified simulation-to-stimulation pipeline.

When compared experimentally to a mature, empirically tuned bang-bang protocol, the simulation-derived control signal exhibited distinct strengths and limitations. The bang-bang strategy consistently produced higher power output and cadence, reflecting years of iterative refinement, long-term participant adaptation, and the use of deliberate stimulation asymmetry to compensate for inter-limb imbalance. In contrast, the simulation-derived signal was generated without manual tuning and relied solely on predictive modeling and constrained optimization. While this resulted in lower peak performance, it produced more consistent left-right balance and smoother temporal coordination, achieved through pre-activation and controlled co-contraction rather than amplitude-based compensation. These findings indicate that the simulation-derived approach does not yet surpass the performance of highly optimized empirical protocols, but offers a fundamentally different value: a reproducible, transparent, and extensible method for generating stimulation strategies. Rather than replacing bang-bang control, the proposed framework provides a principled baseline from which individualized and trike-specific refinements can be systematically developed. While the experimental validation was conducted with a single highly trained participant, the proposed framework itself is not participant-specific and is designed to generalize across FES cycling setups through appropriate model adaptation and constraint specification.

Taken together, the contributions of this thesis extend beyond the specific experimental outcomes. The work demonstrates that predictive simulations can serve as an active design tool for FES control, capable of generating stimulation strategies that are physiologically plausible, experimentally translatable, and adaptable to individual constraints. By validating this approach across two progressively refined studies, the thesis establishes a methodological foundation upon which future developments, such as cadence-adaptive stimulation, personalized musculoskeletal models, delay-aware control formulations, and closed-loop optimization, can be built. Although demonstrated in the context of FES cycling, the principles developed in

this thesis could be directly applicable to other forms of FES-assisted movement, including standing and walking. In this sense, the primary legacy of this work is not a single optimal stimulation pattern, but a flexible and extensible framework that bridges simulation and experimentation, enabling more systematic, transparent, and scalable approaches to FES control.

10.1 FUTURE WORK DIRECTIONS EMERGING FROM THIS THESIS

The present thesis established and experimentally validated for the first time a predictive simulation-to-stimulation workflow for functional electrical stimulation (FES) cycling, progressing from a proof-of-concept framework to a physiologically richer and experimentally more robust case study implementation. While the major limitations of the initial study were systematically addressed, several research directions naturally emerge from the results and methodological advances presented here. The following future work directions are organized approximately by increasing complexity and expected time investment, ranging from short-term experimental refinements to long-term doctoral-level research programs.

10.1.1 Experimental characterization of crank resistance

One feasible experimental study concerns a systematic characterization of crank resistance across the available gear configurations of the tricycle. In the present work, a constant resistive torque of 8 Nm was adopted based on prior studies and practical feasibility. However, this value remains a heuristic estimation of the actual mechanical load experienced during cycling in the available setup.

Future work could involve instrumented measurements of crank torque across different gears and trainer configurations to construct an empirical resistance map as a function of cadence and gear ratio. Such characterization would remove an additional heuristic parameter from the simulation framework, enabling more accurate matching between simulated and experimental conditions.

10.1.2 Experimental characterization of system and muscle delay

A second feasible extension of this work concerns the empirical characterization of the full system delay inherent to real-time FES cycling. In the second study, a speed-dependent phase shift was introduced to compensate for delays associated with crank angle sensing, signal processing, stimulation delivery, and neuromuscular activation (Equation 7.4). Although this phase shift proved robust in practice, its proportionality constant was determined through empirical tuning.

A systematic experimental protocol could be designed to quantify the total delay between crank angle identification and the onset of measurable mechanical response. A simple approach consists of positioning the participant's leg at a known crank angle, delivering isolated stimulation pulses, and measuring the time difference until detectable crank motion or power generation occurs. Repeating this procedure across muscle groups at different moments would allow the characterization of muscle-specific delays, which are expected to differ for different fatigue levels, and between quadriceps and hamstrings due to distinct excitation-activation dynamics and anatomical properties. Such measurements would enable a principled, experiment-specific phase shift formulation that naturally incorporates hardware and signal processing latency, and neuromuscular delay, reducing reliance on heuristic tuning.

Once such delays are experimentally characterized, a natural next step is to incorporate system delay directly into the simulation environment. Rather than applying a phase shift to stimulation profiles, delay effects could be embedded into muscle excitation-activation dynamics by modifying activation and deactivation time constants. This approach would allow predictive simulations to account for real-world timing constraints inherently, enabling direct evaluation of how delay influences coordination features such as pre-activation and co-contraction.

10.1.3 Optimal positioning and biomechanical configuration

Another short-to-medium term extension involves optimizing the mechanical configuration of the FES cycling system itself. Bike fitting literature suggests that joint angle configuration strongly influences power production, comfort, and fatigue (FONDA *et al.*, 2014; MILLOUR

et al., 2022; BINI; HUME, 2025). By integrating joint-angle-based fitting criteria into the simulation framework, different positioning strategies could be evaluated systematically under identical stimulation conditions (PAIRE *et al.*, 2024). This would enable comparison of empirically derived fitting rules with simulation-based optimization, informing individualized tricycle setup prior to training or competition.

10.1.4 Integrated data platform

The experimental validation in this thesis relied on multiple sensing systems, including instrumented pedals, a smart trainer, external crank encoders, and commercial software not specifically designed for low-power and low-cadence FES cycling. A valuable future direction is the development of a unified data acquisition and control platform that integrates crank kinematics, pedal forces, stimulation parameters, and system state within a single synchronized framework.

Such integration would enable higher sampling rates, reduce dependency on proprietary software, and improve temporal alignment between stimulation events and measured mechanical responses. Beyond improving data quality, a unified system would also facilitate advanced control strategies and real-time monitoring.

10.1.5 Closed-loop and adaptive stimulation strategies

A further research direction involves transitioning from open-loop stimulation profiles toward closed-loop control. Initial studies could focus on adjusting a single stimulation parameter, such as pulse width or amplitude, to regulate crank cadence despite fatigue or external disturbances. More advanced controllers could adapt stimulation timing, including the phase shift, in response to cadence deviations. Ultimately, integrating fatigue estimation or prediction, potentially via observer-based approaches, could enable controllers that maintain target performance over extended sessions. These developments would complement the predictive framework presented here by adding robustness to physiological variability.

10.1.6 Adaptive stimulation via forward dynamics and learning-based control

A natural extension of the JNER framework is the removal of the constant cadence reference. While predictive optimal control is well-suited for deriving physiologically consistent stimulation strategies, it becomes computationally limited when spanning long time horizons or wide ranges of cycling speeds. As a result, using predictive simulations alone is not practical.

An alternative pathway is the use of forward dynamics combined with learning-based control strategies, such as reinforcement learning or adaptive machine learning approaches. Starting from the simulation-derived control signals validated experimentally in this thesis, learning-based controllers could be initialized with the physiologically meaningful stimulation patterns and subsequently adapted to reproduce the experimentally measured cycling behavior. This strategy would preserve the biomechanical insight provided by predictive simulations while leveraging the computational efficiency of forward dynamics.

By iteratively adapting stimulation profiles, such a framework could generate a continuous mapping between cadence and optimal stimulation timing and intensity (e.g., across 20-60 rpm), effectively producing a cadence-indexed library of control signals. This approach would reduce or potentially eliminate the need for explicit phase-shift compensation, as cadence-dependent timing adaptations would emerge naturally from the learning process. Developing and validating such a cadence-adaptive stimulation framework constitutes a complete, well-scoped master's-level research project, and would not be feasible without the simulation-to-stimulation validation established in this thesis.

10.1.7 Participant-specific muscle parameter identification and model personalization

At a doctoral research level, one of the most promising future directions is participant-specific muscle parameter identification. Using the experimentally measured kinematics and simulation-derived muscle activation patterns as references, muscle-tendon parameters could be estimated via optimization (e.g., using the *MocoParameter* tool within OpenSim Moco). This study would be complemented by experimental muscle characterization using ultrasound imaging and an isokinetic dynamometer, enabling comparison between simulation-based and

measurement-based parameter identification. Hybrid strategies that combine both sources of information may offer a powerful and practical pathway toward personalized neuromusculoskeletal modeling. The resulting models would not constitute a full digital twin, but rather a highly informed approximation of an individual's neuromuscular system. With sufficiently accurate models, extension to more complex movements, such as FES-assisted walking, would become feasible.

10.1.8 Formal stability analysis of the FES cycling system

Finally, a long-term theoretical extension involves formal stability analysis of the coupled stimulation-cycling system under diverse operating conditions. While the present work demonstrates experimentally that the system can sustain stable cycling under both bang-bang and simulation-derived stimulation strategies, it does not address whether such behavior is guaranteed, robust, or fragile to perturbations.

A central open question is whether the neuromusculoskeletal system driven by electrically stimulated muscles is provably stable under a given stimulation profile, or whether observed asymmetries and oscillations reflect instability, suboptimal control, or other coordination phenomena. In particular, delays, fatigue-induced parameter drift, and asymmetric stimulation could, in principle, destabilize the cycling motion or induce limit-cycle distortions that are not easily detectable from short experimental trials alone.

Tools such as PIETOOLS provide a framework for analyzing infinite-dimensional and delay-differential systems, and could be used to study stability, robustness margins, and delay sensitivity of the stimulation-cycling system (PEET, 2021). Such an analysis would shift the focus from observing what the system does to formally proving why it does not fail, complementing the predictions obtained using optimal control. Although developing a tractable mathematical abstraction of the full neuromusculoskeletal system is a substantial challenge and lies beyond the scope of this thesis, formal certification of stability would represent a powerful theoretical counterpart to the experimental validation achieved.

10.2 LIST OF PUBLICATIONS

- Simpósio de Engenharia Biomédica (SEB 2023): (LIMA *et al.*, 2023) - Utilização de sensores inerciais e IMM para detecção de eletroestimulação em ciclismo. (Published).
- Congresso Brasileiro de Engenharia Biomédica (CBEB 2024): (PERES *et al.*, 2025c) - Feasibility of Low-Cost Alternatives to Estimate Hip and Knee Angles of Adapted Cycling Movement. (Published).
- International Conference on NeuroRehabilitation (ICNR 2024): (PAIRE *et al.*, 2024) - Preliminary results of predictive simulation in cycling rehabilitation using diverse human and bicycle models. (Published).
- International Conference on NeuroRehabilitation (ICNR 2024): (FRANCO *et al.*, 2025) - Preliminary results: a comparative study of knee kinematics and dynamics with NanoStim and motion capture systems. (Published).
- International Conference on Rehabilitation Robotics (ICORR 2025): (PERES *et al.*, 2025a) - Validating Predictive Simulation-Derived Electrical Stimulation Cycling in a Person with Spinal Cord Injury. (Pubished).
- Journal of NeuroEngineering and Rehabilitation (JNER): (PERES *et al.*, 2025b) - From Simulation to Stimulation: A Predictive Synergy-Based Control Strategy for FES Cycling in a Person with SCI. (Under review).
- A PRISMA-Guided Systematic Review of Musculoskeletal Modelling Approaches in Lower-limb Cycling Biomechanics. (In preparation).

REFERENCES

AHMAD, M. K. I.; SHAMSUDIN, A. U.; SOOMRO, Z. A.; RAHIM, R. A.; IBRAHIM, B. S. K. K.; HUQ, M. S. Closed-loop Functional Electrical Stimulation (FES) – cycling rehabilitation with phase control Fuzzy Logic for fatigue reduction control strategies for stroke patients. *SINERGI*, Universitas Mercu Buana, v. 28, n. 1, p. 63, dez. 2023. ISSN 1410-2331. Disponível em: <http://dx.doi.org/10.22441/sinergi.2024.1.007>. Cited in page 20.

ALASHRAM, A. R.; ANNINO, G.; MERCURI, N. B. Changes in spasticity following functional electrical stimulation cycling in patients with spinal cord injury: A systematic review. *The Journal of Spinal Cord Medicine*, Taylor & Francis, v. 45, n. 1, p. 10–23, 2022. Disponível em: <https://doi.org/10.1080/10790268.2020.1763713>. Cited in page 82.

ALIBEJI, N. A.; MOLAZADEH, V.; DICIANNO, B. E.; SHARMA, N. A Control Scheme That Uses Dynamic Postural Synergies to Coordinate a Hybrid Walking Neuroprosthesis: Theory and Experiments. *Frontiers in Neuroscience*, Frontiers Media SA, v. 12, abr. 2018. ISSN 1662-453X. Disponível em: <http://dx.doi.org/10.3389/fnins.2018.00159>. Cited in page 4.

AMBROSINI, E.; FERRANTE, S.; FERRIGNO, G.; MOLTENI, F.; PEDROCCHI, A. Cycling Induced by Electrical Stimulation Improves Muscle Activation and Symmetry During Pedaling in Hemiparetic Patients. *IEEE Transactions on Neural Systems and Rehabilitation Engineering*, Institute of Electrical and Electronics Engineers (IEEE), v. 20, n. 3, p. 320–330, maio 2012. ISSN 1558-0210. Disponível em: <http://dx.doi.org/10.1109/TNSRE.2012.2191574>. Cited in page 42.

AMBROSINI, E.; FERRANTE, S.; SCHAUER, T.; FERRIGNO, G.; MOLTENI, F.; PEDROCCHI, A. An Automatic Identification Procedure to Promote the use of FES-Cycling Training for Hemiparetic Patients. *Journal of Healthcare Engineering*, Wiley, v. 5, n. 3, p. 275–292, jan. 2014. ISSN 2040-2309. Disponível em: <http://dx.doi.org/10.1260/2040-2295.5.3.275>. Cited 2 times in pages 18 and 19.

AMBROSINI, E.; MARCHIS, C. D.; PEDROCCHI, A.; FERRIGNO, G.; MONTICONE, M.; SCHMID, M.; D'ALESSIO, T.; CONFORTO, S.; FERRANTE, S. Neuro-Mechanics of Recumbent Leg Cycling in Post-Acute Stroke Patients. *Annals of Biomedical Engineering*, Springer Science and Business Media LLC, v. 44, n. 11, p. 3238–3251, jun. 2016. ISSN 1573-9686. Disponível em: <http://dx.doi.org/10.1007/s10439-016-1660-0>. Cited in page 85.

ANDERSEN, T.; Padilha Lanari Bo, A.; WATKINS, G.; MOHAMMAD, S.; MCEWAN, A. 7 - Neural stimulation technologies. In: PRAKASH, P.; SRIMATHVEERAVALLI, G. (Ed.). *Principles and Technologies for Electromagnetic Energy Based Therapies*. Academic Press, 2022. p. 235–254. ISBN 978-0-12-820594-5. Disponível em: <https://www.sciencedirect.com/science/article/pii/B9780128205945000113>. Cited in page 1.

ANDERSON, F. C.; PANDY, M. G. A Dynamic Optimization Solution for Vertical Jumping in Three Dimensions. *Computer Methods in Biomechanics and Biomedical Engineering*, Informa UK Limited, v. 2, n. 3, p. 201–231, jan. 1999. ISSN 1476-8259. Disponível em: <http://dx.doi.org/10.1080/10255849908907988>. Cited in page 34.

ANDERSON, F. C.; PANDY, M. G. Dynamic Optimization of Human Walking. *Journal of Biomechanical Engineering*, ASME International, v. 123, n. 5, p. 381–390, maio 2001. ISSN 1528-8951. Disponível em: <http://dx.doi.org/10.1115/1.1392310>. Cited in page 34.

ANDERSSON, J. A. E.; GILLIS, J.; HORN, G.; RAWLINGS, J. B.; DIEHL, M. CasADi: a software framework for nonlinear optimization and optimal control. *Mathematical Programming Computation*, Springer Science and Business Media LLC, v. 11, n. 1, p. 1–36, jul. 2018. ISSN 1867-2957. Disponível em: <http://dx.doi.org/10.1007/s12532-018-0139-4>. Cited in page 29.

BAPTISTA, R. S.; MOREIRA, M. C. C.; PINHEIRO, L. D. M.; PEREIRA, T. R.; CARMONA, G. G.; FREIRE, J. P. D.; BASTOS, J. A. I.; BO, A. P. L. User-centered design and spatially-distributed sequential electrical stimulation in cycling for individuals with paraplegia. *Journal of NeuroEngineering and Rehabilitation*, Springer Science and Business Media LLC, v. 19, n. 1, maio 2022. ISSN 1743-0003. Disponível em: <http://dx.doi.org/10.1186/s12984-022-01014-6>. Cited 5 times in pages 2, 8, 9, 18, and 30.

BAUTMANS, I.; VANTIEGHEM, S.; GORUS, E.; GRAZZINI, Y.-R.; FIERENS, Y.; POOL-GOUDZWAARD, A.; METS, T. Age-related differences in pre-movement antagonist muscle co-activation and reaction-time performance. *Experimental Gerontology*, v. 46, n. 8, p. 637–642, 2011. ISSN 0531-5565. Disponível em: <https://www.sciencedirect.com/science/article/pii/S0531556511000684>. Cited in page 49.

BELLMAN, M. J.; CHENG, T.-H.; DOWNEY, R. J.; HASS, C. J.; DIXON, W. E. Switched Control of Cadence During Stationary Cycling Induced by Functional Electrical Stimulation. *IEEE Transactions on Neural Systems and Rehabilitation Engineering*, Institute of Electrical and Electronics Engineers (IEEE), v. 24, n. 12, p. 1373–1383, dez. 2016. ISSN 1558-0210. Disponível em: <http://dx.doi.org/10.1109/tnsre.2015.2500180>. Cited in page 20.

BERNSTEIN, N. A. *The Co-ordination and Regulation of Movements*. Oxford: Pergamon Press, 1967. Cited in page 4.

BINI, R. R.; HUME, P. Examining the Effectiveness of Bike Fitting. *Sports Medicine*, Springer Science and Business Media LLC, v. 55, n. 9, p. 2059–2063, maio 2025. ISSN 1179-2035. Disponível em: <http://dx.doi.org/10.1007/s40279-025-02242-1>. Cited 2 times in pages 90 and 91.

BO, A. P.; FONSECA, L. O. da; GUIMARAES, J. A.; FACHIN-MARTINS, E.; PAREDES, M. E.; BRINDEIRO, G. A.; SOUSA, A. C. C. de; DORADO, M. C.; RAMOS, F. M. Cycling with Spinal Cord Injury: A Novel System for Cycling Using Electrical Stimulation for Individuals with Paraplegia, and Preparation for Cybathlon 2016. *IEEE Robotics & Automation Magazine*, v. 24, n. 4, p. 58–65, Dec 2017. ISSN 1558-223X. Cited 9 times in pages 8, 9, 10, 12, 18, 30, 72, 73, and 81.

BRAMBILLA, C.; SCANO, A. The Number and Structure of Muscle Synergies Depend on the Number of Recorded Muscles: A Pilot Simulation Study with OpenSim.

Sensors, MDPI AG, v. 22, n. 22, p. 8584, nov. 2022. ISSN 1424-8220. Disponível em: <http://dx.doi.org/10.3390/s22228584>. Cited in page 85.

BRAZ, G. P.; RUSSOLD, M.; DAVIS, G. M. Functional Electrical Stimulation Control of Standing and Stepping After Spinal Cord Injury: A Review of Technical Characteristics. *Neuromodulation: Technology at the Neural Interface*, Elsevier BV, v. 12, n. 3, p. 180–190, jul. 2009. ISSN 1094-7159. Disponível em: <http://dx.doi.org/10.1111/j.1525-1403.2009.00213.x>. Cited in page 1.

CASAS, J.; CHANG, C.-H.; BROSE, S. W.; DUENAS, V. H. Switched Adaptive Integral Concurrent Learning for Powered FES-Cycling. *IEEE Transactions on Automation Science and Engineering*, Institute of Electrical and Electronics Engineers (IEEE), v. 21, n. 3, p. 4905–4916, jul. 2024. ISSN 1558-3783. Disponível em: <http://dx.doi.org/10.1109/TASE.2023.3305185>. Cited in page 20.

CHEUNG, V. C. K.; CHEUNG, B. M. F.; ZHANG, J. H.; CHAN, Z. Y. S.; HA, S. C. W.; CHEN, C.-Y.; CHEUNG, R. T. H. Plasticity of muscle synergies through fractionation and merging during development and training of human runners. *Nature Communications*, Springer Science and Business Media LLC, v. 11, n. 1, ago. 2020. ISSN 2041-1723. Disponível em: <http://dx.doi.org/10.1038/s41467-020-18210-4>. Cited 2 times in pages 4 and 74.

CLANCY, C. E.; GATTI, A. A.; ONG, C. F.; MALY, M. R.; DELP, S. L. Muscle-driven simulations and experimental data of cycling. *Scientific Reports*, Springer Science and Business Media LLC, v. 13, n. 1, dez. 2023. ISSN 2045-2322. Disponível em: <http://dx.doi.org/10.1038/s41598-023-47945-5>. Cited 2 times in pages 21 and 35.

CO, K.; BEGON, M.; BAILLY, F.; MOISSENET, F. Optimal control-driven functional electrical stimulation: A PRISMA-ScR scoping review. *Computers in Biology and Medicine*, v. 199, p. 111311, 2025. ISSN 0010-4825. Disponível em: <https://www.sciencedirect.com/science/article/pii/S0010482525016658>. Cited 3 times in pages 3, 4, and 22.

COSTE, C. A.; WOLF, P. FES-Cycling at Cybathlon 2016: Overview on Teams and Results. *Artificial Organs*, Wiley, v. 42, n. 3, p. 336–341, mar. 2018. ISSN 1525-1594. Disponível em: <http://dx.doi.org/10.1111/aor.13139>. Cited in page 2.

COUSIN, C.; DUENAS, V.; DIXON, W. FES Cycling and Closed-Loop Feedback Control for Rehabilitative Human–Robot Interaction. *Robotics*, MDPI AG, v. 10, n. 2, p. 61, abr. 2021. ISSN 2218-6581. Disponível em: <http://dx.doi.org/10.3390/robotics10020061>. Cited 2 times in pages 74 and 82.

CROSSLEY, C. B.; WORSEY, M. T.; DIAMOND, L. E.; SAXBY, D. J.; WACKWITZ, T.; BOURNE, M. N.; LLOYD, D. G.; PIZZOLATO, C. A calibrated EMG-informed neuromusculoskeletal model can estimate hip and knee joint contact forces in cycling better than static optimisation. *Journal of Biomechanics*, Elsevier BV, v. 182, p. 112586, mar. 2025. ISSN 0021-9290. Disponível em: <http://dx.doi.org/10.1016/j.jbiomech.2025.112586>. Cited in page 21.

DAVIS, G. M.; HAMZAID, N. A.; FORNUSEK, C. Cardiorespiratory, Metabolic, and Biomechanical Responses During Functional Electrical Stimulation Leg Exercise: Health and Fitness Benefits. *Artificial Organs*, Wiley, v. 32, n. 8, p. 625–629, ago. 2008. ISSN 1525-1594. Disponível em: <http://dx.doi.org/10.1111/j.1525-1594.2008.00622.x>. Cited in page 1.

de Sousa, A. C. C.; RAMOS, F. M.; Narvaez Dorado, M. C.; da Fonseca, L. O.; Lanari Bó, A. P. A Comparative Study on Control Strategies for FES Cycling Using a Detailed Musculoskeletal Model. *IFAC-PapersOnLine*, v. 49, n. 32, p. 204–209, 2016. ISSN 2405-8963. Cyber-Physical & Human-Systems CPHS 2016. Disponível em: <https://www.sciencedirect.com/science/article/pii/S2405896316328877>. Cited 4 times in pages 2, 21, 64, and 72.

DELEY, G.; DENUZILLER, J.; CASILLAS, J.-M.; BABAULT, N. One year of training with FES has impressive beneficial effects in a 36-year-old woman with spinal cord injury. *The Journal of Spinal Cord Medicine*, Informa UK Limited, v. 40, n. 1, p. 107–112, dez. 2015. ISSN 2045-7723. Disponível em: <http://dx.doi.org/10.1080/10790268.2015.1117192>. Cited in page 1.

DELP, S.; LOAN, J.; HOY, M.; ZAJAC, F.; TOPP, E.; ROSEN, J. An interactive graphics-based model of the lower extremity to study orthopaedic surgical procedures. *IEEE Transactions on Biomedical Engineering*, Institute of Electrical and Electronics Engineers (IEEE), v. 37, n. 8, p. 757–767, 1990. ISSN 0018-9294. Disponível em: <http://dx.doi.org/10.1109/10.102791>. Cited in page 34.

DELP, S. L.; ANDERSON, F. C.; ARNOLD, A. S.; LOAN, P.; HABIB, A.; JOHN, C. T.; GUENDELMAN, E.; THELEN, D. G. OpenSim: Open-Source Software to Create and Analyze Dynamic Simulations of Movement. *IEEE Transactions on Biomedical Engineering*, v. 54, n. 11, p. 1940–1950, 2007. Cited 3 times in pages 23, 24, and 25.

DEMBIA, C. L.; BIANCO, N. A.; FALISSE, A.; HICKS, J. L.; DELP, S. L. OpenSim Moco: Musculoskeletal optimal control. *PLOS Computational Biology*, Public Library of Science (PLoS), v. 16, n. 12, p. e1008493, dez. 2020. ISSN 1553-7358. Disponível em: <http://dx.doi.org/10.1371/journal.pcbi.1008493>. Cited 2 times in pages 28 and 37.

FARHOUD, A.; ERFANIAN, A. Fully Automatic Control of Paraplegic FES Pedaling Using Higher-Order Sliding Mode and Fuzzy Logic Control. *IEEE Transactions on Neural Systems and Rehabilitation Engineering*, v. 22, n. 3, p. 533–542, 2014. Cited in page 20.

FEBRER-NAFRíA, M.; NASR, A.; EZATI, M.; BROWN, P.; FONT-LLAGUNES, J. M.; MCPHEE, J. Predictive multibody dynamic simulation of human neuromusculoskeletal systems: a review. *Multibody System Dynamics*, Springer Science and Business Media LLC, v. 58, n. 3–4, p. 299–339, nov. 2022. ISSN 1573-272X. Disponível em: <http://dx.doi.org/10.1007/s11044-022-09852-x>. Cited 2 times in pages 3 and 21.

FONDA, B.; SARABON, N.; LI, F.-X. Validity and reliability of different kinematics methods used for bike fitting. *Journal of Sports Sciences*, Informa UK Limited, v. 32, n. 10, p. 940–946, fev. 2014. ISSN 1466-447X. Disponível em: <http://dx.doi.org/10.1080/02640414.2013.868919>. Cited 2 times in pages 90 and 91.

FONSECA, L. O. d.; Bó, A. P.; GUIMARãES, J. A.; GUTIERREZ, M. E.; FACHIN-MARTINS, E. Cadence Tracking and Disturbance Rejection in Functional Electrical Stimulation Cycling for Paraplegic Subjects: A Case Study. *Artificial Organs*, Wiley, v. 41, n. 11, nov. 2017. ISSN 1525-1594. Disponível em: <http://dx.doi.org/10.1111/aor.13055>. Cited 3 times in pages 2, 20, and 72.

FRANCO, T.; PERES, A.; FONT-LLAGUNES, J. M.; SOUSA, A. C. C. de. A Preliminary Comparative Study of Knee Kinematics and Dynamics with NanoStim and Motion Capture

Systems. In: _____. *Converging Clinical and Engineering Research on Neurorehabilitation V*. Springer Nature Switzerland, 2025. p. 588–592. ISBN 9783031775888. Disponível em: <http://dx.doi.org/10.1007/978-3-031-77588-8_115>. Cited in page 94.

FRAZãO, M.; FIGUEIREDO, T. de G.; CIPRIANO, G. Should We Use the Functional Electrical Stimulation-Cycling Exercise in Clinical Practice? Physiological and Clinical Effects Systematic Review With Meta-analysis. *Archives of Physical Medicine and Rehabilitation*, 2024. ISSN 0003-9993. Disponível em: <https://www.sciencedirect.com/science/article/pii/S0003999324010578>. Cited 4 times in pages 2, 8, 16, and 42.

FREGLY, B. J. A Conceptual Blueprint for Making Neuromusculoskeletal Models Clinically Useful. *Applied Sciences*, v. 11, n. 5, 2021. ISSN 2076-3417. Disponível em: <https://www.mdpi.com/2076-3417/11/5/2037>. Cited 5 times in pages 3, 21, 23, 24, and 81.

FéVOTTE, C.; IDIER, J. Algorithms for Nonnegative Matrix Factorization with the β-Divergence. *Neural Computation*, v. 23, n. 9, p. 2421–2456, 09 2011. ISSN 0899-7667. Disponível em: <https://doi.org/10.1162/NECO_a_00168>. Cited in page 58.

GLASER, R. M. Physiologic Aspects of Spinal Cord Injury and Functional Neuromuscular Stimulation. *Central Nervous System Trauma*, Mary Ann Liebert Inc, v. 3, n. 1, p. 49–62, jan. 1986. ISSN 0737-5999. Disponível em: <http://dx.doi.org/10.1089/cns.1986.3.49>. Cited in page 2.

GROOTE, F. D.; KINNEY, A. L.; RAO, A. V.; FREGLY, B. J. Evaluation of Direct Collocation Optimal Control Problem Formulations for Solving the Muscle Redundancy Problem. *Annals of Biomedical Engineering*, Springer Science and Business Media LLC, v. 44, n. 10, p. 2922–2936, mar. 2016. ISSN 1573-9686. Disponível em: <http://dx.doi.org/10.1007/s10439-016-1591-9>. Cited 3 times in pages 23, 35, and 37.

HAKANSSON, N. A.; HULL, M. L. Muscle Stimulation Waveform Timing Patterns for Upper and Lower Leg Muscle Groups to Increase Muscular Endurance in Functional Electrical Stimulation Pedaling Using a Forward Dynamic Model. *IEEE Transactions on Biomedical Engineering*, Institute of Electrical and Electronics Engineers (IEEE), v. 56, n. 9, p. 2263–2270, set. 2009. ISSN 1558-2531. Disponível em: <http://dx.doi.org/10.1109/tbme.2009.2020175>. Cited 3 times in pages 2, 21, and 83.

HAKANSSON, N. A.; HULL, M. L. The Effects of Stimulating Lower Leg Muscles on the Mechanical Work and Metabolic Response in Functional Electrically Stimulated Pedaling. *IEEE Transactions on Neural Systems and Rehabilitation Engineering*, Institute of Electrical and Electronics Engineers (IEEE), v. 18, n. 5, p. 498–504, out. 2010. ISSN 1558-0210. Disponível em: <http://dx.doi.org/10.1109/tnsre.2010.2052132>. Cited in page 9.

HAKANSSON, N. A.; HULL, M. L. Can the efficacy of electrically stimulated pedaling using a commercially available ergometer be improved by minimizing the muscle stress–time integral? *Muscle and Nerve*, Wiley, v. 45, n. 3, p. 393–402, fev. 2012. ISSN 1097-4598. Disponível em: <http://dx.doi.org/10.1002/mus.22302>. Cited 2 times in pages 2 and 21.

HAMID, S.; HAYEK, R. Role of electrical stimulation for rehabilitation and regeneration after spinal cord injury: an overview. *European Spine Journal*, Springer Science and Business Media LLC, v. 17, n. 9, p. 1256–1269, ago. 2008. ISSN 1432-0932. Disponível em: <http://dx.doi.org/10.1007/s00586-008-0729-3>. Cited in page 1.

HAYASHIBE, M.; SHIMODA, S. Synergetic motor control paradigm for optimizing energy efficiency of multijoint reaching via tacit learning. *Frontiers in Computational Neuroscience*, Frontiers Media SA, v. 8, 2014. ISSN 1662-5188. Disponível em: <http://dx.doi.org/10.3389/fncom.2014.00021>. Cited in page 4.

HENNEMAN, E.; SOMJEN, G.; CARPENTER, D. O. Excitability and inhibitability of motoneurons of different sizes. *Journal of Neurophysiology*, American Physiological Society, v. 28, n. 3, p. 599–620, maio 1965. ISSN 1522-1598. Disponível em: <http://dx.doi.org/10.1152/jn.1965.28.3.599>. Cited in page 13.

HERING, G. O.; BERTSCHINGER, R.; STEPAN, J. A quadriceps femoris motor pattern for efficient cycling. *PLOS ONE*, Public Library of Science, v. 18, n. 3, p. 1–28, 03 2023. Disponível em: <https://doi.org/10.1371/journal.pone.0282391>. Cited in page 48.

HILL, A. V. The heat of shortening and the dynamic constants of muscle. *Proceedings of the Royal Society of London. Series B - Biological Sciences*, v. 126, p. 136–195, 1938. Cited 2 times in pages 26 and 35.

HöHLER, C.; ENDO, S.; HERMSDöRFER, J.; CAZENAVE, L.; KAVIANIRAD, H.; JAHN, K.; KREWER, C. Repetitive Grasping After Stroke Assisted by Functional Electrical Stimulation. *Artificial Organs*, Wiley, jun. 2025. ISSN 1525-1594. Disponível em: <http://dx.doi.org/10.1111/aor.15033>. Cited in page 1.

HOOK, M. A.; GRAU, J. W. An animal model of functional electrical stimulation: evidence that the central nervous system modulates the consequences of training. *Spinal Cord*, Springer Science and Business Media LLC, v. 45, n. 11, p. 702–712, ago. 2007. ISSN 1476-5624. Disponível em: <http://dx.doi.org/10.1038/sj.sc.3102096>. Cited in page 82.

HUG, F.; TURPIN, N. A.; COUTURIER, A.; DOREL, S. Consistency of muscle synergies during pedaling across different mechanical constraints. *Journal of Neurophysiology*, American Physiological Society, v. 106, n. 1, p. 91–103, jul. 2011. ISSN 1522-1598. Disponível em: <http://dx.doi.org/10.1152/jn.01096.2010>. Cited 6 times in pages 12, 49, 73, 74, 75, and 83.

HUNT, K.; FANG, J.; SAENGSUWAN, J.; GROB, M.; LAUBACHER, M. On the efficiency of FES cycling: A framework and systematic review. *Technology and Health Care*, SAGE Publications, v. 20, n. 5, p. 395–422, set. 2012. ISSN 1878-7401. Disponível em: <http://dx.doi.org/10.3233/THC-2012-0689>. Cited 11 times in pages 1, 2, 4, 10, 11, 12, 13, 14, 15, 18, and 42.

HUNT, K.; STONE, B.; NEGARD, N.-O.; SCHAUER, T.; FRASER, M.; CATHCART, A.; FERRARIO, C.; WARD, S.; GRANT, S. Control strategies for integration of electric motor assist and functional electrical stimulation in paraplegic cycling: utility for exercise testing and mobile cycling. *IEEE Transactions on Neural Systems and Rehabilitation Engineering*, Institute of Electrical and Electronics Engineers (IEEE), v. 12, n. 1, p. 89–101, mar. 2004. ISSN 1558-0210. Disponível em: <http://dx.doi.org/10.1109/tnsre.2003.819955>. Cited in page 18.

IBITOYE, M. O.; HAMZAID, N. A.; HAYASHIBE, M.; HASNAN, N.; DAVIS, G. M. Restoring prolonged standing via functional electrical stimulation after spinal cord injury: A systematic review of control strategies. *Biomedical Signal Processing and*

Control, Elsevier BV, v. 49, p. 34–47, mar. 2019. ISSN 1746-8094. Disponível em: <http://dx.doi.org/10.1016/j.bspc.2018.11.006>. Cited in page 1.

JAEGER, L.; BAPTISTA, R. d. S.; BASLA, C.; CAPSI-MORALES, P.; KIM, Y. K.; NAKAJIMA, S.; PIAZZA, C.; SOMMERHALDER, M.; TONIN, L.; VALLE, G.; RIENER, R.; SIGRIST, R. How the cybathlon competition has advanced assistive technologies. *Annual Review of Control, Robotics, and Autonomous Systems*, Annual Reviews, v. 6, n. Volume 6, 2023, p. 447–476, 2023. ISSN 2573-5144. Disponível em: <https://www.annualreviews.org/content/journals/10.1146/annurev-control-071822-095355>. Cited 2 times in pages 2 and 8.

KAINZ, H.; FALISSE, A.; PIZZOLATO, C. Neuromusculoskeletal modeling in health and disease. *Brazilian Journal of Motor Behavior*, Brazilian Journal for Motor Behavior, v. 18, abr. 2024. ISSN 1980-5586. Disponível em: <http://dx.doi.org/10.20338/bjmb.v18i1.420>. Cited 2 times in pages 3 and 21.

KAJGANIC, P.; BERGERON, V.; METANI, A. ICEP: An Instrumented Cycling Ergometer Platform for the Assessment of Advanced FES Strategies. *Sensors*, MDPI AG, v. 23, n. 7, p. 3522, mar. 2023. ISSN 1424-8220. Disponível em: <http://dx.doi.org/10.3390/s23073522>. Cited in page 19.

KAPADIA, N.; MOINEAU, B.; POPOVIC, M. R. Functional Electrical Stimulation Therapy for Retraining Reaching and Grasping After Spinal Cord Injury and Stroke. *Frontiers in Neuroscience*, Frontiers Media SA, v. 14, jul. 2020. ISSN 1662-453X. Disponível em: <http://dx.doi.org/10.3389/fnins.2020.00718>. Cited in page 1.

KELLY, M. An Introduction to Trajectory Optimization: How to Do Your Own Direct Collocation. *SIAM Review*, v. 59, n. 4, p. 849–904, 2017. Disponível em: <https://doi.org/10.1137/16M1062569>. Cited in page 21.

KENNEDY, V.; LONG, M. D.; WALTERS, J.; ADEWUYI, A. A.; FRANZ, C. K. Applications of advances in therapeutic electrical stimulation techniques and technologies in precision peripheral nerve repair: a narrative review. *Advanced Technology in Neuroscience*, Ovid Technologies (Wolters Kluwer Health), v. 2, n. 2, p. 97–101, abr. 2025. ISSN 3050-6824. Disponível em: <http://dx.doi.org/10.4103/atn.atn-d-24-00023>. Cited in page 1.

KIM, C.-S.; EOM, G.-M.; HASE, K.; KHANG, G.; TACK, G.-R.; YI, J.-H.; JUN, J.-H. Stimulation Pattern-Free Control of FES Cycling: Simulation Study. *IEEE Transactions on Systems, Man, and Cybernetics, Part C (Applications and Reviews)*, v. 38, n. 1, p. 125–134, 2008. Cited 3 times in pages 21, 74, and 83.

KIM, E.; KIM, S.; KWON, Y. W.; SEO, H.; KIM, M.; CHUNG, W. G.; PARK, W.; SONG, H.; LEE, D. H.; LEE, J.; LEE, S.; JEONG, I.; LIM, K.; PARK, J. Electrical stimulation for therapeutic approach. *Interdisciplinary Medicine*, Wiley, v. 1, n. 2, abr. 2023. ISSN 2832-6245. Disponível em: <http://dx.doi.org/10.1002/INMD.20230003>. Cited in page 1.

KIMURA, K.; IMANAKA, K.; KITA, I. The effects of different instructions for preparatory muscle tension on simple reaction time. *Human Movement Science*, v. 21, n. 5, p. 947–960, 2002. ISSN 0167-9457. Current issues in motor control and coordination. Disponível em: <https://www.sciencedirect.com/science/article/pii/S0167945702001525>. Cited in page 48.

KONG, L.; YANG, K.; LI, H.; WU, X.; ZHANG, Q. Comparison of Lower-Limb Muscle Synergies Between Young and Old People During Cycling Based on Electromyography Sensors—A Preliminary Cross-Sectional Study. *Sensors*, MDPI AG, v. 24, n. 20, p. 6755, out. 2024. ISSN 1424-8220. Disponível em: <http://dx.doi.org/10.3390/s24206755>. Cited in page 12.

LAI, A. K. M.; ARNOLD, A. S.; WAKELING, J. M. Why are Antagonist Muscles Co-activated in My Simulation? A Musculoskeletal Model for Analysing Human Locomotor Tasks. *Annals of Biomedical Engineering*, Springer Science and Business Media LLC, v. 45, n. 12, p. 2762–2774, set. 2017. ISSN 1573-9686. Disponível em: <http://dx.doi.org/10.1007/s10439-017-1920-7>. Cited in page 49.

LAUBACHER, M.; AKSöZ, E. A.; BERSCH, I.; HUNT, K. J. The road to Cybathlon 2016 - Functional electrical stimulation cycling Team IRPT/SPZ. *European Journal of Translational Myology*, PAGEPress Publications, v. 27, n. 4, dez. 2017. ISSN 2037-7452. Disponível em: <http://dx.doi.org/10.4081/ejtm.2017.7086>. Cited 3 times in pages 18, 72, and 81.

LAUBACHER, M.; AKSöZ, E. A.; BINDER-MACLEOD, S.; HUNT, K. J. Comparison of proximally versus distally placed spatially distributed sequential stimulation electrodes in a dynamic knee extension task. *European Journal of Translational Myology*, PAGEPress Publications, v. 26, n. 2, jun. 2016. ISSN 2037-7452. Disponível em: <http://dx.doi.org/10.4081/ejtm.2016.6016>. Cited in page 2.

LEE, D. D.; SEUNG, H. S. Algorithms for non-negative matrix factorization. In: *Proceedings of the 14th International Conference on Neural Information Processing Systems*. Cambridge, MA, USA: MIT Press, 2000. (NIPS'00), p. 535–541. Cited in page 58.

LI, Z.; GUIRAUD, D.; HAYASHIBE, M. Inverse Estimation of Multiple Muscle Activations From Joint Moment With Muscle Synergy Extraction. *IEEE Journal of Biomedical and Health Informatics*, Institute of Electrical and Electronics Engineers (IEEE), v. 19, n. 1, p. 64–73, jan. 2015. ISSN 2168-2208. Disponível em: <http://dx.doi.org/10.1109/JBHI.2014.2342274>. Cited 2 times in pages 4 and 85.

LIMA, L. F.; FARIA, B. Mendes de; BAPTISTA, R. de S.; GARCIA, M. P.; PERES, A. B. Utilização de sensores inerciais e imm para detecção de eletroestimulação em ciclismo. Zenodo, 2023. Disponível em: <https://zenodo.org/record/8397274>. Cited in page 94.

MACENSKI, S.; FOOTE, T.; GERKEY, B.; LALANCETTE, C.; WOODALL, W. Robot Operating System 2: Design, architecture, and uses in the wild. *Science Robotics*, v. 7, n. 66, p. eabm6074, 2022. Disponível em: <https://www.science.org/doi/abs/10.1126/scirobotics.abm6074>. Cited in page 31.

MACERATESI, F.; FEBRER-NAFRíA, M.; FONT-LLAGUNES, J. M. Calibrated muscle models improve tracking simulations without enhancing gait predictions. *PLOS One*, Public Library of Science (PLoS), v. 20, n. 7, p. e0327172, jul. 2025. ISSN 1932-6203. Disponível em: <http://dx.doi.org/10.1371/journal.pone.0327172>. Cited in page 84.

MAFFIULETTI, N. A.; GONDIN, J.; PLACE, N.; STEVENS-LAPSLEY, J.; VIVODTZEV, I.; MINETTO, M. A. Clinical Use of Neuromuscular Electrical Stimulation for Neuromuscular Rehabilitation: What Are We Overlooking? *Archives of Physical Medicine and Rehabilitation*, Elsevier BV, v. 99, n. 4, p. 806–812, abr. 2018. ISSN 0003-9993. Disponível em: <http://dx.doi.org/10.1016/j.apmr.2017.10.028>. Cited in page 1.

MARQUEZ-CHIN, C.; POPOVIC, M. R. Functional electrical stimulation therapy for restoration of motor function after spinal cord injury and stroke: a review. *BioMedical Engineering OnLine*, Springer Science and Business Media LLC, v. 19, n. 1, maio 2020. ISSN 1475-925X. Disponível em: <http://dx.doi.org/10.1186/s12938-020-00773-4>. Cited in page 1.

MATEO, S.; BERGERON, V.; CHEMINON, M.; GUINET-LACOSTE, A.; POUGET, M.-C.; JACQUIN-COURTOIS, S.; LUAUTé, J.; NAZARE, J.-A.; SIMON, C.; RODE, G. Functional electrical stimulation-cycling favours erectus position restoration and walking in patients with critical COVID-19. A proof-of-concept controlled study. *Annals of Physical and Rehabilitation Medicine*, Elsevier BV, v. 64, n. 6, p. 101516, nov. 2021. ISSN 1877-0657. Disponível em: <http://dx.doi.org/10.1016/j.rehab.2021.101516>. Cited in page 1.

MCDANIEL, J.; LOMBARDO, L. M.; FOGLYANO, K. M.; MARASCO, P. D.; TRIOLO, R. J. Cycle Training Using Implanted Neural Prostheses: Team Cleveland. *European Journal of Translational Myology*, PAGEPress Publications, v. 27, n. 4, dez. 2017. ISSN 2037-7452. Disponível em: <http://dx.doi.org/10.4081/ejtm.2017.7087>. Cited 2 times in pages 9 and 18.

METANI, A.; POPOVIć-MANESKI, L.; MATEO, S.; LEMAHIEU, L.; BERGERON, V. Functional electrical stimulation cycling strategies tested during preparation for the First Cybathlon Competition – a practical report from team ENS de Lyon. *European Journal of Translational Myology*, PAGEPress Publications, v. 27, n. 4, dez. 2017. ISSN 2037-7452. Disponível em: <http://dx.doi.org/10.4081/ejtm.2017.7110>. Cited 4 times in pages 19, 72, 73, and 81.

MILLARD, M.; UCHIDA, T.; SETH, A.; DELP, S. L. Flexing Computational Muscle: Modeling and Simulation of Musculotendon Dynamics. *Journal of Biomechanical Engineering*, ASME International, v. 135, n. 2, fev. 2013. ISSN 1528-8951. Disponível em: <http://dx.doi.org/10.1115/1.4023390>. Cited in page 35.

MILLOUR, G.; VELáSQUEZ, A. T.; DOMINGUE, F. A literature overview of modern biomechanical-based technologies for bike-fitting professionals and coaches. *International Journal of Sports Science & Coaching*, SAGE Publications, v. 18, n. 1, p. 292–303, out. 2022. ISSN 2048-397X. Disponível em: <http://dx.doi.org/10.1177/17479541221123960>. Cited 2 times in pages 90 and 91.

MOLL, I.; VLES, J. S. H.; SOUDANT, D. L. H. M.; WITLOX, A. M. A.; STAAL, H. M.; SPETH, L. A. W. M.; JANSSEN-POTTEN, Y. J. M.; COENEN, M.; KOUDIJS, S. M.; VERMEULEN, R. J. Functional electrical stimulation of the ankle dorsiflexors during walking in spastic cerebral palsy: a systematic review. *Developmental Medicine & Child Neurology*, Wiley, v. 59, n. 12, p. 1230–1236, ago. 2017. ISSN 1469-8749. Disponível em: <http://dx.doi.org/10.1111/dmcn.13501>. Cited in page 1.

NIGHTINGALE, E. J.; RAYMOND, J.; MIDDLETON, J. W.; CROSBIE, J.; DAVIS, G. M. Benefits of FES gait in a spinal cord injured population. *Spinal Cord*, Springer Science and Business Media LLC, v. 45, n. 10, p. 646–657, jul. 2007. ISSN 1476-5624. Disponível em: <http://dx.doi.org/10.1038/sj.sc.3102101>. Cited in page 1.

PAIRE, L.; PERES, A.; BAPTISTA, R.; FONT-LLAGUNES, J. M.; SOUSA, A. C. C. de. Preliminary Results of Predictive Simulation in Cycling Rehabilitation Using Diverse

Human and Bicycle Models. In: _____. *Converging Clinical and Engineering Research on Neurorehabilitation V*. Springer Nature Switzerland, 2024. p. 483–486. ISBN 9783031775840. Disponível em: <http://dx.doi.org/10.1007/978-3-031-77584-0_94>. Cited 2 times in pages 91 and 94.

PARK, S.; CALDWELL, G. E.; UMBERGER, B. R. A direct collocation framework for optimal control simulation of pedaling using OpenSim. *PLOS ONE*, Public Library of Science, v. 17, n. 2, p. 1–17, 02 2022. Disponível em: <https://doi.org/10.1371/journal.pone.0264346>. Cited 2 times in pages 21 and 29.

PARK, S.-Y.; LEE, S.-Y.; KANG, H. C.; KIM, S.-M. EMG analysis of lower limb muscle activation pattern during pedaling: Experiments and computer simulations. *International Journal of Precision Engineering and Manufacturing*, Springer Science and Business Media LLC, v. 13, n. 4, p. 601–608, abr. 2012. ISSN 2005-4602. Disponível em: <http://dx.doi.org/10.1007/s12541-012-0077-4>. Cited in page 21.

PEET, M. M. A Partial Integral Equation (PIE) representation of coupled linear PDEs and scalable stability analysis using LMIs. *Automatica*, Elsevier BV, v. 125, p. 109473, mar. 2021. ISSN 0005-1098. Disponível em: <http://dx.doi.org/10.1016/j.automatica.2020.109473>. Cited in page 93.

PERES, A. B.; CARMONA, G. G.; GONCALVES, C.; SOUSA, A. C. C. de; BAPTISTA, R. de S. Validating Predictive Simulation-Derived Electrical Stimulation Cycling in a Person with Spinal Cord Injury. In: *2025 International Conference On Rehabilitation Robotics (ICORR)*. IEEE, 2025. p. 1245–1250. Disponível em: <http://dx.doi.org/10.1109/icorr66766.2025.11063118>. Cited 6 times in pages 3, 6, 22, 30, 35, and 94.

PERES, A. B.; CARMONA, G. G.; SOUSA, A. C. C. de; BAPTISTA, R. d. S. From Simulation to Stimulation: A Predictive Synergy-Based Control Strategy for FES Cycling in a Person with SCI. Springer Science and Business Media LLC, dez. 2025. Disponível em: <http://dx.doi.org/10.21203/rs.3.rs-8176477/v1>. Cited 6 times in pages 4, 6, 22, 30, 35, and 94.

PERES, A. B.; GARCIA, M. P.; BAPTISTA, R. de S. Feasibility of Low-Cost Alternatives to Estimate Hip and Knee Angles of Adapted Cycling Movement. In: _____. *XXIX Brazilian Congress on Biomedical Engineering - Volume 1: Biomedical Robotics, Rehabilitation, Biomechanics, and Biomedical Signal Processing*. Springer Nature Switzerland, 2025. p. 638–646. ISBN 9783031936463. Disponível em: <http://dx.doi.org/10.1007/978-3-031-93646-3_66>. Cited in page 94.

PERKINS, T.; DE, N.; DONALDSON, N.; FITZWATER, R.; PHILLIPS, G.; WOOD, D. Leg powered paraplegic cycling system using surface functional electrical stimulation. *Proc. 7th Int. Workshop on FES*, 01 2001. Cited in page 2.

PETROFSKY, J. S. New algorithm to control a cycle ergometer using electrical stimulation. *Medical & Biological Engineering & Computing*, Springer Science and Business Media LLC, v. 41, n. 1, p. 18–27, jan. 2003. ISSN 1741-0444. Disponível em: <http://dx.doi.org/10.1007/BF02343534>. Cited in page 19.

POPOVIC, D.; SINKJÆR, T. *Control of movement for the physically disabled: control for rehabilitation technology*. Germany: Springer, 2000. ISBN 1-85233-279-4. Cited 12 times in pages 1, 2, 3, 9, 10, 13, 14, 15, 18, 23, 37, and 86.

POPOVIC, M. R.; CURT, A.; KELLER, T.; DIETZ, V. Functional electrical stimulation for grasping and walking: indications and limitations. *Spinal Cord*, Springer Science and Business Media LLC, v. 39, n. 8, p. 403–412, ago. 2001. ISSN 1476-5624. Disponível em: <http://dx.doi.org/10.1038/sj.sc.3101191>. Cited in page 1.

RABELO, M.; JUCá, R. V. B. de M.; LIMA, L. A. O.; RESENDE-MARTINS, H.; Bó, A. P. L.; FATTAL, C.; AZEVEDO-COSTE, C.; FACHIN-MARTINS, E. Overview of FES-Assisted Cycling Approaches and Their Benefits on Functional Rehabilitation and Muscle Atrophy. In: _____. *Muscle Atrophy*. Springer Singapore, 2018. p. 561–583. ISBN 9789811314353. Disponível em: <http://dx.doi.org/10.1007/978-981-13-1435-3_26>. Cited 2 times in pages 2 and 8.

RIENER, R. The Cybathlon promotes the development of assistive technology for people with physical disabilities. *Journal of NeuroEngineering and Rehabilitation*, Springer Science and Business Media LLC, v. 13, n. 1, maio 2016. ISSN 1743-0003. Disponível em: <http://dx.doi.org/10.1186/s12984-016-0157-2>. Cited in page 2.

RUSHTON, D. Functional Electrical Stimulation and rehabilitation—an hypothesis. *Medical Engineering & Physics*, IOP Publishing, v. 25, n. 1, p. 75–78, jun. 2002. ISSN 1873-4030. Disponível em: <http://dx.doi.org/10.1016/S1350-4533(02)00040-1>. Cited in page 82.

RYAN, M. M.; GREGOR, R. J. EMG profiles of lower extremity muscles during cycling at constant workload and cadence. *Journal of Electromyography and Kinesiology*, v. 2, n. 2, p. 69–80, 1992. ISSN 1050-6411. Disponível em: <https://www.sciencedirect.com/science/article/pii/105064119290018E>. Cited in page 48.

SADOWSKY, C. L.; HAMMOND, E. R.; STROHL, A. B.; COMMEAN, P. K.; EBY, S. A.; DAMIANO, D. L.; WINGERT, J. R.; BAE, K. T.; MCDONALD, J. W. Lower extremity functional electrical stimulation cycling promotes physical and functional recovery in chronic spinal cord injury. *The Journal of Spinal Cord Medicine*, Informa UK Limited, v. 36, n. 6, p. 623–631, nov. 2013. ISSN 2045-7723. Disponível em: <http://dx.doi.org/10.1179/2045772313Y.0000000101>. Cited in page 1.

SANDRINI, G.; HOMBERG, V.; SALTUARI, L.; SMANIA, N.; PEDROCCHI, A. *Advanced Technologies for the Rehabilitation of Gait and Balance Disorders*. Springer International Publishing, 2018. (Biosystems & Biorobotics). ISBN 9783319727363. Disponível em: <https://books.google.com.br/books?id=YtBJDwAAQBAJ>. Cited in page 16.

SCHEER, J. W. van der; GOOSEY-TOLFREY, V. L.; VALENTINO, S. E.; DAVIS, G. M.; HO, C. H. Functional electrical stimulation cycling exercise after spinal cord injury: a systematic review of health and fitness-related outcomes. *Journal of NeuroEngineering and Rehabilitation*, Springer Science and Business Media LLC, v. 18, n. 1, jun. 2021. ISSN 1743-0003. Disponível em: <http://dx.doi.org/10.1186/s12984-021-00882-8>. Cited in page 2.

SCHMOLL, M.; GUILLOU, R. L.; FATTAL, C.; COSTE, C. A. OIDA: An optimal interval detection algorithm for automatized determination of stimulation patterns for FES-Cycling in individuals with SCI. *Journal of NeuroEngineering and Rehabilitation*, Springer Science and Business Media LLC, v. 19, n. 1, abr. 2022. ISSN 1743-0003. Disponível em: <http://dx.doi.org/10.1186/s12984-022-01018-2>. Cited 3 times in pages 8, 12, and 19.

SCOTT, W.; ADAMS, C.; FISHER, J.; FISHER, S.; JONES, K.; MATHIEU, B. Electrically elicited quadriceps muscle torque: Comparison at three knee angles. *Physiotherapy Theory and Practice*, Informa UK Limited, v. 37, n. 6, p. 729–735, jul. 2019. ISSN 1532-5040. Disponível em: <http://dx.doi.org/10.1080/09593985.2019.1639867>. Cited in page 40.

SO, R. C.; NG, J. K.-F.; NG, G. Y. Muscle recruitment pattern in cycling: a review. *Physical Therapy in Sport*, Elsevier BV, v. 6, n. 2, p. 89–96, maio 2005. ISSN 1466-853X. Disponível em: <http://dx.doi.org/10.1016/j.ptsp.2005.02.004>. Cited 2 times in pages 12 and 49.

SOUSA, A. C. C. de; FONT-LLAGUNES, J. M. Predictive Framework for Electrical Stimulation Cycling in Spinal Cord Injury. *IFAC-PapersOnLine*, Elsevier BV, v. 58, n. 24, p. 332–337, 2024. ISSN 2405-8963. Disponível em: <http://dx.doi.org/10.1016/j.ifacol.2024.11.059>. Cited 4 times in pages 34, 35, 56, and 84.

SOUSA, A. C. C. de; SOUSA, F. S. C.; BAPTISTA, R. de S.; BO, A. P. L. Passive Knee Orthoses Assistance in Functional Electrical Stimulation Cycling in an Individual With Spinal Cord Injury. *IEEE Transactions on Neural Systems and Rehabilitation Engineering*, Institute of Electrical and Electronics Engineers (IEEE), v. 29, p. 690–698, 2021. ISSN 1558-0210. Disponível em: <http://dx.doi.org/10.1109/TNSRE.2021.3070468>. Cited in page 34.

THRASHER, T.; POPOVIC, M. Functional electrical stimulation of walking: Function, exercise and rehabilitation. *Annales de Réadaptation et de Médecine Physique*, Elsevier BV, v. 51, n. 6, p. 452–460, jul. 2008. ISSN 0168-6054. Disponível em: <http://dx.doi.org/10.1016/j.annrmp.2008.05.006>. Cited in page 1.

TONG, R. K. Y.; WANG, X.; LEUNG, K. W. C.; LEE, G. T. Y.; LAU, C. C. Y.; WAI, H. W.; PANG, P. M. K.; LEUNG, H. C. How to prepare a person with complete spinal cord injury to use surface electrodes for FES trike cycling. In: *2017 International Conference on Rehabilitation Robotics (ICORR)*. IEEE, 2017. p. 801–805. Disponível em: <http://dx.doi.org/10.1109/icorr.2017.8009346>. Cited in page 18.

TURPIN, N. A.; WATIER, B. Cycling Biomechanics and Its Relationship to Performance. *Applied Sciences*, v. 10, n. 12, 2020. ISSN 2076-3417. Disponível em: <https://www.mdpi.com/2076-3417/10/12/4112>. Cited in page 49.

UHLRICH, S. D.; UCHIDA, T. K.; LEE, M. R.; DELP, S. L. Ten steps to becoming a musculoskeletal simulation expert: a half-century of progress and outlook for the future. *Journal of biomechanics*, Elsevier, v. 154, p. 111623, 2023. Cited 3 times in pages 3, 21, and 24.

WäCHTER, A.; BIEGLER, L. T. On the implementation of an interior-point filter line-search algorithm for large-scale nonlinear programming. *Mathematical Programming*, Springer Science and Business Media LLC, v. 106, n. 1, p. 25–57, abr. 2005. ISSN 1436-4646. Disponível em: <http://dx.doi.org/10.1007/s10107-004-0559-y>. Cited in page 29.

WAKELING, J. M.; HORN, T. Neuromechanics of Muscle Synergies During Cycling. *Journal of Neurophysiology*, American Physiological Society, v. 101, n. 2, p. 843–854, fev. 2009. ISSN 1522-1598. Disponível em: <http://dx.doi.org/10.1152/jn.90679.2008>. Cited in page 12.

WANG, G.; ZHAO, Y.; SUN, M.; DONG, W.; ZHU, S. Different Control Methods for FES Cycling:Review. In: *2024 IEEE 24th International Conference on Software Quality, Reliability, and Security Companion (QRS-C)*. [S.l.: s.n.], 2024. p. 759–766. Cited 2 times in pages 74 and 82.

WARNER, H.; AUDU, M. L.; LABROZZI, G. C.; MAKOWSKI, N. S.; TRIOLO, R. J. Experimental feasibility of personalized functional neuromuscular stimulation stepping patterns developed in silico. *Frontiers in Bioengineering and Biotechnology*, Frontiers Media SA, v. 13, jul. 2025. ISSN 2296-4185. Disponível em: <http://dx.doi.org/10.3389/fbioe.2025.1609734>. Cited 2 times in pages 4 and 21.

WORSEY, M. T.; CROSSLEY, C. B.; WACKWITZ, T.; COLLINGS, T.; BOURNE, M. N.; PIZZOLATO, C. Muscle forces and powers during sprint cycling at optimal cadence. *Journal of Biomechanics*, Elsevier BV, v. 191, p. 112890, out. 2025. ISSN 0021-9290. Disponível em: <http://dx.doi.org/10.1016/j.jbiomech.2025.112890>. Cited in page 21.

YAMAGUCHI, G. T.; ZAJAC, F. E. A planar model of the knee joint to characterize the knee extensor mechanism. *Journal of Biomechanics*, Elsevier BV, v. 22, n. 1, p. 1–10, 1989. ISSN 0021-9290. Disponível em: <http://dx.doi.org/10.1016/0021-9290(89)90179-6>. Cited in page 34.

ZHANG, Q.; HAYASHIBE, M.; FRAISSE, P.; GUIRAUD, D. FES-Induced Torque Prediction With Evoked EMG Sensing for Muscle Fatigue Tracking. *IEEE/ASME Transactions on Mechatronics*, Institute of Electrical and Electronics Engineers (IEEE), v. 16, n. 5, p. 816–826, out. 2011. ISSN 1941-014X. Disponível em: <http://dx.doi.org/10.1109/TMECH.2011.2160809>. Cited 2 times in pages 2 and 14.

ZOULIAS, I. D.; ARMENGOL, M.; POULTON, A.; ANDREWS, B.; GIBBONS, R.; HARWIN, W. S.; HOLDERBAUM, W. Novel instrumented frame for standing exercising of users with complete spinal cord injuries. *Scientific Reports*, Springer Science and Business Media LLC, v. 9, n. 1, set. 2019. ISSN 2045-2322. Disponível em: <http://dx.doi.org/10.1038/s41598-019-49237-3>. Cited in page 1.